Journal of Statistical Physics, Vol. 110, Nos. 3–6, March 2003 (© 2003)

Monte Carlo Studies of Wetting, Interface Localization and Capillary Condensation[1]

Kurt Binder,[2] David Landau,[3] and Marcus Müller[2]

Received February 12, 2002; accepted July 5, 2002

We present a brief review of Monte Carlo simulations of ferromagnetic Ising lattices in a film geometry with surface magnetic fields. The seminal work of Nakanishi and Fisher [*Phys. Rev. Lett.* **49**:1565 (1982)] showed how phase transitions in such models are related to wetting in systems with short range forces; and we will show how theoretical concepts about critical and tricritical wetting, interface localization-delocalization, and capillary condensation can be tested in this and similar models. After reviewing the qualitative, phenomenological description of these phenomena on a mean field level, we will summarize predictions of scaling theories. Comments will be made about the models studied and simulation techniques as well as the specific problems that occur in the relevant finite size scaling analysis. The resulting simulational data have prompted considerable new theoretical efforts, but there are still unsolved problems with respect to critical wetting. We will also present results for interface localization-delocalization transitions in both Ising models and lattice polymer mixtures in a thin film geometry and show that theory can account for many, but not all, aspects of the simulations. In systems with asymmetric boundary fields rather complex phase diagrams can result, and these should be relevant for corresponding experiments. The simulational evidence is fully compatible with the scaling predictions of Fisher and Nakanishi [*J. Chem. Phys.* **75**:5875 (1981)] on capillary condensation. To conclude we shall summarize the major unanswered theoretical questions in this rich field of inquiry.

KEY WORDS: Ising models; Monte Carlo simulation; wetting transition; capillary waves; finite size scaling.

[1] Dedicated to Professor Michael E. Fisher on the occasion of his 70th birthday.

[2] Institut für Physik, Johannes Gutenberg-Universität, D-55099 Mainz, Staudinger Weg 7, Germany; e-mail: kurt.binder@uni-mainz.de

[3] Center for Simulational Physics, The University of Georgia, Athens, Georgia 30602-2451.

0022-4715/03/0300-1411/0 © 2003 Plenum Publishing Corporation

1. INTRODUCTION: PHENOMENOLOGICAL DESCRIPTION OF WETTING, INTERFACE LOCALIZATION-DELOCALIZATION, AND CAPILLARY CONDENSATION

When a small amount of liquid on the surface of a solid substrate coexists with saturated gas, we may either observe that this liquid exists in the form of droplets touching the surface with a well-defined contact angle Θ (see Fig. 1), or that the liquid is spread out into a homogenous film on the surface. In the latter case one says that the surface is wetted by the fluid, while in the former case the substrate surface is termed "non-wet" or "incompletely wet" (i.e., if $0 < \Theta < \pi/2$). It has been known for about 200 years that the contact angle is determined by a competition between three interface free energies, namely the surface tension wall-gas σ_{wg}, the surface tension between wall and liquid σ_{wl}, and the interface tension

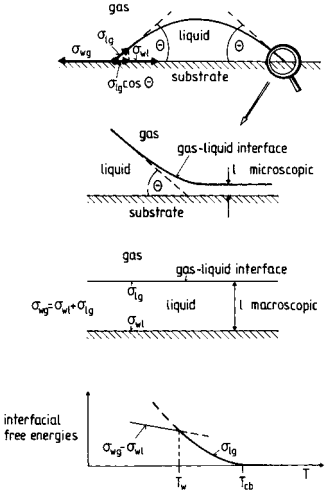

Fig. 1. Schematic cross section of a (macroscopic) droplet of liquid, coexisting with saturated gas, on a non-wet substrate surface showing: (upper part) the contact angle Θ and the interpretation of Young's equation in terms of mechanical equilibrium of the surface tensions on the contact line; (middle part) A magnified view of the three-phase contact line where the liquid-gas interface meets the substrate surface. On scales of a few molecular diameters this contact line is rounded away, since the liquid-gas interface bends over into a flat liquid film of microscopically small thickness l (of the order of a few molecular diameters). Note that the shape of the profile near the three-phase contact line shown here qualitatively refers to the simplest case—namely a situation close to a continuous wetting transition, as will be discussed below. In contrast, the wet surface is coated by a liquid film of macroscopic thickness $l \to \infty$ (in practice l may remain finite because of gravity, finite size, etc.). (bottom part) Illustration of a (first-order) wetting transition in terms of the temperature dependence of the various interface free energies.

between liquid and gas σ_{lg}.[1] The formal relationship is given by Young's equation:[1]

$$\cos\Theta = (\sigma_{wg} - \sigma_{wl})/\sigma_{lg} \qquad \text{if} \quad \sigma_{wg} \leqslant \sigma_{wl} + \sigma_{lg}. \tag{1}$$

If the inequality in Eq. (1) is not fulfilled, there is no real solution for Θ, and $\sigma_{wg} = \sigma_{wl} + \sigma_{lg}$. By forming a liquid film of mesoscopic thickness that uniformly coats the surface, the system lowers its free energy with respect to the state in which it is incompletely wet. The wet surface thus formally corresponds to $\Theta = 0$.

Since the interface free energies in Eq. (1) depend on temperature (and possibly on other control parameters) it is quite natural to expect that by suitable variation of parameters one can induce a transition where the state of the surface changes from incompletely wet to completely wet. Thus, it is surprising that a Landau-type theory of such a wetting transition was first proposed only about 25 years ago.[2] Figure 2 shows the resulting generic phase diagram and (coarse-grained[3]) density profile, and the variation of the surface excess density ρ_s in various situations is also drawn schematically. Here it is implied that the wetting transition, that is observed when the temperature T is raised through T_w along a path where one stays with the bulk density ρ exactly at the gas branch $\rho_{\text{coex}}^{(1)}$ of the coexistence curve (by controlling the gas pressure or the chemical potential $\mu = \mu_{\text{coex}}(T)$), is a first-order transition. With a suitable choice for the interactions between the fluid particles and the wall, it is also possible to have a second-order wetting transition ("critical wetting").[4–6] In this case, there is no prewetting line. The marginal case where the conditions have been fine-tuned such that the prewetting line just starts to disappear, i.e., the prewetting critical point and the wetting transition coincide, corresponds to a "tricritical wetting transition." Approaching T_w along the coexistence curve from below, the thickness of the fluid film absorbed on the wall diverges to infinity in a continuous fashion, while for a first-order transition l is still finite as $T \to T_w^-$ and then jumps discontinuously to infinity. In Section 2.1. we shall see how this behavior and an explicit description of the density profiles (shown schematically in Fig. 2) emerge from a Ginzburg–Landau-type theory.

From the viewpoint of thermodynamics, both wetting and prewetting transitions can be considered as singularities of the surface excess free energy of the fluid, $f_{wg}(T, \mu)$. At this point, it is of interest to recall that a description of surface phase transitions in terms of the singular behavior of a surface excess free energy contribution of a semi-infinite system has also been discussed for the surface critical behavior of Ising ferromagnets.[7] Figure 3 presents the associated phase diagram.[7, 8]

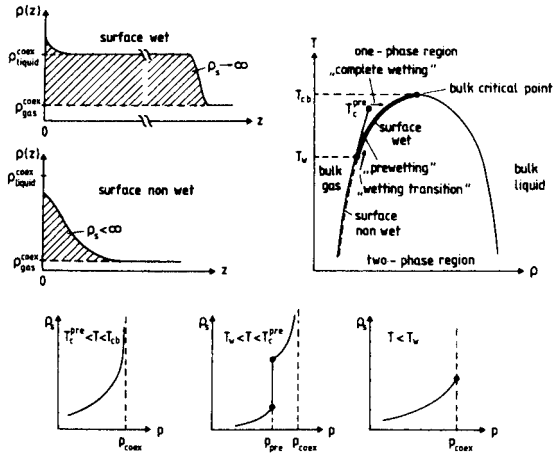

Fig. 2. (right part) Schematic phase diagram of a *semi-infinite* fluid in contact with a wall; (left part) corresponding profiles of the coarse-grained local density $\rho(z)$ as function of the distance z from the wall at $z = 0$. The interface distance l from the wall in Fig. 1 may be identified as the location of the inflection point in the profile. In the temperature (T)-density (ρ) plane, the coexistence curve separates saturated gas with liquid in the bulk. The enclosed two-phase region ends at the bulk critical point (T_{cb}). The wetting transition is a singularity of the surface excess free energy associated with the wall and occurs at a temperature T_w along the gas branch of the coexistence curve. The corresponding density profile may change from a non-wet state of the surface (surface excess density ρ_s, the integral of the shaded region, being finite) to a wet state either continuously ("critical wetting") or via a discontinuous jump at T_w. In the latter case, a further discontinuity at the "prewetting transition" occurs in the one-phase region, ending at a prewetting critical temperature T_c^{pre}. The figure shows (lower part) the schematic "adsorption isotherms" for "complete wetting" of the wall (when the pressure p of the gas approaches its value p_{coex} at the liquid-gas coexistence curve) and a further discontinuity at the prewetting transition for $T_w < T < T_c^{\mathrm{pre}}$. In contrast, for $T < T_w$ (surface non-wet) ρ_s reaches a finite limit for $p \to p_{\mathrm{coex}}$.

As is well known, the Ising model in a magnetic field H can be reinterpreted in terms of a lattice gas model in a chemical potential. This is done by relating a density variable c_i ($c_i = 1$ if a lattice site i is occupied by a fluid particle and $c_i = 0$ if it is empty) to an Ising spin $S_i = \pm 1$ by $c_i = (1 + S_i)/2$. In terms of the phase diagram of the bulk fluid in Fig. 2, phase coexistence between liquid and gas occurs for $H = 0$, and the particle-hole symmetry of the lattice gas implies a mirror symmetry of the bulk phase diagram along the critical density $\rho_c = \langle c_i \rangle_{T=T_c} = 1/2$. Therefore, it is natural that wetting phenomena (tacitly restricting attention to systems with short range forces between the fluid particles and the wall) can be described by an Ising Hamiltonian appropriate for a semi-infinite lattice (the coordinate z being restricted to $z \geqslant 0$). We represent the wall by the

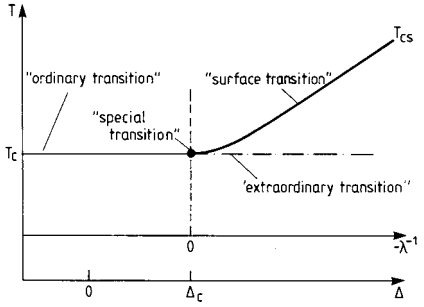

Fig. 3. Surface phase diagram of a Ising ferromagnet with nearest-neighbor interaction J in the bulk and coupling J_s in the surface plane, and zero surface field $H_1 = 0$ as a function of temperature T. If $\Delta = J_s/J - 1$ exceeds the critical value Δ_c, the surface orders at a temperature $T_{cs} > T_{cb}$ where the bulk is still disordered. The point $T = T_{cb}$, $J_s/J = J_{sc}/J$, where this "surface transition" at T_{sc} merges with the bulk transition at T_{cb}, is called the "special transition" or "surface-bulk multicritical point." Note that $\Delta - \Delta_c$ can be interpreted as an inverse of an "extrapolation length"[8] denoted as λ. From Binder.[8]

plane $z = 0$, assuming then that its physical effect can be modeled by a surface magnetic field H_1 acting only on the spins in the first lattice plane ($n = 1$) adjacent to the wall, and by a different choice of the exchange interaction J_s in the plane, as depicted in Fig. 3. Thus, this Hamiltonian can be written as

$$\mathscr{H}_{\text{Ising}}^{(s\cdot i)} = -J \sum_{\langle i,j\rangle \text{ bulk}} S_i S_j - J_s \sum_{\langle i,j\rangle \in \text{plane } n=1} S_i S_j - H \sum_i S_i - H_1 \sum_{i \in \text{plane } n=1} S_i \tag{2}$$

and obviously for $H = 0$, $H_1 = 0$ it contains the problem discussed in Fig. 3 as a special case.

At this point we mention that for the case $H = 0$ but $H_1 \neq 0$ and $\Delta < \Delta_c$ in Fig. 3 ($\Delta = \Delta_c$ corresponds to $J_S = J_{SC}$ in Eq. (2)) an additional type of surface transition occurs, which describes critical adsorption at walls for the liquid-gas critical point.[11,12] When $H_1 \neq 0$, then at $T = T_c$ there exists a non-zero magnetization at the surface of an Ising ferromagnet also for $\Delta < \Delta_c$, similar to the case $\Delta > \Delta_c$ and $H_1 = 0$, where the "extraordinary transition" (Fig. 3) occurs. Unlike the latter, this so-called "normal transition" ($H_1 \neq 0$ and $\Delta < \Delta_c$) can be easily realized in fluids and binary mixtures.[9,10] It turns out, that the critical behavior of the extraordinary and the "normal transitions" are identical.[11,12] Note that a fluid that undergoes wetting invariably undergoes the "normal transition" at its

surface for $T = T_c$ and at the critical pressure $p = p_c$ or critical density $\rho = \rho_c$ in the bulk.

An important advance in our theoretical understanding of wetting phenomena was made by Nakanishi and Fisher[13] who clarified the relation between wetting and surface critical phenomena more precisely. As is illustrated in Fig. 4, the surface critical temperature T_{cs} can be viewed as a special point on the critical line of prewetting transitions $T_c^{\text{pre}} = T_{cs}(H, H_1)$, and similarly the surface-bulk multicritical point is the (singular) endpoint of the line of tricritical wetting transitions in the space of variables $(T, H = 0, H_1, J_s/J)$ at T_{cb}. Thus, this picture shows in which regions of the parameters $T, H_1, J_s/J$ one can expect critical wetting or first-order wetting, respectively.[14] A further consequence of this relation[13] between surface critical behavior[7,8] and wetting is the fact that the scaling properties of surface critical behavior (in the presence of the fields $H \to 0$ and $H_1 \to 0$) also fixes the critical exponents that describe the vanishing of the critical fields $H_{1c}(T)$, $H_{1t}(T)$ of critical and tricritical wetting transitions as $T \to T_{cb}$ (see Section 2.3).

Figure 4 also emphasizes an important symmetry of the Ising model: when we change the sign of all the spins $\{S_i\}$ and of the fields H and H_1, the Hamiltonian is left completely invariant. As a consequence, the parts of the phase diagrams in Fig. 4 that are in the $H = 0$ plane are symmetric

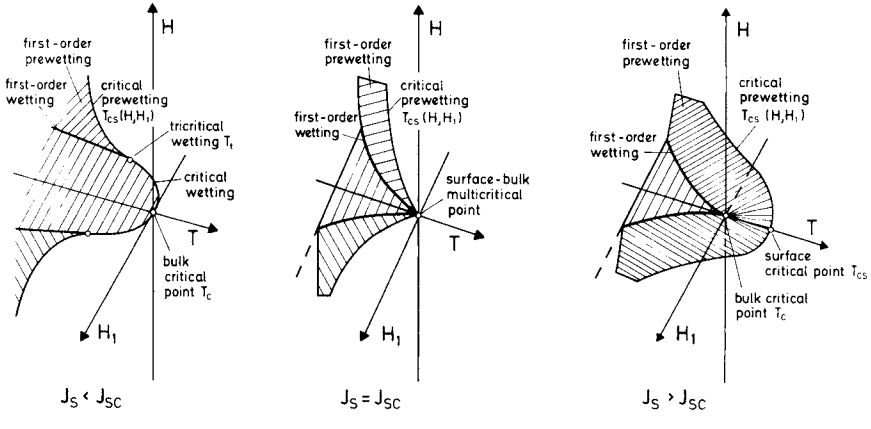

Fig. 4. Schematic phase diagrams for a semi-infinite Ising magnet in the vicinity of the bulk critical point T_{cb} as a function of temperature T, bulk field H, and surface field H_1. In the shaded part of the plane $H = 0$ the system is non-wet for $T < T_c$, while outside of it, for $T < T_c$, it is wet. The wetting transition is shown by a thin line where it is second-order and by a thick line where it is first-order. First-order prewetting surfaces terminate in the plane $H = 0$ at the first-order wetting line. Critical and multicritical points are indicated in the figure. After Nakanishi and Fisher.[13]

around the line $H_1 = 0$ (i.e., the temperature axis). Thus, wetting transitions occur for both positive and negative H_1, but it is important to realize that wetting transitions with $H_1 < 0$ belong to the branch of the coexistence curve with positive magnetization, and transitions with $H_1 > 0$ belong to the branch of the coexistence curve with negative magnetization. Since the mapping between the Ising magnet and the lattice gas implies the correspondence between the magnetization m of the magnet and the density ρ of the lattice gas according to $\rho = (1-m)/2$, only the case with $H_1 < 0$ describes a wetting transition of a liquid layer forming when a saturated gas is in contact with a wall. The case with $H_1 > 0$ then describes the opposite effect, i.e., the formation of a "drying layer" of gas when a fluid at the coexistence curve (i.e., saturated with gas) is in contact with a wall that "dislikes" the fluid. In the picture of the contact angle, Fig. 1, this corresponds to contact angle $\Theta > \pi/2$. In the phase diagram of Fig. 2, this would correspond to taking a mirror image along the line $\rho = \rho_c$ (thus, one then expects also a "predrying" line ending at a "predrying critical point" T^{pre} in the bulk liquid; this is described by the first-order "prewetting" sheets in the phase diagrams of Fig. 4 for positive H_1—in Fig. 4 no distinction in nomenclature between "wetting" and "drying" was made, and henceforth we also shall not make such a distinction speaking of "wetting" irrespective of whether physically a liquid or a gas layer form).

A very useful interpretation of the wetting transition is to consider it as an "interface unbinding transition": in the non-wet state, the interface is tightly bound to the wall, while in the wet state the interface is "free," far away from the wall. This description can be made explicit in terms of the behavior of the effective interface potential $V_{\text{eff}}(l)$ describing the free energy cost of placing a (straight) interface at the distance l from the wall. Figure 5 presents a qualitative sketch that shows how this interface potential behaves at a second-order wetting transition and at a first-order wetting transition, respectively.[4–6] In Section 2.2 this description and its consequences will be worked out in more detail.

We now briefly discuss the extension of these considerations to the case when the system is not semi-infinite, but rather we have to deal with a thin film of thickness D, confined by two parallel surface planes. In terms of an Ising model description, we may generalize Eq. (2) as follows

$$\mathscr{H}_{\text{Ising}}^{(\text{film})} = -J \sum_{\langle i,j\rangle \text{ bulk}} S_i S_j - J_s \sum_{\langle i,j\rangle \text{ surfaces}} S_i S_j$$

$$- H \sum_i S_i - H_1 \sum_{i \in \text{plane } n=1} S_i - H_D \sum_{i \in \text{plane } n=D} S_i \qquad (3)$$

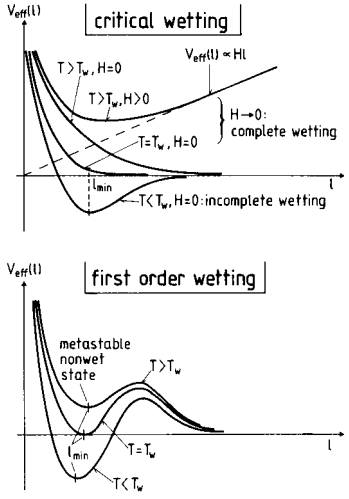

Fig. 5. Schematic variation of the effective interface potential $V_{\text{eff}}(l)$ for critical and complete wetting (upper part) and for first-order wetting (lower part). $V_{\text{eff}}(l)$ describes the excess free energy of having the interface a distance l from the wall as compared to the situation where $l \to \infty$ at $H = 0$ (the "completely wet" state). Equilibrium states are found from minimizing this potential with respect to the interface position, $dV_{\text{eff}}(l)/dl|_{l_{\min}} = 0$. For $T < T_w$, $l_{\min}$ is finite. For a second-order wetting transition $l_{\min}$ increases smoothly to infinity as $T \to T_w$ and for $T > T_w$ a metastable non-wet minimum does not exist. $V_{\text{eff}}(l_{\min}) = 0$ at T_w for a finite value of $l_{\min}$ at the first-order wetting transition, and for a range of temperatures above T_w a minimum with $V_{\text{eff}}(l_{\min}) > 0$, corresponding to a metastable non-wet state, still exists. The equilibrium solution hence exhibits a discontinuous jump from a finite $l_{\min}$ to $l_{\min} \to \infty$ at T_w. If a non-zero field $H > 0$ is present, the interface potential $\propto Hl$ at large distances (for the case $H_1 < 0$ so that the wetting layer corresponds to a region of negative magnetization). Therefore, a finite minimum position $l_{\min}$ is always found for $T > T_w$ if $H > 0$. As $H \to 0$, we again find $l_{\min} \to \infty$ ("complete wetting").

Here we have specialized to the case where the change of exchange constants is the same in both surface planes, while we still allow for different surface magnetic fields, $H_1 \neq H_D$. A particularly interesting situation is the case of antisymmetric surface fields, $H_1 = -H_D$, because then the system may undergo an interface localization-delocalization transition in zero external field $H = 0$, see Fig. 6.[15]

If we would consider the corresponding semi-infinite system, and approach the wetting transition temperature $T_w(H_1) = T_w(H_D = -H_1)$ from below, interfaces would unbind either from the left wall or the right wall, as described above. Note that with this antisymmetric choice of boundary conditions the order parameter profile across the system exhibits only a

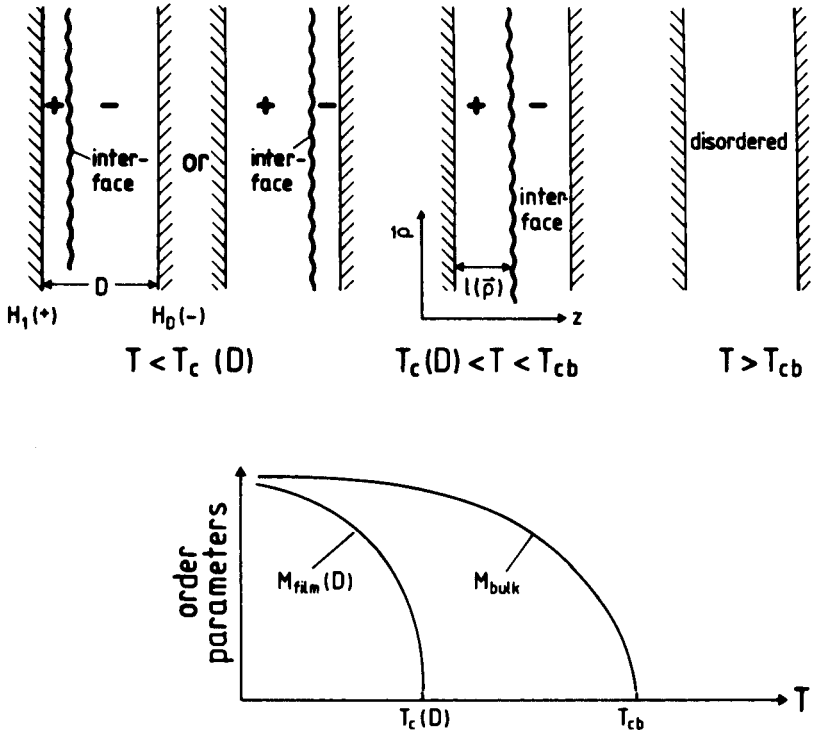

Fig. 6. Schematic description of the interface localization-delocalization transition of an Ising model confined between two walls a distance D apart, where a positive field H_1 acts at the left wall while a negative field H_D acts on the right wall. For $T < T_c(D)$ the interface is bound either to the left or the right wall, and the average magnetization $m_{\text{film}}(D)$ of the film is then non-zero. For $T_c(D) < T < T_{cb}$, however, the interface fluctuates (delocalized) in the center of the film, and thus $m_{\text{film}}(D) = 0$ even though there is still a non-zero bulk magnetization $\pm m_{\text{bulk}}$ in an infinite system as well as locally in the film away from the interface. For $T > T_{cb}$, however, the film is disordered (apart from the response to the surface fields near the walls). The description of the interface in terms of a coordinate $z = l(\vec{\rho})$, with $\vec{\rho}$ being the coordinates in the plane formed by the left wall, is also indicated. From Binder *et al.*[15]

single interface in equilibrium. Therefore this interface localization-delocalization phase transition is in a sense a finite size analog of the wetting transition, and for $D \to \infty$ the transition temperature $T_c(D)$ approaches the wetting transition temperature $T_w(H_1)$ rather than the bulk transition temperature T_{cb}.[16] This is also made plausible by a consideration of the effective interface potential $V_{\text{eff}}(l)$ for this case (cf. Fig. 7). Superimposing a potential of the type shown in Fig. 5 for the left wall at $z = 0$, and a mirror image of that potential for the right wall at $z = D$, one obtains potentials which are symmetric around $l = D/2$, as drawn in Fig. 7. Depending on the

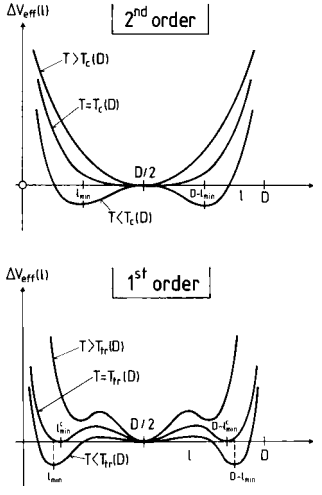

Fig. 7. Schematic variation of the effective interface potential difference $\Delta V_{\text{eff}}(l) = V_{\text{eff}}(l) - V_{\text{eff}}(D/2)$ for thin Ising films of thickness D, for the second-order (upper part) and first-order (lower part) interface localization-delocalization phase transitions.

character of the underlying wetting transition, one expects that either second-order or first-order interface localization-delocalization phase transitions occur: in the second-order case, the two positions of the minima (at $l = l_{\min}$ and at $l = D - l_{\min}$, respectively) merge smoothly at $l = D/2$ as $T \to T_c(D)$ from below. This is the case that was assumed in Fig. 6, a continuous vanishing of the order parameter at $T_c(D)$. However, a discontinuous first-order type behavior is also possible, and then the position of the minimum $l_{\min}$ increases only to $l^c_{\min}$ (or decreases only down to $D - l^c_{\min}$, respectively) at $T_{\text{trip}}(D)$ where the minimum at $D/2$ then takes over.

The discussion of interface localization-delocalization presented so far is restricted to the case $H = 0$, and indeed in the second-order case there is no transition for $H \neq 0$. However, this is not true in the first order case since remnants of the prewetting transition lines that existed for the semi-infinite case do still exist for the thin film, and in the space of variables (T, H) these (first-order) transitions merge at the point $H = 0, T = T_{\text{trip}}(D)$, thus producing a triple point. This case becomes of practical interest when we remember a further physical interpretation of the Ising model, namely as a model for a binary mixture (A, B) in which spin down may represent species A, and spin up species B. In fact, in a thin film of thickness D of a binary mixture on a substrate, it is quite common that a layered geometry of a phase-separated state is realized when the substrate energetically prefers one component, while the other surface (e.g., against air or vacuum)

favors the other component. The magnetic field H of the Ising model translates into the chemical potential difference $\Delta\mu$ between the species, and the magnetization m is related to the relative concentration $\phi = \phi_A$ of the mixture, $\phi = (1-m)/2$. In this case it is natural,[17,18] of course, to discuss how the properties of the film change with temperature keeping its concentration constant rather than $\Delta\mu$. This is illustrated in Fig. 8 for the case of a mixture that in the bulk is strictly symmetric, assuming strict antisymmetry of the surface forces (i.e., $H_1 = -H_D$) as well. Then, the concentration that corresponds to the triple point is $\phi_{\text{trip}} = 1/2$, but it is of interest to consider films that have different concentrations. Figure 8 indicates qualitatively that even above the bulk critical temperature we expect

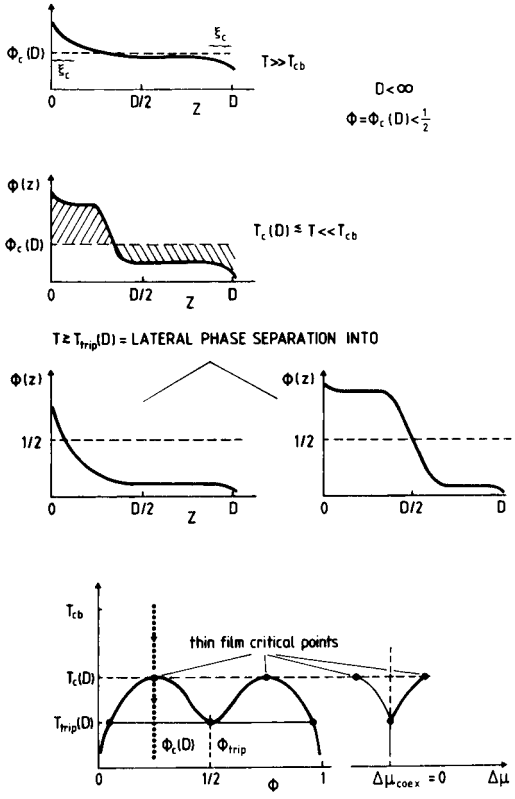

Fig. 8. Schematic concentration profiles $\phi(z)$ of a binary mixture across a thin film of thickness D, at the critical concentration of the thin film, $\phi = \phi_c(D) < 1/2$, at three different temperatures (upper part). The lower part shows the phase diagram of the thin film, in the canonical ensemble $\{(T, \phi)$ plane, left$\}$ and in the semi-grandcanonical ensemble $\{(T, \Delta\mu)$ plane, right$\}$. From Binder *et al.*[18]

some surface enrichment of the preferred species near the appropriate walls, but this surface enrichment is restricted to distances of the order of the bulk correlation length ξ_b, which for $T \gg T_{cb}$ is much less than D except for ultrathin films. But when T approaches T_{cb}, ξ_b grows and ultimately becomes comparable to D. This also means that the system forms an interface from the A-rich side of the film to the B-rich side which has a width of the same order as the film thickness. Below T_{cb}, ξ_b decreases again, and one can distinguish a layered structure with an A-rich domain and a B-rich domain, separated by an interface whose width is much smaller than D. The concentrations inside the domains resemble the values of the concentrations $\phi_{\text{coex}}^{(1)}$, $\phi_{\text{coex}}^{(2)}$ at the two branches of the coexistence curve in the bulk, and the thickness of the domains is given by the lever rule, in order to satisfy the overall concentration of the film that has been chosen. The condition, that the overall concentration is fixed, enforces a lateral phase separation, in the directions parallel to the wall two different phases must coexist. For the example shown, and temperatures $T_{\text{trip}}(D) < T < T_c(D)$, one phase is a state with an interface bound to the wall at $z = 0$, whereas the other phase is a state with a delocalized interface, almost in the middle of the film. When one crosses $T_{\text{trip}}(D)$, a second transition occurs, to another state of lateral phase separation. In the one phase the interface is bound to the left wall, and in the other phase the interface is bound to the right wall. While in the semi-grand canonical ensemble of the mixture (with $\Delta\mu = \text{const}$) only a single phase transition is always encountered when T is varied, we have here in general two successive transitions. Only when one chooses the concentration ϕ_{trip} of the triple point, will one go to the phase-separated state with interfaces bound to both walls in a single transition (Fig. 9). Thus, we emphasize that the consideration of different systems (Ising magnets vs. liquid-gas systems or binary mixtures) in thin film geometry is not just a trivial exercise but involves different physics.

The finding that the critical temperature $T_c(D)$ for antisymmetric boundary conditions is unrelated to T_{cb}, see Figs. 7–9, irrespective of the thickness D of the film as long as $D < \infty$, seems paradoxical at first sight. One must keep in mind, however, that near T_{cb} there is indeed a transition to a kind of "longitudinal phase separation": i.e., two domains of opposite sign of the order parameter form, separated by an interface running parallel to the walls, as sketched qualitatively in Fig. 6. This transition is gradual (Figs. 8 and 9) and not associated with any singularity in the thermodynamic potential, and, consequently, it does not show up in the phase diagram. Of course, the extent of this rounding gets the smaller the larger D becomes. Finite size scaling arguments, to be discussed later, yield the result that the temperature region ΔT over which the transition is smeared out scales as $\Delta T / T_{cb} \propto D^{-1/\nu}$, where ν is the critical exponent of the

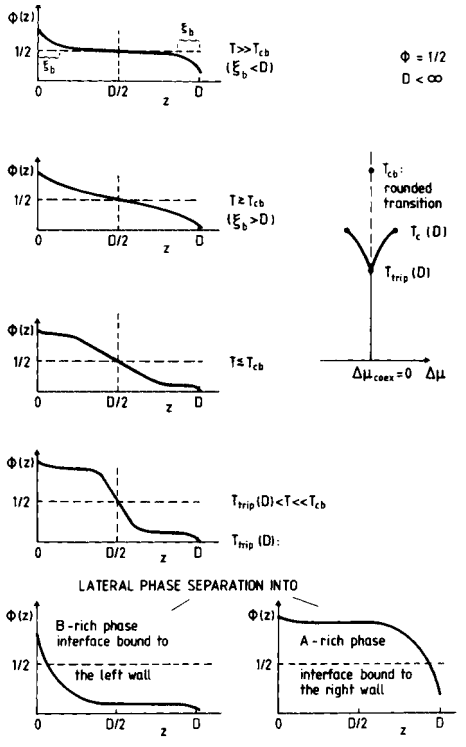

Fig. 9. Schematic concentration profiles $\phi(z)$ across a thin film of thickness D at the bulk critical concentration $\phi_{\text{crit}} = 1/2$, assuming that the left wall energetically prefers A and the right wall prefers B with the same strength, at several temperatures (left part). The right part shows the corresponding schematic phase diagram in the semi-grandcanonical ensemble. For further explanations see text. From Binder *et al.*[18]

correlation length in the bulk. Hence, for large D it hence may be difficult to distinguish experimentally this rounded transition from a true thermodynamic phase transition. It is also interesting to discuss the case of antisymmetric boundary conditions in an enlarged parameter space that includes a gradient ΔH in the field across the film.[19, 20] Then the critical temperature $T_c(D)$ discussed above becomes the end point of a critical line $T_c(D, \Delta H)$, and for sufficiently large ΔH the difference $T_{cb} - T_c(D, \Delta H)$ also becomes very small and is again proportional to $D^{-1/\nu}$. Since it is not straightforward to apply a variable ΔH in the laboratory, and—unfortunately—we are not aware of any simulations addressing this extended model, we shall not discuss it any further in this article.

Of course, the case of strictly antisymmetric surface fields ($H_1 = -H_D$) is a simplifying idealization, and one really needs to consider the case

which lacks any particular symmetry of the surface fields,[21] however we shall defer a discussion of this situation to Section 3.6. But there is another generic case, $H_1 = H_D$, i.e., confinement of the system by two walls of the same kind. In the context of liquid-gas transitions in confined geometry, this is known as "capillary condensation."[22–28] It was already discovered in the 19th century that in a capillary the condensation of a gas occurs at a lower pressure p than the coexistence pressure p_{coex} necessary to induce condensation in the bulk. Again, here we are not concerned with a description of this behavior in any chemically realistic atomistic detail but rather follow the pioneering studies of Fisher and Nakanishi[24, 25] once more and base our treatment on the thin film Ising Hamiltonian, Eq. (3). For simplicity, we now consider the case where the corresponding semi-infinite system has only a second-order wetting transition. This transition for finite film thickness is rounded off, and then the liquid-gas transition in the bulk of the thin film is the only transition that needs to be considered. The case where analogs of the prewetting transitions still exist for the film[29] will be considered in Section 3.5 (cf. Fig. 43). In the present case, the resulting phase diagram is shown in Fig. 10. While in the bulk lattice gas system ($D \to \infty$) the condensation from gas to liquid occurs along the line $H = 0$ that ends in the bulk critical point T_{cb}, in the thin film this transition line is now shifted to negative values of the field, which describes the effect mentioned above that condensation occurs at a lower pressure than in the bulk. Simple bond-counting arguments show that the transition line at $T = 0$ starts at $H = -2H_1/D$, but estimating the location $T_c(D)$, $H_c(D)$ of the critical point is a non-trivial matter (Section 3.5). Scaling arguments[24] that yield the D-dependence of the shift of T_c, $\Delta T_c = T_{cb} - T_c(D)$ and $\Delta H_c = H_c(D)$ (cf. Fig. 10) will be summarized in Section 2.3.

In the next sections, we shall enhance this qualitative phenomenological description with more detailed arguments, including the treatment by a Ginzburg–Landau-type mean field theory (Section 2.1.), and calculations

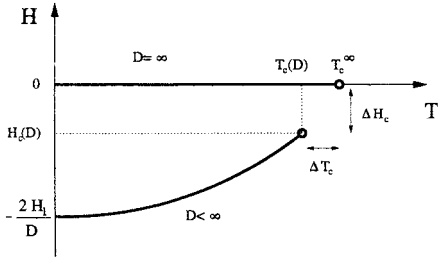

Fig. 10. Schematic phase boundary for an Ising film of thickness D with a field H_1 acting on both surfaces in the plane of temperature T and bulk field H.

based on the effective interface Hamiltonian (Section 2.2). Effects of thermal fluctuations will be addressed, introducing the concept of capillary waves (Section 2.2) and summarizing the main predictions resulting from scaling arguments and renormalization group treatments (Section 2.3). Monte Carlo results will then be reviewed in Section 3, first briefly describing the techniques of simulation (Section 3.1) and finite size scaling analysis (Section 3.2), and then presenting results for critical wetting (Section 3.3), interface localization-delocalization and capillary condensation in Ising models (Sections 3.4 and 3.5) and in polymer mixtures (Section 3.6). Finally, Section 4 summarizes our conclusions.

At this point, we have to mention that a variety of closely related topics will not be treated in this article: e.g., we shall not review computer simulations studying the shape of sessile droplets (Fig. 1, top), see, e.g., refs. 30–32, and corresponding results on the line tension,[33–37, 53] and the behavior of the interface near the three-phase contact line. For instance, it has been predicted[36, 38] that near first order wetting transitions the qualitative behavior differs from the sketch in Fig. 1, because the interfacial profile intersects the dashed asymptote which forms the contact angle Θ. To our knowledge, this feature has not yet been confirmed by simulations (the nanoscopic size of the simulated droplets[30–32] precludes even accurate estimates of Θ). Also, we will not consider wetting on cylinders[39–41] or in cylindrical tubes[42] or other non-planar geometries. As a final point of this disclaimer, we are also not concerned with wetting of a third phase at interfaces between coexisting phases, wetting near grain boundaries or defect planes, etc.[43, 44] as well as wetting near "triple junctions":[45] only wetting at walls (adsorbates in contact with substrates or so-called "spectator phases"[5, 45]) will be considered.

2. THEORY

2.1. Ginzburg–Landau Type Mean Field Theories

A well-known method to derive the Ginzburg–Landau-type mean field theory appropriate for the models defined by the Hamiltonians Eqs. (2) and (3) starts from a layer-wise molecular field approximation.[7, 8, 46–48] (Note that the result is much more general than this derivation.) Thus we consider a lattice model, assuming that the external wall is the plane $z = 0$ in our coordinate system, and denote the coordination number of lattice sites in planes parallel to this plane as $q_{||}$, while the coordination number in the positive z-direction perpendicular to these planes is $q_{\perp}$ (e.g., $q_{||} = 4$ and $q_{\perp} = 1$ for the simple cubic lattice). We label the plane directly adjacent to the external wall (i.e., the surface plane of our system) by an index

$n = 1$, and the planes are indexed consecutively, $n = 2, 3, \ldots$ as we move away from the wall. In the molecular field approximation, the average magnetization $m_n = \langle S_i \rangle$ of spins whose lattice site i is in the nth layer then is given by

$$m_n = \tanh[(H + q_{||} J m_n + q_\perp J m_{n-1} + q_\perp J m_{n+1})/k_B T], \qquad n \geqslant 2 \tag{4}$$

$$m_1 = \tanh[(H + H_1 + q_{||} J_s m_1 + q_\perp J m_2)/k_B T], \qquad n = 1 \tag{5}$$

Assuming that the temperatures of interest are close to T_{cb} and the fields H and H_1 are small enough such that $|m_n| \ll 1$ for all n, we can expand $\operatorname{artanh}(m_n) \approx m_n + m_n^3/3$ and also replace differences by differentials, denoting $m_n = m(z)$,

$$m_{n\pm1} = m(z) \pm a \frac{\partial m(z)}{\partial z} + \frac{a^2}{2} \frac{\partial^2 m(z)}{\partial z^2}, \tag{6}$$

a being the lattice spacing. As discussed in ref. 48, Eq. (6) is only accurate for large correlation length ξ_b, since it amounts to approximations equivalent to putting $\exp(a/\xi_b) \approx 1 + a/\xi_b$.

Accepting Eq. (6), we than replace Eqs. (4) and (5) by a second-order non-linear differential equation. Using henceforth $a = 1$ as our unit of length, we obtain

$$\left[1 - \frac{(q_{||} + 2q_\perp) J}{k_B T} \right] m(z) + \frac{1}{3} m^3(z) - \frac{q_\perp J}{k_B T} \frac{\partial^2 m(z)}{\partial z^2} = \frac{H}{k_B T}, \tag{7}$$

supplemented by a boundary condition at the surface, $z = 0$,

$$\left[1 - \frac{q_{||} J_s + q_\perp J}{k_B T} \right] m(0) + \frac{1}{3} m^3(0) - \frac{q_\perp J}{k_B T} \left. \frac{\partial m(z)}{\partial z} \right|_{z=0} = \frac{H + H_1}{k_B T}. \tag{8}$$

Due to the non-linear character of Eqs. (4) and (5), the results obtained from the discrete set of difference equations are not equivalent to the results following from the differential equation, Eqs. (7) and (8). For all temperatures $T < T_{cb}$ Eqs. (4) and (5) yield an infinite sequence of layering transitions,[14, 49] when $H \to 0$ while Eqs. (7) and (8) yield at most a single transition (prewetting) followed by complete wetting.[46, 47] But a treatment of the problem beyond mean field implies[14] that the infinite sequence of layering transitions in the Ising model can only occur for $T < T_R$, where T_R is the roughening transition temperature of an interface between coexisting bulk phases.[50, 51] For $T > T_R$, the interface is a smooth object, delocalized due to capillary wave excitations,[4–6, 8, 51–56] and under these circumstances

the description in terms of Eqs. (7) and (8) is more appropriate than by Eqs. (4) and (5). Being interested in the modelling of liquid-gas transitions and liquid-liquid unmixing, where interfaces always are smooth, we know that the localization of interfaces at lattice planes as it occurs in the Ising model for $T < T_R$ really must be considered as a lattice artefact. Thus, we shall only be concerned with temperatures sufficiently above T_R in this article, such that this problem will not play any role.

It is convenient to rescale Eqs. (7) and (8) in terms of the bulk magnetization m_b and the correlation length ξ_b, noting that in the molecular field approximation $k_B T_{cb} = (q_{||} + 2q_\perp)\, J$. Using the standard results[8]

$$m_b = \sqrt{3(1 - T/T_{cb})}\,, \qquad \xi_b = \sqrt{\frac{q_\perp}{2(q_{||} + 2q_\perp)}}\,(1 - T/T_{cb})^{-1/2}, \tag{9}$$

we define rescaled fields h, h_1 as follows

$$h = \frac{H}{\sqrt{3}\, k_B T_{cb}}\,(1 - T/T_{cb})^{-3/2}, \qquad h_1 = \frac{H_1}{\sqrt{3}\, k_B T_{cb}}\,(1 - T/T_{cb})^{-3/2}. \tag{10}$$

The boundary condition at the surface will then involve a parameter g,

$$g = 1 + 2\xi_b^2 \left[\frac{q_{||} J_s}{q_\perp J} - 1 - \frac{q_{||}}{q_\perp} \right]. \tag{11}$$

With the rescaled order parameter μ and the rescaled distance ζ from the surface defined as

$$\mu(\zeta) = m(z)/m_b, \qquad \zeta = z/(2\xi_b), \tag{12}$$

Eq. (7) turns into a rescaled equation for the bulk that no longer contains any parameter,

$$\frac{1}{2}\frac{\mathrm{d}^2\mu(\zeta)}{\mathrm{d}\zeta^2} + \mu(\zeta) - \mu^3(\zeta) + h = 0. \tag{13}$$

The only parameter appears in the boundary condition,

$$\gamma \left.\frac{\mathrm{d}\mu(\zeta)}{\mathrm{d}\zeta}\right|_{\zeta = 0} + g\mu(0) + h + h_1 = 0. \tag{14}$$

Here the third order term of Eq. (8) was already omitted, because it yields only unimportant corrections to the leading behavior. We have also allowed for a general coefficient γ (instead of ξ_b) for the first term of

Eq. (14). As is well known,[8] Eqs. (13) and (14) can also be thought of as the result of minimizing an effective free energy functional,

$$\frac{1}{2\xi_b A}\frac{\delta \Delta\mathscr{F}[\mu(\zeta)]/k_B T_{cb}}{\delta\mu(\zeta)} = 0, \tag{15}$$

where

$$\frac{\Delta\mathscr{F}}{k_B T_{cb}} = \int_0^\infty \mathrm{d}\zeta \left\{ \frac{1}{2}\left[\frac{\mathrm{d}\mu(\zeta)}{\mathrm{d}\zeta}\right]^2 - \mu^2(\zeta) + \frac{1}{2}\mu^4(\zeta) - h\mu(\zeta) - \frac{1}{\gamma}\left[h_1\mu(\zeta) + \frac{1}{2}g\mu^2(\zeta)\right]\delta(\zeta)\right\}. \tag{16}$$

Near T_{cb} the correlation length $\xi_b \gg 1$, and therefore $|g| \gg 1$, Eq. (11), if we are not very close to the surface-bulk multicritical point,[7, 8, 57] which in the molecular field approximation occurs for (ref. 7)

$$J_{SC}/J = 1 + q_\perp/q_{||}. \tag{17}$$

Since the approximations made in Eqs. (6)–(8) require that the limit $\xi_b \to \infty$ is taken first, the 1 on the rhs of Eq. (11) is actually negligible against the other term, and, hence, the multicritical value of g is $g = 0$. The sign of g is controlled by the sign of $J_s - J_{sc}$.

In the absence of fields h, h_1, we note that $g > 0$ for $J_S > J_{SC}$; then, Eqs. (13) and (14) show that the surface layer is ordered—the surface orders before the bulk.[7, 8, 35] Conversely, g is negative for $J_S < J_{SC}$, which is the situation considered in the following. At this point we emphasize, however, that Eqs. (13)–(16) can be justified on much more general grounds than by the present derivation based on Eqs. (4) and (5), if we do not insist on the particular relations Eqs. (9), (11), and (17), and allow h_1/γ, g/γ in Eq. (16) to be phenomenological parameters. Before we show how Eqs. (13)–(16) are used to describe wetting phenomena, we recall how Eq. (13) is solved to describe the profile of an interface between two bulk phases, of opposite sign of the order parameter, that coexist for $h = 0$. I.e., the equation

$$\frac{1}{2}\frac{\mathrm{d}^2\mu(\zeta)}{\mathrm{d}\zeta^2} + \mu(\zeta) - \mu^3(\zeta) = 0 \tag{18}$$

must be solved with the boundary conditions

$$\mu(\zeta \to \pm\infty) \to \pm 1, \qquad \lim_{\zeta \to \pm\infty}\frac{\mathrm{d}\mu}{\mathrm{d}\zeta} = 0. \tag{19}$$

This problem is formally analogous to a problem in classical mechanics, namely the motion of a point particle of unit mass in a potential $U(x) = x^2 - x^4/2$, $\ddot{x} = -dU/dx$, if we identify position x with μ and time t with ζ. The energy of this problem is then chosen to be $E = 1/2$, so the particle starts at $t = -\infty$ at the left potential well with zero velocity, and comes to rest again for $t \to \infty$ at the right potential well. The velocity $\dot{x}$ (corresponding to the slope $d\mu/d\zeta$ of the interface profile) is maximal for $x = 0$ ($\mu = 0$, respectively). Since conservation of energy implies $E = U + \dot{x}^2/2 = \text{const}$, multiplication of Newton's law by $\dot{x}$ and integration over time from $t = -\infty$ to t yields $\dot{x}^2/2 = -(x^2-1) + (x^4-1)/2 = (1-x^2)^2/2$. Analogously, we find the scaled order parameter profile is given by

$$[1 - \mu^2(\zeta)]^2 = (\mathrm{d}\mu/\mathrm{d}\zeta)^2, \qquad \mu(\zeta) = \tanh(\zeta), \tag{20}$$

or transforming back to the original coordinates

$$m(z) = m_b \tanh(z/2\xi_b). \tag{21}$$

This shows that in mean field theory the intrinsic width of the interface is $w_0 = 2\xi_b$.

The interface free energy, defined as the excess contribution of a system containing one interface relative to that of a homogeneous system where $m(z) = m_b$ everywhere, can be shown to be (normalized per unit area of the interface area A)

$$\sigma = \frac{\Delta F_{\text{int}}}{k_B T A} = \frac{1}{3} m_b^4 \xi_b \int_{-\infty}^{+\infty} d\zeta \left(\frac{\mathrm{d}\mu}{\mathrm{d}\zeta}\right)^2 = \frac{2}{9} m_b^4 \xi_b. \tag{22}$$

If we define a critical exponent λ and amplitude $\hat{\sigma}$ of this interface tension via $\sigma = \hat{\sigma}(1 - T/T_{cb})^{\lambda}$, this mean field theory yields $\lambda = 3/2$.

Now for a problem of a free surface of a semi-infinite system which is at phase coexistence ($h = 0$) in the bulk, the problem is still described by the first equation of Eq. (20), since Eqs. (13) and (18) are identical. The order parameter profile of the free surface problem is still of the form $\mu(\zeta) = \pm\tanh(\zeta + \zeta_0)$, for a state in the regime where the wall is incompletely wet. Then ζ_0 (and the sign of the above solution) have to be chosen such that the boundary conditions at $\zeta = 0$ and $\zeta \to \infty$ are fulfilled. For the wet case the profile has the form $\mu(\zeta) = \pm\coth(\zeta + \zeta_0)$ instead, cf. Fig. 11. Note that the spin up—spin down symmetry of the bulk part of our Ising model (cf. Eq. (3)) implies that both "wetting" and the opposite phenomenon, "drying," can occur. By "wetting" we denote here a macroscopically thick film of up-spins, fluid atoms, for the lattice gas; B-atoms, for the

A-rich *AB*-mixture, etc. intruding at the wall. "Drying" means a film of down-spins (gas layer at the surface of the "lattice fluid"; *A*-atoms, for the *B*-rich *AB*-mixture, etc.). The constants ζ_0, ζ_0' are then found from requiring that $\partial\mu(\zeta)/\partial\zeta = \pm|\mu^2(\zeta)-1|$ must also satisfy the boundary condition, Eq. (14). In the wet (or dry) case, the boundary condition at $\zeta \to \infty$, $\mu(\zeta) = -1$ (or $\mu(\zeta) = +1$), is satisfied by adding to the solution $\mu(\zeta) = \pm\coth(\zeta+\zeta_0)$ the solution $\mu(\zeta) = \mp\tanh(\zeta-\zeta_i)$ with $\zeta_i \to \infty$ as well. From a graphical analysis of these equations, the so-called "Cahn construction"[2] (Fig. 12) one derives the wetting phase diagram (see Fig. 13) which displays both second-order and first-order wetting transitions, separated by a wetting tricritical point.[47] We here only focus on the second-order wetting transition, noting that then Eqs. (14) and (20) yield

$$\mu^2(0)-1 = [h_1 + g\mu(0)]/\gamma. \tag{23}$$

Since $\mu^2(0) = 1$ at critical wetting (Fig. 12), we conclude that $h_{1c} = -g$ (Fig. 13), and the constant ζ_0 becomes

$$\zeta_0 = -\text{arctanh}(\mu(0)) = -\text{arctanh}\left[\frac{h_{1c}}{2\gamma} + \sqrt{\frac{h_{1c}^2}{4\gamma^2}+1-\frac{h_1}{\gamma}}\ \right], \tag{24}$$

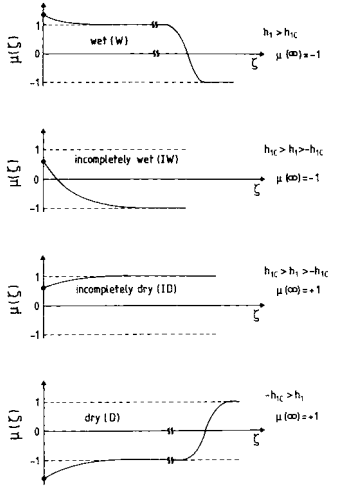

Fig. 11. Profiles of the normalized order parameter $\mu(\zeta)$ as a function of the rescaled distance ζ from the wall for different states of the surface and/or the bulk: wet (W), incompletely wet (IW), incompletely dry (ID) and dry (D). From Puri and Binder.[47]

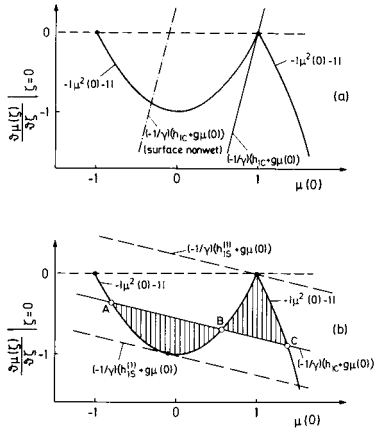

Fig. 12. Plot of $\partial\mu(\zeta)/\partial\zeta|_{\zeta=0}$ versus $\mu(0)$ for: (a) second-order wetting; (b) and a first-order wetting. The solution consistent with the boundary condition is the intersection of the curve $|\mu_c^2(0)-1|$ with the straight line $[h_1+g\mu(0)]/\gamma$: In case (a) this solution is unique for all choices of h_1/γ (for g/γ fixed). Critical wetting occurs where the solution is at $\mu(0)=+1$; then $\partial\mu(\zeta)/\partial\zeta|_{\zeta=0}=0$, and the interface is an infinite distance away from the surface. For $h_1>h_{1c}$ the surface is non-wet while for $h_1\geqslant h_{1c}$ the surface is wet. In case (b) the solution is unique for $h_1<h_{1s}^{(1)}$ (only a non-wet state occurs) and for $h>h_{1s}^{(2)}$ (only a wet state occurs). For $h_{1s}^{(2)}>h_1>h_{1s}^{(1)}$ there are three intersections, denoted by A, B, C. B is always unstable, while A is stable and C metastable for $h_{1c}>h>h_{1s}^{(1)}$; and A is metastable and C is stable for $h_{1s}^{(2)}>h>h_{1c}$. At h_{1c}, where the exchange of stability between A and C occurs (i.e., the first-order wetting) the shaded areas are equal. This construction is the surface counterpart of the well-known Maxwell construction for the first-order liquid-gas transition in the bulk. Note that for $\mu(0)<-1$ the parabola continues to positive values, but this part is not shown here. It would be needed to describe profiles that approach the gas density (corresponding to $\mu(0)=-1$) from below. From Schmidt and Binder.[46]

which for h_1 near h_{1c} reduces to

$$\zeta_0 \approx -\operatorname{arctanh}\left[1-\frac{h_1-h_{1c}}{2\gamma(1-h_1/2\gamma)}\right] \approx \frac{1}{2}\ln\frac{h_1-h_{1c}}{(2\gamma-h_1)}+\text{const} \tag{25}$$

This relation shows that the thickness of the wetting film diverges logarithmically when one approaches the second-order wetting transition from the non-wet side.

At this point we briefly discuss the argument of Cahn[2] that wetting should always occur near a critical point: Since the Young equation (Eq. (1)) implies that at the wetting transition $\sigma_{lg}=\sigma_{wg}-\sigma_{wl}$, and while one expects that σ_{lg} exceeds $\Delta\sigma=\sigma_{wg}-\sigma_{wl}$ at low temperatures, σ_{lg} vanishes at T_{cb} with a larger exponent than $\Delta\sigma$. Hence the curves σ_{lg} and $\Delta\sigma$ must cross each

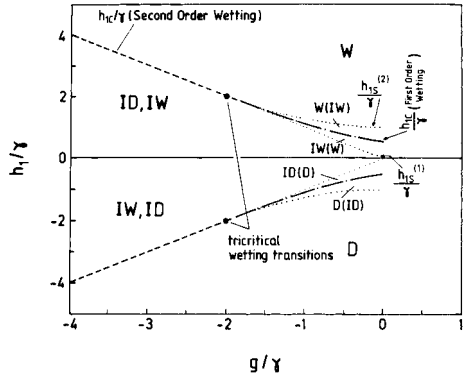

Fig. 13. Phase diagram of the Ginzburg–Landau model for wetting and drying in the space of variables g/γ and h_1/γ. Regions are labeled according to the stable static solution for those parameters (metastable states, if any, are listed in brackets): wet (W), dry (D), incompletely wet (IW) and incompletely dry (ID). Note that the phase diagram is symmetric around the abscissa if the meaning of W and D is interchanged. Second-order phase boundaries are shown as dashed lines and given by $h_{1c} = \pm g($ for $g/\gamma < -2)$. First-order phase boundaries are shown as dash-dotted curves; surface spinodals are shown as dotted curves, $h_{1s}^{(1)} = -g$ and $h_{1s}^{(2)}/\gamma = 1 + (g/2\gamma)^2$, $g > -2\gamma$ (upper half plane). Of course, the first order wetting transition as well as the surface spinodals continue smoothly to the region $g > 0$, see, e.g., ref. 44, but are not shown here in order not to complicate the labeling of the diagram. From Puri and Binder.[47]

other in the critical region. In fact, Cahn[2] originally assumed that $\Delta\sigma$ behaves like the order parameter $\Delta\sigma \propto m_b$ in the bulk, but one uses rather the surface order parameter: $\Delta\sigma \propto m_1 \propto (1 - T/T_{cb})^{\beta_1}$ with $\beta_1 = 1$, and using (see Eq. (22)) $\sigma_{lg} \propto (1 - T/T_{cb})^{(d_u - 1)\nu}$ (where, within mean field approximation, $d_u = 4$ is the upper critical dimension and $(d_u - 1)\nu = 3/2$) one would obtain $(1 - T_w/T_{cb})^{1/2} \propto$ const from $\sigma_{lg}/\Delta\sigma = 1$. However, as discussed in detail by Iglói and Indekeu,[44] this relation for T_w is not always supported by an explicit calculation within Landau theory.

In fact, Cahn[2] did not discuss at all the possibility of critical wetting, he discussed first order wetting only. For this case Iglói and Indekeu[44] obtained that $\Delta\sigma$ for $T - T_{cb}^-$ becomes a non-zero constant, which implies that the distance of T_w from T_{cb} scales as $H_1 \propto (J_S - J_{SC})(1 - T_w/T_{cb})^{3/2}$, while the original Cahn result (with bulk exponent $\beta = 1/2$) accidentally holds for tricritical wetting: $H_1 \propto (1 - T_w/T_{cb})^1$ and $J_S = J_{SC}$.

Thus, although, the argument of Cahn[2] was wrong, his conclusion that near a critical point wetting should always occur is supported by Landau theory.[44] As discussed by Iglói and Indekeu,[44] critical point wetting is connected with the presence of a non-zero surface order

parameter at T_c. This order can be imposed by a surface field ("normal transition," see Section 1) or occurs spontaneously ("extraordinary transition," see Fig. 3). In contrast, whenever the surface at T_{cb} undergoes an "ordinary transition" (which happens in the present model for $J_S < J_{SC}$ and $H_1 = 0$ only), no wetting transition can occur. This relation between the existence of surface order at T_{cb} and occurrence of wetting transitions is useful to understand the relations between wetting at grain boundaries and at walls.[44]

In this context, we mention that approaching a wetting transition at phase coexistence (i.e., for $H = 0$ in the present model) from the non-wet side, the contact angle Θ vanishes continously for both first order and second order wetting transitions. Noting that $\Delta\sigma$ and σ_{lg} meet under a finite angle in Fig. 1 (lower part), which describes a first order wetting transition, the relations $\cos\theta \approx 1 - \Theta^2/2$ and $\sigma_{lg} - \Delta\sigma \propto 1 - T/T_w$ yield $\Theta \propto (1 - T/T_w)^{1/2}$. In contrast, for critical wetting. $\Delta\sigma$ and σ_{lg} meet tangentially at T_w, i.e., $\sigma_{lg} - \Delta\sigma \propto (1 - T/T_w)^2$ and, hence, $\Theta \propto (1 - T/T_w)$. Of course, these relations are born out explicitly by the present Landau theory.

Before we discuss the singular behavior of other quantities at the wetting transition, we recall some further relations from general surface thermodynamics. We note that the surface excess order parameter m_s, which can be defined in terms of the layer order parameters m_n as (ref. 8)

$$m_s = \sum_{n=1}^{\infty} (m_n - m_b), \tag{26}$$

can also be found as the derivative of the surface excess free energy with respect to the bulk field, analogously to the order parameter m_b in the bulk,

$$m_s = -\frac{\partial \mathscr{F}_s(T, H, H_1)}{\partial H}\bigg|_{T, H_1} \qquad m_b = -\frac{\partial \mathscr{F}_b(T, H)}{\partial H}\bigg|_{T}. \tag{27}$$

Here both the surface free energy density $\mathscr{F}_s$ and bulk free energy density $\mathscr{F}_b$ are normalized per lattice site of the basic semi-infinite Ising lattice model, Eq. (2). The relation between Eqs. (26) and (27) is readily understood by considering a thin film of thickness D in the limit $D \to \infty$: then the total free energy of the film can be split in bulk and surface terms, A being the area of a free surface of the film,[8, 57]

$$\frac{F_{\text{film}}(T, H, H_1, D)}{AD} = \mathscr{F}_b(T, H) + \frac{2}{D}\mathscr{F}_s(T, H, H_1), \quad D \to \infty, \tag{28}$$

$$m_{\text{film}} = \sum_{n=1}^{\infty} m_n = -\frac{1}{AD}\frac{\partial F_{\text{film}}(T, H, H_1, D)}{\partial H}\bigg|_{T, H_1, D}. \tag{29}$$

The factor 2 in Eq. (28) appears simply because there are two equivalent free surfaces in this geometry. From Eqs. (27)–(29) we recognize that $m_{\text{film}} = m_b + \frac{2}{D} m_s$ with $m_s = \lim_{D\to\infty} \sum_{n=1}^{D/2} (m_n - m_b)$, i.e., Eq. (26). The local order parameter at the surface then results as a derivative of $\mathscr{F}_s$ with respect to the local field H_1 conjugate to it,

$$m_1 = -\left.\frac{\partial \mathscr{F}_s(T, H, H_1)}{\partial H_1}\right|_{T,H}. \tag{30}$$

It also is of interest to consider "susceptibilities," defined in analogy with the bulk response function

$$\chi_b = \left.\frac{\partial m_b}{\partial H}\right|_T = -\left.\frac{\partial^2 \mathscr{F}_b(T, H)}{\partial H^2}\right|_T; \tag{31}$$

but since there are two fields, three susceptibilities result:

$$\chi_s = \left.\frac{\partial m_s}{\partial H}\right|_{T,H_1} = -\left.\frac{\partial^2 \mathscr{F}_s}{\partial H^2}\right|_{T,H_1}, \tag{32}$$

$$\chi_1 = \left.\frac{\partial m_1}{\partial H}\right|_{T,H_1} = \left.\frac{\partial m_s}{\partial H_1}\right|_{T,H} = -\left.\frac{\partial^2 \mathscr{F}_s}{\partial H \partial H_1}\right|_T, \tag{33}$$

and

$$\chi_{11} = \left.\frac{\partial m_1}{\partial H_1}\right|_{T,H} = -\left.\frac{\partial^2 \mathscr{F}_s}{\partial H_1^2}\right|_{T,H}. \tag{34}$$

Of course, the surface excess susceptibility can also be written analogously to Eq. (26), in terms of susceptibility χ_n defined as response functions to fields H_n acting solely in the nth layer, $\chi_n \equiv (\partial m_s/\partial H_n)_{T,H} = (\partial m_n/\partial H)_{T,H_n}$

$$\chi_s = \sum_{n=1}^{\infty} (\chi_n - \chi_b) \tag{35}$$

At a second-order phase transition in the bulk, quantities like m_b and χ_b exhibit singularities described by power laws involving the well-know critical exponents[58] β_b, γ_b and amplitudes $\hat{B}$, $\hat{\Gamma}_\pm$

$$m_b = \hat{B}(1 - T/T_{cb})^{\beta_b}, \qquad \chi_b|_{H=0} = \hat{\Gamma}_\pm\, |1 - T/T_{cb}|^{-\gamma_b}. \tag{36}$$

In Eq. (36), the $\pm$ signs refer to above (+) and below (−) T_{cb} respectively. In analogy with Eq. (36) one now may define critical exponents associated

with the singularities of the various surface quantities at a critical wetting transition temperature $T_w(H_1)$, namely[4–6]

$$m_s \propto (1-T/T_w)^{-\beta_s}, \qquad m_1 - m_1(T_w) \propto (1-T/T_w)^{\beta_1} \tag{37}$$

$$\chi_s \propto |1-T/T_w|^{-\gamma_s}, \qquad \chi_1 \propto |1-T/T_w|^{-\gamma_1}, \qquad \chi_{11} \propto |1-T/T_w|^{-\gamma_{11}} \tag{38}$$

Since the wetting transition temperature $T_w = T_w(H_1)$ depends on the surface field H_1, we can approach the wetting transition alternatively by varying T at fixed H_1 (as was implicitly assumed in Eqs. (37) and (38)), or by varying the surface field H_1 at fixed T. In the latter case the critical field $H_{1c}(T)$ simply is the inverse function of $T_w(H_1)$, and the argument $T_w - T$ in Eqs. (37) and (38) can then simply be replaced by $H_{1c} - H_1$. Since the surface excess magnetization m_s is simply related to the rescaled interface distance ζ_0 from the wall as $m_s \propto \xi_b m_b \zeta_0$, we conclude from Eqs. (25) and (37) that $\beta_s = 0$ (logarithmic divergence) in mean field theory. With some algebra one can also derive[46]

$$\tilde{\chi}_1 = \left.\frac{\partial \mu_s}{\partial h_1}\right|_T = [g - 2\gamma \tanh(-\zeta_0)]^{-1} [1 + \tanh(-\zeta_0)]^{-1} \propto (h_{1c} - h_1)^{-1}, h_1 \to h_{1c}. \tag{39}$$

and one can also show that $\gamma_s = 1$, $\gamma_{11} = 0$ (jump singularity) and $\beta_1 = 1$. Of course, Landau theory in the bulk (predicting $\beta_b = 1/2$ and $\gamma_b = 1$) is known to be, in general, rather unreliable due to the neglect of thermal fluctuations. The actual critical exponents of systems with short range forces differ from the predictions of Landau theory for system dimensionalities $d < d^* = 4$. Similarly, we expect that fluctuation effects on critical wetting also may alter the critical behavior substantially, as will be discussed in Section 2.3.

Of course, the Landau treatment can be extended from the semi-infinite case[7, 8] discussed so far to the case of thin films with symmetric[24, 25] and antisymmetric[16, 59–61] boundary fields.

For simplicity, we first briefly describe the antisymmetric case at zero bulk field $H = 0$. Instead of Eq. (16) the (rescaled) free energy functional becomes

$$\begin{aligned} \frac{1}{2\xi_b A}\frac{\Delta \mathscr{F}(D)}{k_B T} = & \int_{-D/(4\xi_b)}^{+D/(4\xi_b)} \mathrm{d}\zeta \left\{ \frac{1}{2}\left[\frac{\mathrm{d}\mu(\zeta)}{\mathrm{d}\zeta}\right]^2 - \mu^2(\zeta) + \frac{1}{2}\mu^4(\zeta) \right\} \\ & - \frac{1}{\gamma}\left[h_1 \mu(-D/(4\xi_b)) + \frac{1}{2} g \mu^2(-D/(4\xi_b)) \right] \\ & - \frac{1}{\gamma}\left[h_D \mu(D/(4\xi_b)) + \frac{1}{2} g \mu^2(D/(4\xi_b)) \right] \end{aligned} \tag{40}$$

Here the origin $\zeta = 0$ was chosen in the center of the thin film, so the two surfaces occur at $z = \pm D/2$ or $\zeta = \pm D/(4\xi_b)$, respectively. The corresponding Euler–Lagrange equation still is given by Eq. (13), with $h = 0$ in the present case, but instead of Eq. (14) (and the boundary condition $\mu(\zeta \to \infty) \to \pm 1$) we now have

$$\gamma \left. \frac{\mathrm{d}\mu(\zeta)}{\mathrm{d}\zeta} \right|_{\zeta = -D/(4\xi_b)} + g\mu(-D/(4\xi_b)) + h_1 = 0, \tag{41}$$

$$-\gamma \left. \frac{\mathrm{d}\mu(\zeta)}{\mathrm{d}\zeta} \right|_{\zeta = D/(4\xi_b)} + g\mu(D/(4\xi_b)) - h_D = 0. \tag{42}$$

After multiplication of the Euler–Lagrange equation with $\mu' \equiv d\mu/d\zeta$ one can integrate Eq. (13) once to find

$$\left(\frac{\mathrm{d}\mu}{\mathrm{d}\zeta}\right)^2 = (\mu^2(\zeta) - 1)^2 - 4\,\Delta p(D) \tag{43}$$

where the integration constant was denoted as $1 - 4\,\Delta p(D)$, for the sake of consistency with the notation of Parry and Evans.[59] For $D \to \infty$, when we stay in the phase where the interface between the regions of positive and negative order parameter is in the center of the thin film (cf. Fig. 6), we expect that $(d\mu/d\zeta)^2 \to 0$ for $\mu(\zeta) = \pm 1$ (corresponding to the flat regions around $\pm m_b$ in Fig. 14), and thus the constant $\Delta p(D \to \infty) \to 0$. With some algebra one can show that for $D \to \infty$

$$\Delta p \approx 2C(1 - \tilde{\mu}_\infty) \exp(-D/2\xi_b), \tag{44}$$

where the constant C has a numerical value close to 4, and the quantity $\tilde{\mu}_\infty$ is an abbreviation for the local order parameter on the right surface $\mu(\zeta = D/4\xi_b)$ in the limit $D \to \infty$, as long as $\tilde{\mu}_\infty > 1$. Note that in the semi-infinite system, the transition from the wet state to the non-wet state occurs when $\tilde{\mu}_\infty = 1$, while in a thin film we reach a phase transition (where the antisymmetric profile of $m(z)$ shown in Fig. 14 becomes unstable[59]) for a value of $\tilde{\mu}_\infty$ slightly larger than $\tilde{\mu}_\infty = 1$, namely, at a value of the field $|h_1|$ slightly larger than $|h_{1c}|$. This field can be identified[59] from the maximum $\Delta p(D)$ as functions of D. With some algebra one finds that there is a shift of this transition point relative to the wetting transition given by[59]

$$|h_{1c}(D) - h_{1c}(\infty)| \propto \exp(-D/2\xi_b) \qquad \text{for} \quad D \to \infty. \tag{45}$$

Another interesting consequence that can be derived from Eqs. (40)–(43) is the fact that in this confined situation of Fig. 14 the interfacial width $w_0(D)$ is reduced in comparison with that for a free interface

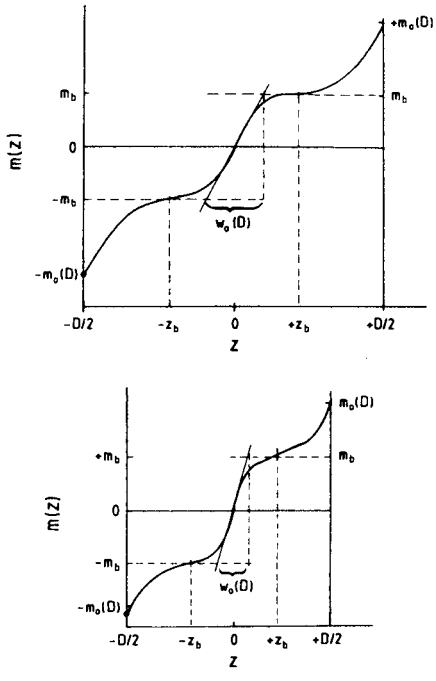

Fig. 14. Schematic order parameter profiles $m(z)$ versus z, for a thin Ising film of thickness D confined between walls at $z=-D/2$ and $z=+D/2$. A negative surface field H_1 acts on the left wall and a positive surface field $H_D=-H_1$ acts on the right wall. The field $|H_1|$ is large enough that the local magnetization $m_0(D)$ at the wall exceeds the bulk magnetization m_b, and an interface (of width $w_0(D)$) forms in the center of the film. If D gets small (lower part), a flat part in the profile near $\pm m_b$ does no longer occur, and then the width $w_0(D)$ becomes substantially reduced in comparison to its asymptotic value $w_0(D\to\infty)=2\xi_b$. From Binder *et al.*[61]

between bulk phases in a macroscopically thick film.[61] This "squeezing" of a confined interface can be approximately described as[61]

$$\frac{w_0(D)}{w_0(\infty)}\approx\sqrt{1+16\frac{h_1-h_{1c}}{\gamma}\frac{\exp(-D/2\xi_b)}{1+h_{1c}/(2\gamma)}}\ . \tag{46}$$

However, as we shall discuss below, it becomes difficult to identify an "intrinsic" profile and an "intrinsic" width w_0 of an interface when one goes beyond mean field theory and allows for capillary-wave type fluctuations of the local position of the interface center in directions parallel to the interface itself.

When we now include the term $-h\mu(\zeta)$ involving the bulk field in Eq. (40), and consider the case of symmetric wall fields $h_1=h_D$, we recover

the Landau theory of capillary condensation as treated by Nakanishi and Fisher.[25] In the general case, this problem can only be solved numerically.[25] The problem is analytically soluble only for the case of very weak wall fields $h_1 \to 0$, as far as the shift of the critical point relative to the bulk is concerned (cf. Fig. 10). One finds[25]

$$T_c(D) - T_{cb} \propto -D^{-2}, \qquad H_c(D) \propto -H_1 D^{-2} \tag{47}$$

and the magnetization at the midpoint of the profile (i.e., at $\zeta = 0$) is related to the magnetization at the surface $\mu_1 = \mu(\zeta = \pm D/4\xi_b)$ by[25]

$$\mu_{\text{mid}} \equiv \mu(\zeta = 0) = -\left(\frac{32}{9\pi} - 1\right)\mu_1. \tag{48}$$

2.2. The Effective Interface Hamiltonian; Capillary Waves

The mean field theory, described in the previous subsection, is suitable for a description of phase transitions in the bulk as well as surface and interface behavior within a common framework. Being interested in interface unbinding transitions such as wetting phenomena in semi-infinite geometry or interface localization-delocalization in films with competing walls, we note that the temperatures of interest typically are not close to T_{cb}, however. Then the length scales of interest, such as the mean distance of an interface from the wall to which it is bound, and the correlation length $\xi_{\|}$ of fluctuations of its local distance (Fig. 15) are much larger than

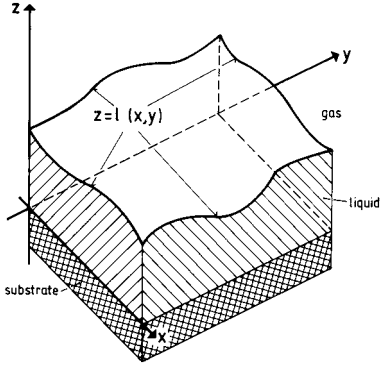

Fig. 15. Coarse-grained description of a liquid-gas interface, where the "intrinsic" profile and local structure of the interface are disregarded, and the interface is treated as an "elastic membrane" at position $z = l(x, y)$. This approximation is also called the "sharp kink" approximation for the interface profile.

the correlation length ξ_b of order parameter fluctuations in the bulk (or the "intrinsic width" $w_0 = 2\xi_b$ according to mean field theory, as argued above). Under such conditions, it is tempting to disregard variations of the order parameter in the bulk, away from the interface, altogether, and focus on the local position $l(x, y)$ of the interface as the single degree of freedom (Fig. 15). In other words, one attempts to provide a description of the liquid-gas interface in terms of the capillary wave Hamiltonian ($\vec{\rho} = (x, y)$)[4–6, 52–56, 59, 62]

$$\mathcal{H}_{\text{eff}}(\{l\}) = \int d\vec{\rho} \left[\frac{\sigma}{2} (\nabla l)^2 + V_{\text{eff}}\{l(\vec{\rho})\} \right] \tag{49}$$

where σ is just the liquid-gas interface tension σ_{lg}. Here σ is treated as a given input-parameter to the theory but, in principle, it has to be calculated from a more microscopic theory (e.g., Landau theory, Eq. (22)). Actually the Hamiltonian describes the excess free energy of the system associated with a fluctuating interface at positions $\{l(\vec{\rho})\}$ relative to a perfectly flat interface at distance $l \to \infty$ (which has the free energy cost $\sigma \int d\vec{\rho} = \sigma A$, A being the area of a flat interface). It also assumes that there are no overhangs of the interface, so $l(\vec{\rho})$ is a single-valued function, and that the interface is almost flat, i.e., $(\nabla l)^2$ is very small everywhere ($\int d\vec{\rho}[1 + (\nabla l)^2/2]$ simply represents the actual area of the distorted interface in Fig. 15).

The term $V_{\text{eff}}(l)$ describes the interaction of the interface in Fig. 15 with the substrate surface. Assuming short range forces between the substrate atoms and the atoms of the fluid that forms the liquid film on the substrate, one writes[59]

$$V_{\text{eff}}(l) = -\delta\varepsilon a_0 e^{-\kappa l} + b e^{-2\kappa l} - hl, \qquad \delta\varepsilon = (T_w - T)/T_w \tag{50}$$

for the case of the system that undergoes a second-order wetting transition at $\delta\varepsilon = 0$ in Eq. (50). According to the mean field theory of the previous subsection, the decay length κ^{-1} of the effective interface potential should simply be the correlation length. h is a (rescaled) bulk field which in the present subsection we normalize as $h \equiv 2m_b H$, while a_0, b are phenomenological positive constants. In fact, the form of this potential (cf. Eq. (50)) can be justified from the more detailed mean field theory of the previous section[63, 64] and we can relate the constants a_0, b as well as the location of the wetting transition temperature T_w to the parameters in the Hamiltonian (H_1, J_s, J, cf. Eq. (2)). Qualitatively, the shape of $V_{\text{eff}}(l)$ has already been sketched in the upper part of Fig. 5.

If we disregard the fluctuations of the local interface position at this point of the treatment, we can find the equilibrium position of the interface by minimizing $V_{\text{eff}}(l)$ with respect to l,

$$\frac{\mathrm{d}V_{\text{eff}}(l)}{\mathrm{d}l} = 0 \Rightarrow\ h = 2\kappa b \exp(-2\kappa l) - \delta\varepsilon\, \kappa a_0 \exp(-\kappa l) \tag{51}$$

For $h = 0$ and $\delta\varepsilon > 0$, i.e., $T < T_w$, on the non-wet side of the transition, we again find the well-known logarithmic divergence of the thickness of the wetting layer,

$$l = -\frac{1}{\kappa} \ln(a_0\, \delta\varepsilon / 2b) \tag{52}$$

consistent with our previous calculation (cf. Eq. (25)). For $\delta\varepsilon < 0$ and $h = 0$ the minimum occurs for $l \to \infty$, i.e., an unbound interface. However, it then is of interest to consider the question how l diverges when $h \to 0$ ("complete wetting").[4–6] Again one finds a logarithmic divergence,

$$l \approx -\frac{1}{\kappa} \ln(h / [-\delta\varepsilon\, \kappa a_0]). \tag{53}$$

Of course, in this framework it is also easy to describe a first-order wetting transition rather than critical wetting. This occurs when the constant b in Eq. (50) is negative rather than positive, and then one needs a higher order term ($c \exp(-3\kappa l)$ with $c > 0$) to obtain a finite solution for l in the non-wet case. Indeed, the effective interface potential (with positive constants a_0, b, c)

$$V_{\text{eff}}(l) = -\delta\varepsilon a_0 e^{-\kappa l} - b e^{-2\kappa l} + c e^{-3\kappa l} - hl \tag{54}$$

for $h = 0$ displays indeed the behavior sketched qualitatively in the lower part of Fig. 5. The temperature corresponding to $\delta\varepsilon = 0$ now is not the wetting transition temperature, however, but rather the "spinodal" of the wet phase, since one finds that the first-order wetting transition occurs for

$$\delta\varepsilon_{\text{tr}} = -\frac{b^2}{4ca_0}, \tag{55}$$

and a metastable non-wet phase exists up to the "spinodal temperature"

$$\delta\varepsilon_{\text{sp}} = -\frac{b^2}{3ca_0}, \tag{56}$$

Such "surface spinodals" have also been obtained from the Ginzburg–Landau treatment of first-order wetting transitions, of course (cf. Fig. 13). Thus, $\delta\varepsilon$ in Eq. (54) needs to be reinterpreted as $(T^{w}_{sp}-T)/T_w$ in the present case. The interface position at the first-order wetting transition is straightforwardly found as

$$l_{\rm tr} = -\frac{1}{\kappa}\ln(2c/b)\,. \tag{57}$$

One can also locate the prewetting transition lines to find that they terminate at the prewetting critical point located at

$$\delta\varepsilon_c^{\rm pre} = 16\,\delta\varepsilon_{\rm tr}/9, \qquad l_c^{\rm pre} = -\frac{1}{\kappa}\ln(9c/2b). \tag{58}$$

For completeness, we mention the case of the tricritical wetting transition, which in this framework is simply described by the special case when b vanishes, and hence

$$l = -\frac{1}{2\kappa}\ln(3c/a_0\,\delta\varepsilon), \qquad \text{for} \quad h=0, \quad \delta\varepsilon = (T_w-T)/T_w > 0. \tag{59}$$

This treatment now is easily generalized to the case of interface localization-delocalization in thin films.[15, 16, 59, 65] We now have to superimpose the potentials from the two competing walls. It is convenient to normalize the resulting potential as follows[65]

$$V(l) = V_{\rm eff}(l) + V_{\rm eff}(D-l) - 2V_{\rm eff}(D/2), \tag{60}$$

which yields (for the case $h=0$, using the abbreviation $a \equiv -a_0\,\delta\varepsilon$),

$$\begin{aligned} V(l) = {} & 2a\exp(-\kappa D/2)\{\cosh[\kappa(l-D/2)]-1\} \\ & -2b\exp(-\kappa D)\{\cosh[2\kappa(l-D/2)]-1\} \\ & +2c\exp(-3\kappa D/2)\{\cosh[3\kappa(l-D/2)]-1\} \end{aligned} \tag{61}$$

In general, the phase boundaries depend on the variables a/c, b/c and κD. It is convenient to analyze the situation using the auxiliary variable $\tilde{m}$, which is defined by[65]

$$\begin{aligned} \tilde{m}^2 &= 2\exp(-\kappa D/2)\{\cosh[\kappa(l-D/2)]-1\} \\ &\approx [\exp(-\kappa D/4)\,\kappa(l-D/2)]^2 + \text{higher orders of } (l-D/2) \end{aligned} \tag{62}$$

Thus, to leading order $\tilde{m}$ simply is proportional to the order parameter of the interface localization-delocalization phase transition, since $\tilde{m} \equiv 0$ if the interface is located at $l = D/2$, i.e., in the center of the film (Fig. 6). With some algebra, the reduced interface potential $V(l)$ then can be written in the form[65]

$$V(l) = c[\tilde{m}^2(\tilde{m}^2 - r)^2 + t\tilde{m}^2] \tag{63}$$

where the following abbreviations have been introduced

$$r = \frac{b}{2c} - 3\exp(-\kappa D/2) \tag{64}$$

and ($a_{tr} \equiv \delta\varepsilon_{tr}\, a_0$)

$$t = \frac{a - a_{tr} - b\exp(-\kappa D/2)}{c}. \tag{65}$$

Negative values of r correspond to second-order localization-delocalization transitions, $r = 0$ corresponds to a tricritical transition,[60] and positive values of r give rise to a first-order transition. The quantity t has the meaning of reduced temperature distance from the tricritical transition temperature (for $r \leqslant 0$), and $t = 0$ denotes the triple temperature in the case of a first-order interface localization-delocalization transition (see below). For $r \leqslant 0$ the phase boundaries depend only on the two parameter combinations r and t. In these variables the limit $\kappa D \to \infty$ is particularly transparent: $cr \to b/2$, $ct \to a - a_{tr}$, and $\tilde{m} \to \exp(-\kappa l)$. We now discuss the behavior for finite κD in more detail.

A second-order interface localization-delocalization transition (i.e., $r < 0$) will occur either if the wetting transition is second-order (i.e., $b < 0$ in Eq. (64)), or if the wetting transition is first-order but the film thickness D is small enough to comply with $0 < b < 6c\exp(-\kappa D/2)$. From the treatment[65] reviewed here it becomes particularly transparent that by reducing the thickness D of the film the order of the transition may change from first-order to second-order at a tricritical thickness[66] D_t, which in the present mean field theory becomes $D_t = -\frac{2}{\kappa}\ln(b/6c)$.

Since the coexisting phases are symmetric with respect to exchanging l and $D - l$, phase coexistence occurs at $h = 0$, or $\partial V/\partial l = (\partial V/\partial\tilde{m})(\partial\tilde{m}/\partial l) = 0$. From this condition one obtains for the binodals[65]

$$\tilde{m}^2 = \frac{2|r|}{3}\{\sqrt{1 + 3\Delta t/(4r^2)} - 1), \qquad \Delta t = t_c - t, \quad t_c = -r^2 \tag{66}$$

where Δt denotes the distance from the critical temperature at fixed r. One recognizes two different types of critical behavior, namely (two-dimensional) mean field critical behavior (2dMF) of a system with a single scalar order parameter $m = (l/D - 1/2)$, or (two-dimensional) tricritical mean field behavior (2dTMF);

$$\tilde{m}^2 \to \begin{cases} \Delta t/4\,|r| & \text{for} \quad \Delta t \ll r^2 \text{ (2dMF)} \\ \sqrt{\Delta t/3} & \text{for} \quad \Delta t \gg r^2 \text{ (2dTMF)} \end{cases} \tag{67}$$

Of course, the two-dimensional character of these phase transitions shows up in the critical exponents only if one goes beyond mean field, while on the mean field level the exponents have their standard values, which we can read off from Eq. (67), namely defining $m \propto (\Delta t)^{\beta}$

$$\beta_{\text{2dMF}} = 1/2, \qquad \beta_{\text{2dTMF}} = 1/4. \tag{68}$$

The crossover between mean field critical and tricritical behavior occurs around $|\Delta t_{\text{cross}}| \approx r^2$. As $r \to 0$, the tricritical point is approached and the regime where mean field critical behavior is observable shrinks. At the tricritical point only the tricritical regime (2dTMF) exists, i.e., $\Delta t_{\text{cross}} = 0$, and the binodal takes the particularly simple form, $\tilde{m} = \pm(\Delta t/3)^{1/4}$. These considerations are exemplified in Fig. 16. The crossover in the binodal is illustrated in the inset of Fig. 16(a) for the special case $r = -0.4$.

Of course, the above considerations neglect fluctuations and the behavior close to the transition is governed by two-dimensional Ising critical and tricritical exponents, respectively. The resulting additional crossover between the above mean field behavior and this non-mean field behavior will be discussed below.

If we wish to deal with fluctuations, we have to return to the Hamiltonian $\mathscr{H}_{\text{eff}}(l)$ in Eq. (49) and include now the term $\sigma(\nabla l)^2/2$. A full treatment of this problem requires a complicated renormalization group approach[67–76] and is beyond the scope of the present article, however. Thus we shall restrict the present consideration to Gaussian fluctuations around the mean field results. Thus we write ($\delta l \equiv l(\vec{\rho}) - l_{\text{eq}}$)

$$V_{\text{eff}}\{l(\vec{\rho})\} = V_{\text{eff}}(l_{\text{eq}}) + \frac{1}{2}\left(\frac{\partial^2 V_{\text{eff}}}{\partial l^2}\right)_{l_{\text{eq}}} (\delta l)^2, \tag{69}$$

where now the solution for l found from the minimization of $V_{\text{eff}}(l)$, cf. Eqs. (51)–(53), for instance, is denoted as l_{eq}. Introducing Fourier transforms $l_{\vec{q}}$ of $\delta l(\vec{\rho})$, where $\vec{q}$ is a two-dimensional wave vector oriented

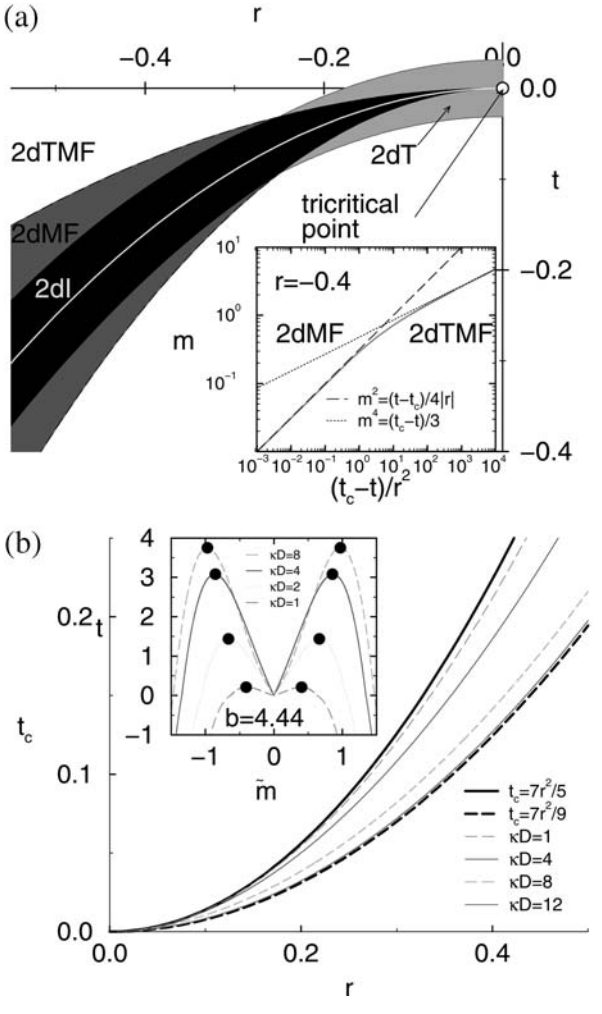

Fig. 16. (a) Illustration of the different regimes for a second-order and tricritical interface localization-delocalization phase transition; 2dTMF-mean field tricritical behavior; 2dMF-mean field critical behavior; 2dI-two-dimensional Ising critical behavior; 2dT—two-dimensional tricritical behavior. The inset shows the temperature dependence of the order parameter $\tilde{m}$ for $r = -0.4$ as calculated within mean field theory (using Eq. (66)). (b) Dependence of the critical temperature t_c on the distance r from the tricritical point. The curves correspond to different values of κD, as indicated in the key. Thick lines, which bracket the behavior, correspond to $t_c = 7r^2/5$ (valid for small κD) and $t_c = 7r^2/9$ (valid in the limit $\kappa D \to \infty$). The inset shows binodals of fixed value $b/c = 4.44$ and several choices of κD as indicated in the key (remember that b/c controls the strength of the first-order wetting transition of a semi-infinite system, cf. Eq. (57). For $b/c = 4.44 > 3\exp(-\kappa D/2)$, and hence $r > 0$, there are two critical points (highlighted by dots) for all values of film thicknesses. From Müller and Binder.[65]

parallel to the interface, we can rewrite the effective interface Hamiltonian, Eq. (49), as

$$\mathscr{H}_{\text{eff}}(\{l\}) = AV_{\text{eff}}(l_{\text{eq}}) + \frac{1}{2(2\pi)^2}\int d\vec{q}\left[\sigma q^2 + \left(\frac{\partial^2 V_{\text{eff}}}{\partial l^2}\right)_{l_{\text{eq}}}\right]|l_{\vec{q}}|^2 \tag{70}$$

From Eq. (70) we can immediately read off that the correlation length $\xi_{\|}$ of local fluctuations of the interface position δl is

$$\xi_{\|} = \sqrt{\sigma/(\partial^2 V_{\text{eff}}/\partial l^2)|_{l_{\text{eq}}}}\,. \tag{71}$$

Noting that the effective Hamiltonian, Eq. (70), is harmonic in the $l_{\vec{q}}$, we can immediately invoke the equipartition theorem to conclude that

$$\frac{\sigma}{2}(q^2 + \xi_{\|}^{-2})\langle|l_{\vec{q}}|\rangle^2 = \frac{1}{2}k_B T, \tag{72}$$

and hence the mean square displacement of the interface position is

$$\langle(\delta l)^2\rangle = \frac{1}{(2\pi)^2}\int d\vec{q}\,\langle|l_{\vec{q}}|\rangle^2 = \frac{k_B T}{(2\pi)^2\sigma}\int d\vec{q}\,\frac{1}{q^2 + \xi_{\|}^{-2}}. \tag{73}$$

Here it is understood that the integration is only extended to some upper cutoff, which we call $q_{\max}$ here, and which is assumed to be of the same order as the inverse of the correlation length ξ_b in the bulk (or the "intrinsic" interfacial width w_0, respectively). Thus,

$$\langle(\delta l)^2\rangle = \frac{k_B T}{2\pi\sigma}\int_0^{q_{\max}}\frac{q\,dq}{q^2 + \xi_{\|}^{-2}} \approx \frac{k_B T}{2\pi\sigma}\ln(\xi_{\|} q_{\max}) \tag{74}$$

for $\xi_{\|} q_{\max} \gg 1$. From Eqs. (73) and (74) it is obvious that the mean square width of the interface diverges for a free interface, which is unbound from the wall(s), for which $V_{\text{eff}}(l) = 0$ and hence $\xi_{\|}^{-1} = 0$. Then the lateral size L of the system acts as a lower cutoff, $q_{\min} = 2\pi/L$, for the q-integrations in Eqs. (73) and (74), and one hence finds the well-known logarithmic size dependence[52–56]

$$\langle(\delta l)^2\rangle \approx \frac{k_B T}{2\pi\sigma}\ln(L q_{\max}) + \text{const.} \tag{75}$$

However, a more precise description of the spectrum of the capillary waves near $q = q_{\max}$ is still a topic of active research.[30, 77–82]

Using now Eqs. (50), (52), and (71), we can calculate the critical behavior of $\xi_{\|}$ as the second-order wetting transition is approached,

$$\xi_{\|} = \kappa^{-1} \sqrt{2b\sigma}\, (a_0 \delta\varepsilon)^{-1} \Rightarrow \xi_{\|} \propto (T_w - T)^{-\nu_{\|}}, \qquad \nu_{\|} = 1. \tag{76}$$

This treatment can be generalized easily to the interface localization-delocalization problem, using now (in the second-order case) Eq. (61) with $b < 0$ (and setting $c \equiv 0$). For $T > T_c(D)$ where $l_{\text{eq}} = D/2$, this yields

$$\left.\frac{\partial^2 V}{\partial l^2}\right|_{l = D/2} = 2 \exp(-\kappa D/2)\, \kappa^2 [-a_0\, \delta\varepsilon + 4b \exp(-\kappa D/2)] \tag{77}$$

and noting that the response function $\bar{\chi}$ can be written as[15]

$$\bar{\chi} \equiv \left.\frac{\partial l_{\text{eq}}}{\partial h}\right|_{T,\, D} = [(\partial^2 V/\partial l)^2_{l = D/2}]^{-1}, \tag{78}$$

we find, using $t \equiv [T_c(D) - T]/T_w$,

$$\bar{\chi} = (2\kappa^2 a_0)^{-1} \exp(\kappa D/2)(-t)^{-1}, \tag{79}$$

with

$$t = \delta\varepsilon - \frac{4b}{a_0} \exp(-\kappa D/2). \tag{80}$$

Equation (80) shows that $T_c(D)$ differs from T_w only by terms that are exponentially small in $\kappa D/2$, and for the case where $b < 0$ in Eq. (61) we always have $T_c(D) < T_w$. Since the susceptibility $\chi = \partial m/\partial H$ then becomes

$$\chi = 4m_b^2 \bar{\chi}/D = \hat{C}^+_{\text{MF}} (-t)^{-\gamma_{\text{MF}}}, \qquad \gamma_{\text{MF}} = 1, \tag{81}$$

we conclude from Eqs. (79) and (81) that the critical amplitude in this mean field (MF) theory is[15]

$$\hat{C}^+_{\text{MF}} = (2m_b^2/\kappa^2 a_0) \exp(\kappa D/2)/D. \tag{82}$$

For the correlation length $\xi_{\|}$ we find from Eqs. (71), (77), and (80) a critical exponent that differs from the wetting case (cf. Eq. (76)), namely

$$\xi_{\|} = \hat{\xi}^+_{\text{MF}} (-t)^{-\nu_{\text{MF}}}, \qquad \nu_{\text{MF}} = \tfrac{1}{2}, \tag{83}$$

and the critical amplitude again has an (unusual!) exponential dependence on the thickness D of the thin film,

$$\hat{\xi}^+_{\text{MF}} = \kappa^{-1} \sqrt{\sigma/2a_0} \exp(\kappa D/4) \tag{84}$$

Expanding the potential $V(l)$ around $l_{eq} = D/2$ up to fourth order, we find that[15]

$$l_{eq} - D/2 = \pm \kappa^{-1} \sqrt{a_0/2b} \exp(\kappa D/4)\, t^{1/2}, \tag{85}$$

and hence the order parameter in this mean field theory again yields the exponent $\beta_{MF} = 1/2$ and the critical amplitude becomes ($m_{MF} = m_b(2l_{eq} - D) = \hat{B}_{MF}\, t^{\beta_{MF}}$)

$$\hat{B}_{MF} = \sqrt{2a_0/b}\, m_b \exp(\kappa D/4)/(\kappa D). \tag{86}$$

This exponential dependence on D exhibited by the critical amplitudes in this phase transition has important consequences when one considers the question over which range of temperature distances t from $T_c(D)$ this mean field theory is valid, and where it breaks down due to the effects of thermal fluctuations. As is well known,[83–85] mean field theory is self-consistent, if the order parameter fluctuations in a correlation volume are small in comparison to the square of the mean order parameter. For the present geometry, one obtains ($\vec{r} \equiv (\vec{\rho}, z)$)

$$\int_0^D dz \int_{\rho < \xi_\parallel} d\vec{\rho}\, [\langle m(\vec{r}')\, m(\vec{r}' + \vec{r})\rangle - m_{MF}^2] \ll D \xi_\parallel^2 m_{MF}^2 \tag{87}$$

Near $T_c(D)$, $\xi_\parallel$ is very much larger than D, and the inhomogeneity of $m(\vec{r})$ in the pure phases (for $z < l(\vec{\rho})$ or $z > l(\vec{\rho})$, respectively) can be ignored—it contributes only a prefactor of order unity. Thus one concludes[15] that Eq. (87) is essentially equivalent to the standard form of the Ginzburg criterion, expressed by the condition that the Ginzburg number Gi is small in comparison to the temperature distance t from $T_c(D)$

$$\begin{aligned} Gi \ll |t|, \qquad Gi &= \hat{C}_{MF}^{+} \hat{B}_{MF}^{-2} k_B T / [(\hat{\xi}_{+}^{MF})^2\, D] \\ &= \exp(-\kappa D/2)[2bk_B T \kappa^2/(a_0 \sigma)] \end{aligned} \tag{88}$$

From Eq. (88) one sees that the Ginzburg number decreases exponentially fast with thickness, and hence the mean field theory of interface localization-delocalization[16, 59] for large D should be very accurate. The same statement applies[65] to the tricritical transition, where $Gi \propto \exp(-\kappa D)$.

At this point, we caution that despite its plausibility and elegance the above description (cf. Eqs. (49)–(88)) in terms of the interface Hamiltonian may suffer from fundamental defects: it is not obvious that the problem really can be fully reduced to the statistical mechanics of only a single collective coordinate $l(\vec{\rho})$. Such a point of view has been emphasized by Parry

and Boulter,[86–91] who showed by several rather compelling arguments that Eq. (49) actually loses important physics (particular with respect to the description of complete wetting) that is still contained in the more microscopic mean field theory (based on Eq. (16), for instance). They pointed out that one can remedy these defects by generalizing Eq. (49) to an effective Hamiltonian with two coupled collective coordinates $(l_1(\vec{\rho}), l_2(\vec{\rho}))$ instead of a single one:

$$\mathscr{H}_{\text{eff}}(\{l_1, l_2\}) = \int d\vec{\rho}\{\tfrac{1}{2}\sigma_{\mu\nu}\nabla l_\mu \cdot \nabla l_\nu + V_{\text{eff}}^{(1)}(l_1) + V_{\text{eff}}^{(2)}(l_2 - l_1)\}, \qquad (89)$$

where $\sigma_{\mu\nu}(\mu, \nu = 1, 2)$ are elements of a symmetric "stiffness matrix." $l_1(\vec{\rho})$ models order parameter fluctuations near the wall which are neglected in the traditional capillary wave theory, and $l_2(\vec{\rho})$ represents the position of the unbinding interface (i.e., the variable analogous to $l(\vec{\rho})$ before). In the simplest case, one can assume that $\sigma_{\mu\nu}$ is diagonal, $V_{\text{eff}}^{(1)}(l_1) = \frac{1}{2}(\sigma_{11}/\xi_\perp^2)\, l_1^2$, $\xi_\perp$ being the transverse correlation length at the wall, and $V_{\text{eff}}^{(2)}$ can be taken to have the same form as $V_{\text{eff}}(l)$ before (cf. Eq. (50)). Then one finds that the length κ^{-1} (which according to the standard mean field theory is just the correlation length ξ_b)[59] is renormalized when one considers complete wetting near a critical wetting transition (h_1 near h_{1c}). Instead of Eq. (53), namely $l_{\text{eq}} \approx -\kappa^{-1} \ln h + \text{const}$, one finds to leading order,[86–91]

$$\langle l \rangle = -\frac{(1+\omega/2)}{\kappa} \ln h + \text{const}, \qquad h \to 0 \qquad (90)$$

where ω is the capillary parameter that enters also the theory of critical wetting,

$$\omega = \frac{k_B T}{4\pi \xi_b^2 \sigma}. \qquad (91)$$

Here we are not giving a full account of these recent developments but rather refer to recent reviews.[91, 92]

2.3. Scaling and Renormalization Group Predictions

As a first step, we consider the consequences of scaling behavior near the bulk critical point in this section, following the pioneering papers of Fisher and Nakanishi.[13, 24, 25]

We consider hence the singular part f_{sing} of the free energy density of a thin film $F_{\text{film}}(T, H, H_1, D)/(AD)$, cf. Eq. (28), and make the standard scaling assumption.[7, 8, 24] Defining $t = (T - T_{cb})/T_{cb}$, we write:

$$f_{\text{sing}}(T, H, H_1, D) = |t|^{2-\alpha} \tilde{f}_{\pm}(D\,|t|^{\nu}, H\,|t|^{-\Delta}, H_1\,|t|^{-\Delta_1}), \tag{92}$$

where we have again assumed that the same field H_1 acts on both surfaces of the thin film, and α is the critical exponent of the specific heat of the three-dimensional Ising model, and $\tilde{f}_{\pm}$ is a scaling function which has two different branches, according to the sign of t. The critical behavior of the bulk correlation length ξ_b is[58, 93, 94]

$$\xi_b = \hat{\xi}_{\pm}\,|t|^{-\nu}, \qquad \nu \approx 0.63, \tag{93}$$

and Eq. (92) thus expresses the principle of finite size scaling that "the film thickness D scales with the correlation length ξ_b."[95–99] While the gap exponent Δ that enters in the scaling power of the bulk magnetic field is known very precisely,[58, 93, 94]

$$\Delta = \gamma + \beta \approx 1.56, \tag{94}$$

the surface counterpart Δ_1 is known with somewhat less precision[8, 100–104]

$$\Delta_1 \approx 0.47 \pm 0.01. \tag{95}$$

In order to consider singularities that occur in Eq. (92) when one keeps D finite and fixed, such as for a consideration of capillary condensation, it is convenient to introduce the scaling variables

$$x \equiv D\,|t|^{\nu}, \qquad w \equiv H_1 D^{\Delta_1/\nu}. \tag{96}$$

Then Eq. (92) can also be written differently, eliminating $|t|$ from the arguments of $\tilde{f}_{\pm}$,

$$f_{\text{sing}}(T, H, H_1, D) = |t|^{2-\alpha} \tilde{f}_{\pm}(x, HD^{\Delta/\nu}/x^{\Delta/\nu}, w/x^{\Delta_1/\nu}) \tag{97}$$

We now investigate the possibility of critical behavior in the thin film. Since the associated critical point is shifted relative to the bulk critical point (T_{cb}, $H = 0$), it must correspond to a singular behavior of the scaling function $\tilde{f}_{\pm}$. At fixed H_1 and fixed D this means that the scaling function $\tilde{f}_{\pm}(x, y, y_1)$ (where $y_1 = w/x^{\Delta_1/\nu}$) has a singularity at a point $x_c(w)$, $y_c(w)$.

Therefore, one obtains for the shifts $\Delta T_c(D)$ and $\Delta H_c(D)$ of the capillary condensation critical point (cf. Fig. 10)[24, 25]

$$\Delta T_c = T_c(D, H_1) - T_{cb} = -B_T D^{-1/\nu} X_c(C H_1 D^{\Delta_1/\nu}), \tag{98}$$

$$\Delta H_c \equiv H_c(D, H_1) = -B_H D^{-\Delta/\nu} Y_c(C H_1 D^{\Delta_1/\nu}). \tag{99}$$

Here B_T, B_H and C are non-universal amplitudes, the scaling functions X_c and Y_c are universal and normalized such that they have the following expansions for small arguments,

$$X_c(Cw) = 1 + (Cw)^2 + \cdots, \qquad Y_c(Cw) = Cw + \mathcal{O}((Cw)^3). \tag{100}$$

Note that $X_c(Cw)$ and $Y_c(Cw)$ are analytic for $w \to 0$, and we have made use of the fact that the symmetries of the Ising model (cf. Eq. (3)) require that X_c is an even function of H_1 and hence, w, while Y_c is an odd function of H_1. From these considerations, we straightforwardly obtain for small H that

$$\Delta T_c = -B_T D^{-1/\nu}, \qquad \Delta H_c = -B_H C H_1 D^{-(\Delta - \Delta_1)/\nu}. \tag{101}$$

An interesting aspect of this result is the question how this result fits together with the Kelvin[23] equation ($\Delta H_c \propto -H_1/D$, cf. Fig. 10) which we expect to hold if we consider temperatures below the capillary condensation critical point for large enough D. This question can be answered by the following argument: If $H_1 = H = 0$, we would have two coexisting phases with magnetization profiles $m^+(z) > 0$ and $m^-(z) = -m^+(z)$ across the film, and both states would have the same free energy $F^+(0, 0) = F^-(0, 0)$. These free energies $F^{\pm}(H, H_1)$ are smooth functions of H and H_1 (for the considered temperature $T < T_c(D)$). Hence one can expand them around $F^+(0, 0)$ and $F^-(0, 0)$ as follows

$$F_+(H, H_1) = F_+(0, 0) - \overline{m^+} H D L^2 - 2 m_1^+ H_1 L^2, \tag{102}$$

$$F_-(H, H_1) = F_-(0, 0) - \overline{m^-} H D L^2 - 2 m_1^- H_1 L^2 \tag{103}$$

where $\overline{m^+}$ and $\overline{m^-}$ refer to the average over the magnetization profiles $m^+(z)$ and $m^-(z)$ in the coexisting states with zero bulk and surface fields, and m_1^+, m_1^- are the respective surface magnetizations. Using the obvious symmetries $\overline{m^-} = -\overline{m^+}$, $m_1^- = -m_1^+$, the condition for phase coexistence $F_+(H, H_1) = F_-(H, H_1)$ then yields

$$H_{\text{coex}}(D, T, H_1) = -\frac{2H_1}{D} \frac{m_1^+(D, T)}{\overline{m^+}(D, T)}. \tag{104}$$

If $D \gg \xi_b$ the profile $m^+(z)$ must approach the spontaneous magnetization in the bulk ($m_b = \hat{B}(-t)^\beta$) almost everywhere, and hence $\overline{m^+}(D, T)$ differs from m_b only by a $1/D$ correction[7, 8] which can be neglected in the order considered. Similarly, $m_1^+(D, T)$ approaches the surface layer magnetization of a semi-infinite system,[7, 8] $m_1 = \hat{B}_1(-t)^{\beta_1}$, where β_1 is the critical exponent of the surface layer magnetization at the "ordinary transition"[7, 8, 57, 105] of an associated semi-infinite system, and $\hat{B}_1$ is critical amplitude analogous to the critical amplitude $\hat{B}$ of the bulk magnetization. Equation (104) then yields

$$H_{\text{coex}}(D, T, H_1) \approx -\frac{2H_1}{D}\frac{\hat{B}_1}{\hat{B}}(-t)^{\beta_1-\beta}, \qquad x = D|t|^\nu \to \infty \tag{105}$$

For D large but finite, crossover occurs from the behavior described by Eq. (105) at $t \approx t_{\text{cross}}$ to the behavior of Eq. (101), t_{cross} being of the same order as the shift of T_c, $t_{\text{shift}} = \Delta T_c / T_{cb} \propto -D^{-1/\nu}$. Thus, $H_{\text{coex}}(D, T_c(D), H_1)$ indeed follows from Eq. (105) in full agreement with Eq. (101). Note the scaling relation $1 + (\beta_1 - \beta)/\nu = (\Delta - \Delta_1)/\nu$ which follows from[7, 8] $\beta = 2 - \alpha - \Delta$ and $\beta_1 = 2 - \alpha - \nu - \Delta_1$. There is also an interesting scaling relation for the slope of the coexistence curve $H_{\text{coex}}(D, T, H_1)$ as $T \to T_c(D)$, namely

$$\begin{aligned}\tan(\Theta) \equiv (\partial H_{\text{coex}}/\partial T)_{H_1} &= \frac{2H_1}{D}\frac{\hat{B}_1}{\hat{B}}\frac{\beta_1 - \beta}{T_{cb}}(-t)^{\beta_1-\beta-1} \propto H_1 D^{-\frac{(\beta_1-\beta-1)}{\nu}-1} \\ &= H_1 D^{-(\Delta-\Delta_1-1)/\nu}.\end{aligned} \tag{106}$$

While in Landau theory[7, 8] $\Delta = 3/2$, $\Delta_1 = 1/2$ so the power of D vanishes, i.e., the slope remains finite and non-zero at $T_c(D)$ in the limit $D \to \infty$, for the three-dimensional Ising model this slope actually vanishes ($(\Delta_1 - \Delta - 1)/\nu \approx 0.14 \pm 0.2$[100–105]), and $\Theta \to 0$ as $D \to \infty$. This result also implies that for capillary condensation field mixing effects[106] can be neglected for $D \to \infty$.

We are now interested in the critical behavior near the critical point of the thin film and hence consider the case $y = y_c(w)$ in Eq. (97), keeping x near $x_c(w)$. For fixed w, the dependence on both w and $y_c(w)$ does not need to be considered explicitly and we can write the singular part of the free energy, the magnetization and the susceptibility of the film as

$$f_{\text{sing}}(T, D) = D^{-3}\,\tilde{\tilde{f}}(x'), \qquad x' \equiv tD^{1/\nu} \tag{107}$$

$$m = D^{-\beta/\nu}\,\tilde{m}(x'), \qquad \chi = D^{\gamma/\nu}\,\tilde{\chi}(x'), \tag{108}$$

with β, γ, ν the exponents of the three-dimensional Ising model. $\tilde{\tilde{f}}(x')$, $\tilde{m}(x')$, and $\tilde{\chi}(x')$ suitable scaling functions that can be derived from $\tilde{f}_{\pm}$, if the latter function is known explicitly. The singularity at $x = x_c(w)$ translates into a singularity of x' at $x'_0(w')$, of course. Following standard assumptions on crossover scaling in systems with a linear dimension being finite,[24, 25, 95–99, 107–111] the specific heat C_V, order parameter m, and susceptibility χ of the thin film result from a corresponding singularity of the respective scaling functions, i.e.

$$\begin{aligned} C_V &\propto D^{2/\nu-3}\,|x'-x'_c|^{-\alpha_2}, \qquad m \propto D^{-\beta/\nu}(x'_c-x')^{\beta_2}, \\ \chi &\propto D^{\gamma/\nu}\,|x'-x'_c|^{-\gamma_2}, \end{aligned} \tag{109}$$

where α_2, β_2, γ_2 are the corresponding exponents of the specific heat, order parameter and susceptibility of a corresponding bulk two-dimensional system. (In the Ising model, the logarithmic singularity [$\alpha_2 = 0$] means the term $|x'-x'_c|^{-\alpha_2}$ needs to be re-interpreted as $\ln|x'-x'_c|$, of course). As a consequence, in terms of the reduced temperature distance $t' = (T-T_c(D))/T_{cb} = (x'-x'_c)\,D^{-1/\nu}$ we obtain

$$\begin{aligned} C_V &\propto D^{2/\nu-3}\ln|t'|, \qquad m \propto D^{(\beta_2-\beta)/\nu}(-t')^{\beta_2}, \\ \chi &\propto D^{(\gamma-\gamma_2)/\nu}\,|t'|^{-\gamma_2}, \qquad t' \to 0. \end{aligned} \tag{110}$$

The crossover from three-dimensional to two-dimensional critical behavior in thin films shows up in a singular variation of the critical amplitudes with film thickness D. Of course, the larger D is the narrower the critical region becomes: only if the variable $|x'-x'_c| \ll 1$ can we expect to see the two-dimensional critical behavior, which requires $|t'| \ll D^{-1/\nu}$.

This general line of reasoning can be extended to discuss wetting transitions near the bulk critical points, and thus derive the phase diagrams already shown in Fig. 4.[13] We simply have to consider the limit of very thick films, $D \to \infty$ which are equivalent to the semi-infinite case in the sense that the free energy of the film can be split into a bulk term and a contribution from the two (equivalent) surfaces, cf. Eq. (28). Consequently, Eq. (92) yields the singular part of the free energy of the system, for $D \to \infty$,

$$\begin{aligned} f_{\text{sing}}(T, H, H_1, D) = {} & |t|^{2-\alpha}\,\tilde{f}_{\pm}^{(\text{bulk})}(H\,|t|^{-\Delta}) \\ & + \frac{2}{D}\,|t|^{2-\alpha-\nu}\,\tilde{f}_{\pm}^{(\text{surface})}(H\,|t|^{-\Delta}, H_1\;|t|^{-\Delta_1}), \end{aligned} \tag{111}$$

where we have anticipated that the bulk part of the free energy must, of course, be independent of H_1. Equation (111) is only sufficient if (in the limit

$H_1 \to 0$) the surface undergoes the "ordinary transition" (cf. Fig. 3),[8, 57] which happens for the case where there is no (or only a subcritical) enhancement of the exchange interactions at the surface of the Ising model. Particularly interesting, however, is the case where one has an enhancement of the exchange interactions such that one stays at or close to the surface-bulk multicritical point[8, 57] (cf. Fig. 3). Denoting the distance from the surface-bulk multicritical point as $g \equiv (J_s - J_{sc})/J$, we need to include g as an additional scaled variable in the singular part of the surface free energy. This leads to[8, 13]

$$f_{\text{sing}}^{(\text{surface})}(T, H, H_1, g) = |t|^{2-\alpha-\nu} \tilde{f}_{\pm}^{\text{SB}}(H\,|t|^{-\Delta}, H_1\,|t|^{-\Delta_1^{\text{SB}}}, g\,|t|^{-\phi}), \qquad (112)$$

where $\tilde{f}_{\pm}^{\text{SB}}$ is now the scaling function of the surface free energy at the surface-bulk multicritical point, Δ_1^{SB} is the analog of the exponent Δ_1 but for the multicritical point, and ϕ is the "crossover exponent" describing the merging of the surface transition line at this multicritical point with bulk transition at temperature T_{cb}, i.e.

$$T_{cs} - T_{cb} \propto g_{\pm}^{1/\phi}. \qquad (113)$$

Of course, Eq. (113) simply results from the reasoning that the surface transition line $T_{cs} = T_{cs}(g)$ is found at the appropriate singularity of the scaling function $\tilde{f}_{\pm}^{\text{SB}}(0, 0, \zeta)$, occurring at some value $\zeta = \zeta_c$. Note that $\phi = 1/2$ in mean field theory;[7, 8, 57] the value of ϕ for the 3d Ising model is not yet known very precisely, but it is believed to be rather close to the mean field result.[100–103] For $g < 0$ the only singularities (in the limit $H_1 \to 0$) occur for $t \to 0$, and in this limit $\tilde{f}_{\pm}^{\text{SB}}$ in Eq. (112) reduces to $\tilde{f}_{\pm}^{(\text{surface})}$ of Eq. (111) again.

We now discuss wetting transitions for this case of subcritical or critical surface exchange enhancement, i.e., for $g \leqslant 0$. From Eq. (111) we conclude, noting that the wetting transition is a singularity of $\tilde{f}_{\pm}^{(\text{surface})}(0, X)$ for $X \equiv H_1(-t)^{-\Delta_1}$ reaching some critical value X_c. Consequently, the surface field H_1 at the wetting transition vanishes according to the following power laws as $t \to 0$,

$$H_{1c} \propto (-t)^{\Delta_1}, \quad g < 0; \qquad H_{1c} \propto (-t)^{\Delta_1^{\text{SB}}}, \quad g = 0. \qquad (114)$$

Again the existing estimates for Δ_1^{SB}, e.g., ref. 101, $\Delta_1^{\text{SB}} \approx 1.04$ differ only slightly from the mean field result,[7, 8] $\Delta_1^{\text{SB}} = 1$.

A discussion of prewetting criticality is particularly interesting: this prewetting critical point must show up as a critical singularity of $\tilde{f}_{\pm}^{(\text{surface})}$, but in general it is a line in the space of variables (H, H_1, t, g) where both H and H_1 are non-zero. Only when one approaches tricritical wetting, do

the wetting transition and the prewetting critical point coincide at $H = 0$. Nakanishi and Fisher[13] now recognized that in the case $g > 0$ the surface transition simply is a point of particular symmetry (where $H = H_1 = 0$) on the line of critical prewetting transitions (see Fig. 3). Since these prewetting transitions belong to the universality class of the two-dimensional Ising model as well, this point is not a singular point on this line.

The limiting case when the surface transition merges with the bulk critical temperature T_{cb} is of special interest. The prewetting critical lines also must end there, and since end points of prewetting critical lines at the coexistence curve ($T \leqslant T_{cb}$, $H = 0$) have the character of tricritical wetting transitions, the surface-bulk multicritical point also is the endpoint of a line of tricritical wetting transitions.

From these considerations and the scaling forms of the surface free energy (cf. Eqs. (111) or (112), respectively) one can work out the asymptotic power laws of the curves in Fig. 3 as $t \to 0$. E.g., tricritical wetting is a singularity of Eq. (112) for $H = 0$, $X' \equiv H_1(-t)^{-\Delta_1^{SB}} = X'_t$ and $Y \equiv g(-t)^{-\phi} = Y_t$. As a consequence, the line of tricritical wetting transitions merges at the surface-bulk multicritical point as

$$(J_{sc} - J_{st})/J \propto (1 - T_t/T_{cb})^{\phi}, \tag{115}$$

where T_t is the tricritical wetting temperature and J_{st} the corresponding surface coupling.

Next we discuss the scaling behavior of the critical and tricritical wetting transitions themselves. Of course, the nature of these singularities *cannot* be concluded from the scaling structure of Eqs. (111) and (112). Similarly, for the case of capillary condensation we also could not use Eq. (92) to show that the transition of the thin film belongs to the universality class of the two-dimensional Ising model; instead we introduced this in Eq. (109) as a hypothesis. For wetting transitions, however, the critical behavior is completely non-trivial, and to analyze it renormalization group treatments of Eqs. (49) and (89) have been proposed.[67–76, 112] Here we shall not describe these theories in detail but summarize only these results which are most pertinent for the analysis of the simulation data shown in Section 3.3.

Assuming that a critical wetting transition occurs at $H_1 = H_{1c}(T)$ and denoting the reduced distance from this wetting transition as $\tilde{t} = (H_{1c} - H_1)/J$, we find a scaling description of the surface free energy per spin $f_s(T, H, H_1)$[112]

$$f_s^{\text{sing}}(T, H, H_1) = \tilde{t}^{2\nu_\parallel} \Omega_1(H\tilde{t}^{-2\nu_\parallel}) + cH \ln[H\Omega_2(H\tilde{t}^{-2\nu_\parallel})], \tag{116}$$

where $\nu_\parallel$ is the critical exponent of the correlation length $\xi_\parallel \propto \tilde{t}^{-\nu_\parallel}$ of interface fluctuations, Ω_1 and Ω_2 are scaling functions, and c is a constant. Note

that there is a single exponent $\nu_{\|}$ describing the singularities at critical wetting. The power of $\tilde{t}$ in front of Ω_1 is a simple consequence of a hyperscaling-type relation for surface critical phenomena: $(d-1)\,\nu_{\|} = 2-\alpha_s$, for $d=3$, α_s being the critical exponent of the surface excess specific heat. While in mean field theory $\nu_{\|}=1$ (cf. Eq. (76)), renormalization group theory predicts that $\nu_{\|}$ is non-universal and depends on the capillarity parameter ω (cf. Eq. (91)),[67–76, 112]

$$\nu_{\|} = \begin{cases} (1-\omega)^{-1} & \text{if} \quad 0 \leqslant \omega \leqslant 1/2, \\ (\sqrt{2}-\sqrt{\omega})^{-2} & \text{if} \quad 1/2 \leqslant \omega \leqslant 2, \\ \infty & \text{if} \quad \omega \geqslant 2\,. \end{cases} \tag{117}$$

Near T_{cb} Fisher and Wen[113] have shown that $\omega \simeq 0.86$, and at all temperatures between the roughening temperature T_R and T_{cb} for the simple cubic nearest-neighbor Ising model ω seems, in fact, to have only a rather weak temperature dependence,[113] implying that for the temperatures of interest $\nu_{\|}$ is close to $\nu_{\|} \approx 4$. Therefore, a very dramatic deviation from the mean field description is predicted.

From Eq. (116) one then can show that, to leading order for $H \to 0$ and $\tilde{f} \to 0$,

$$m_s = -(\partial f_s/\partial H)_{\tilde{t},\,H_1} \approx -c\,\ln[H\Omega_2(H\tilde{t}^{-2\nu_{\|}})], \tag{118}$$

$$\chi_1 = -(\partial^2 f_s/\partial H\,\partial H_1)_{\tilde{t}} \approx \tilde{t}^{-1}\,\tilde{\chi}_1(H\tilde{t}^{-2\nu_{\|}}) \tag{119}$$

and

$$\chi_{11} = -(\partial^2 f_s/\partial H_1^2)_{\tilde{t},\,H} \approx \tilde{t}^{2\nu_{\|}-2}\,\tilde{\chi}_{11}(H\tilde{t}^{-2\nu_{\|}}) \tag{120}$$

where $\tilde{\chi}_1$ and $\tilde{\chi}_{11}$ are suitable scaling functions deriving from Ω_1 and Ω_2. Equation (118) implies for $\tilde{t}=0$ that $m_s \approx -c\ln H$ and for $H \to 0$ (since $\Omega_2(\zeta \to 0) \propto \zeta^{-1}$ to ensure a sensible limit) $m_s \approx -c\ln\tilde{t}$, i.e., results identical to mean field theory (cf. Eq. (37)). On the other hand, we conclude that

$$\chi_1(H=0) \propto \tilde{t}^{-1}, \qquad \chi_1(\tilde{t}=0) \propto H^{-1/2\nu_{\|}} \tag{121}$$

where the second of these relations resulting from the fact that in Eq. (119) the powers of $\tilde{t}$ must cancel for $\tilde{t} \to 0$ at fixed small H. At this point, we also note that Eqs. (119)–(121) should only hold in a strict sense for $0 < \omega < 1/2$, while for $\omega > 1/2$ further logarithmic corrections are predicted[73] which we disregard here for simplicity.

This description can be extended to tricritical wetting, but now the general scaling structure of Eq. (116) needs to be generalized to include another scaling variable v, which at the tricritical point is tangential to the

line $H_{1c}(J_s/J)$ of critical wetting transitions in the space of variables $(H_1, J_s/J)$. Denoting $\Omega_1^{(t)}$, $\Omega_2^{(t)}$ as scaling functions we write,

$$f_s^{\text{sing}}(T, H, H_1, J_s/J) = \tilde{t}^{2\nu_{\parallel}^t}\Omega_1^{(t)}(H\tilde{t}^{-2\nu_{\parallel}^t}, \tilde{t}v^{-1/\phi}) + c^{(t)}H \ln[H\Omega_2^{(t)}(H\tilde{t}^{-2\nu_{\parallel}^t}, \tilde{t}v^{-1/\phi})]. \quad (122)$$

$\nu_{\parallel}^t$ is the tricritical value of the exponent $\nu_{\parallel}$ ($\nu_{\parallel}^t = 3/4$ in mean field theory), and ϕ is the crossover exponent describing the crossover from tricritical to critical wetting ($\phi = 1/2$ in mean field theory). The line of critical wetting transitions is given by a critical value of the scaling variable $\zeta = \tilde{t}v^{-1/\phi}$,

$$\tilde{t}_c v^{-1/\phi} = \zeta_c \quad \text{(critical wetting)} \quad (123)$$

Note that $\tilde{t} \equiv (H_{1t} - H_1)/J$ describes the distance from the tricritical wetting transition. In this case renormalization group theory[70, 72, 114] predicts a non-universal behavior of $\nu_{\parallel}^t$, depending again on the parameter ω, Eq. (91),

$$\nu_{\parallel}^t = \begin{cases} 3/(4-6\omega) & \text{if } 0 \leqslant \omega < 2/9, \\ (\sqrt{2}-\sqrt{\omega})^{-2} & \text{if } 2/9 \leqslant \omega \leqslant 2, \\ \infty & \text{if } \omega \geqslant 2. \end{cases} \quad (124)$$

To complete this section, we discuss the critical behavior of the interface localization-delocalization phase transition, using our discussion of the Ginzburg criterion (cf. Eq. (87)) to conclude that an appropriate crossover scaling variable is[15]

$$\zeta = t \exp(\kappa D/2), \quad (125)$$

where now $t = [T_c(D) - T]/T_w$ as in Eqs. (79)–(86). We hence make the phenomenological assumption that the magnetization of the thin film of thickness D can be written as (cf. Eq. (86)).

$$m = D^{-1} \exp(\kappa D/4)\, t^{1/2}\tilde{m}(\zeta) \quad (126)$$

where for large ζ the crossover scaling function $\tilde{m}(\zeta)$ tends to a constant (cf. Eq. (86)). Now we postulate that for small ζ one must have criticality according to the two-dimensional Ising model, and hence

$$\tilde{m}(\zeta \ll 1) \propto \zeta^{\beta_2 - 1/2}, \qquad \beta_2 = 1/8. \quad (127)$$

From Eqs. (125)–(127) we find[15]

$$m(t \to 0) = \hat{B}(D)\, t^{\beta_2}, \qquad \beta_2 = 1/8$$
$$\hat{B}(D) \propto D^{-1} \exp(\kappa D \beta_2/2) = D^{-1} \exp(\kappa D/16). \tag{128}$$

Next we consider the susceptibility for $T > T_c(D)$ (cf. Eq. (82))

$$\chi = D^{-1} \exp(\kappa D/2)(-t)^{-1}\, \tilde{\chi}(\zeta), \tag{129}$$

where again we conclude that $\tilde{\chi}(\zeta \to -\infty)$ tends to a constant, and Eq. (129) becomes equivalent to Eq. (82), while for $-\zeta \ll 1$

$$\tilde{\chi}(-\zeta \ll 1) \propto (-\zeta)^{-(\gamma_2 - 1)}, \qquad \gamma_2 = 7/4 \tag{130}$$

This yields the critical behavior of the susceptibility in the Ising regime as follows,

$$\chi = \hat{\chi}^+(-t)^{-\gamma_2}, \qquad \hat{\chi}^+ \propto D^{-1} \exp[\kappa D(2-\gamma)/2] = D^{-1} \exp(\kappa D/8). \tag{131}$$

Finally we consider the correlation length $\xi_{\|}$, Eq. (84),

$$\xi_{\|} = \exp(\kappa D/4)(-t)^{-1/2}\, \hat{\xi}(\zeta) \tag{132}$$

where Eq. (84) is reproduced if $\hat{\xi}(\zeta \to -\infty)$ tends to a constant, while for small $(-\zeta)$ one has

$$\tilde{\xi}(-\zeta \ll 1) \propto (-\zeta)^{(1/2)-\nu_2} \qquad \text{with} \quad \nu_2 = 1. \tag{133}$$

The asymptotic critical behavior of the correlation length is

$$\xi_{\|} = \hat{\xi}_{\|}^+(-t)^{-\nu_2}, \qquad \hat{\xi}^+ \propto \exp[\kappa D(1-\nu_2)/2] = 1, \tag{134}$$

hence there is no anomalous film thickness dependence in the critical amplitude of the correlation length.

Lastly, we examine the combination $D\xi_{\|}^2 m^2 \chi^{-1}$ that appears in the Ginzburg criterion (cf. Eq. (88)) again, but now in the Ising critical region rather than in the mean field critical region. Now this combination becomes independent of both t and D, as it should be: in the Ising critical region, this combination reduces to the universal critical amplitude combination $(\hat{\xi}^+)^2\, \hat{B}^2 (\hat{\chi}^+)^{-1}\, D$, which indeed is independent of D, if Eqs. (128), (131), and (134) are inserted.

Of course, the treatment presented in Eqs. (125)–(134) is highly phenomenological[115] and tells nothing about the explicit form of the scaling functions $\tilde{m}$, $\tilde{\chi}$, and $\tilde{\xi}$. To calculate the latter, renormalization group methods will be necessary.

3. MONTE CARLO SIMULATIONS

3.1. Comments About the Simulation Technique of Lattice Models

Simulations of Ising models addressing their bulk critical behavior are abundant, and an impressive level of accuracy has been reached.[94, 116, 117] Most of this work uses Swendsen–Wang–Wolff cluster algorithms[117–120] and has thus been restricted to zero field; however, the present problem demands the inclusion of magnetic fields. In order to use such methods here, an extension of the cluster algorithm that allows for the inclusion of magnetic fields[121–124] must be applied. So far, for the current problem (where in the general case both surface magnetic fields H_1 and a bulk field H are present) only the simplest variant of these extensions was used,[125] namely the "ghost spin algorithm."[121] The coupling of spins to a magnetic field is thereby treated as if it were an additional infinite-range exchange coupling to an extra spin $S_G = \pm 1$. This coupling has the strength $h = |H|$ for spins in the interior of the system and $h = |H_1 + H|$ for spins in the surface layers. In addition to putting bonds in clusters of spins (inside a cluster all spins are connected by exchange interactions and have the same sign) with probability[117–120] $p_B = 1 - \exp(-2J/k_BT)$ one also puts bonds between the spins in clusters and the ghost spin with probability[121] $p_G = 1 - \exp(-2h/k_BT)$, if the orientation of the spin in the cluster is the same as that of the ghost spin [which is $S_G = \text{sign}(H)$ for interior spins and $S_G = \text{sign}(H_1 + H)$ for spins in the surface planes, respectively]. Note that for simplicity, we discuss only the case $J_s = J$ here.

While this extension of the cluster algorithm to the case of non-zero bulk and surface fields is formally exact, discussion of its efficiency is a rather delicate problem: in fact, if h/k_BT is of order unity, p_G is also of order unity and the infinite-range character of this coupling then implies that huge clusters containing a large fraction of the entire simulation volume are created most of the time! It is clear that under such circumstances the algorithm would be rather inefficient; as in the case of zero field for a good performance of the cluster algorithm it is necessary that large clusters are created, but a single large cluster must contain only a negligible fraction of the total volume in the thermodynamic limit. As a consequence, one needs $h/k_BT \ll 1$. Therefore, in the recent study of Dillmann *et al.*[125] where the scaling behavior of the capillary condensation critical point near the bulk critical point was tested, only a single small value of the surface field was used, $H_1 = -0.015J$, and the corresponding bulk fields typically were at least an order of magnitude smaller.

Even for these small values of the fields, the performance of the algorithm has deteriorated significantly in comparison with the case without

any magnetic fields. Typically, one wishes to study systems in a $L \times L \times D$ geometry, with periodic boundary conditions in the x and y-directions, while on the two free $L \times L$ surfaces the surface field H_1 acts.[125–131] For a typical choice of linear dimensions, such as[125] $D = 32$, $L = 128$, at the thin film critical point the correlation time of the magnetization τ_m is of the order $\tau_m \approx 280$ Monte Carlo steps (MCS) per spin for the above choice of H_1 in the ghost spin cluster algorithm, whereas for a corresponding system with $H_1 = 0$, $H = 0$, τ_m is only a few MCS. Thus, while the gain of the cluster algorithm in the zero field case compared to the Metropolis algorithm,[117] where $\tau_m > 10^4$ for $L = 128$, is very significant, in the case with non-zero fields it is only rather modest! This dramatic decrease of the efficiency of the cluster algorithm with increasing strength of the surface (and bulk) fields has prevented a study of systems larger than $L = 128$ near T_{cb} and the dependence on H_1 has also not yet been systematically explored.[125] For the example mentioned ($D = 32$, $L = 128$), runs of length of up to 1.2 million MCS were performed, which is a major effort when one uses a cluster algorithm.

For system parameters where one does not work in the vicinity of the bulk critical temperature of the Ising model, such as for the exploration of wetting phenomena,[126–131] the study of the global phase diagram of capillary condensation (cf. Fig. 10),[131] or the study of interface localization-delocalization,[15, 132–135] standard single spin-flip Metropolis[136] or heatbath[117] algorithms were used. Of course, for interface localization-delocalization and wetting phenomena, the slow relaxation of the long wavelength (capillary wave-type) interface fluctuations is a serious problem limiting the accuracy that can be reached. While for the study of interfaces between coexisting phases in the bulk in the absence of any fields an efficient cluster algorithm has been proposed,[137] it was not used in the research reviewed here since problems were foreseen due to the presence of the non-zero surface fields. Because the second-order interface localization-delocalization phase transition ultimately falls into the universality class of the two-dimensional Ising model (see Section 2.3) it is also doubtful to what extent the interface cluster algorithm would present an advantage very close to $T_c(D)$.

In order to use available computer resources with the single spin flip algorithms most efficiently, vectorizing multispin coding algorithms were used on the supercomputers available at the respective time (a CDC Cyber 205 for the study of critical wetting[129, 130] and capillary condensation,[131] an IBM ES/9000 for the study of interface localization-delocalization.[133–135] However, it was also found to be effective to complement these studies on supercomputers with runs performed on IBM RISC workstations, using

"multilattice"[117] algorithms.[132–135] Nevertheless, it will be clear from the simulation data that will be presented in the following sections that there is still a need to have more efficient algorithms. In this context, initial results,[138] utilizing a combination of the Wang–Landau algorithm[139] with the "*n*-fold way"-algorithm[140] to efficiently sample the density of states of the model system seem rather promising.

An important issue for every Monte Carlo simulation is the quality of the random number generator that is used.[117, 141] In particular, cluster algorithms at critical points of Ising systems are rather sensitive to correlations among the pseudo-random numbers produced by the random number generator.[141, 142] For the work using a cluster algorithm,[125] an improved version of the standard "R250" generator[143] was used, where two generators [one based on the pair of integers (250, 103) and the other with the pair (521, 168)] were combined with the logical exclusive OR (XOR) operation. For the studies with the single-spin-flip algorithm, the standard "R250" generator[143] was judged to be good enough.

We now discuss how phase transitions are located precisely. Depending on the choice of J_s/J, both the wetting transition[126–130] and interface localization-delocalization[132–135] can be either first-order or second-order phase transitions, and the capillary condensation transition (Fig. 10) is a line of first-order phase transitions, ending in a critical point. Only in the vicinity of this critical point is the first-order transition sufficiently weak that a finite size scaling based on multihistogram reweighting[117, 120, 144] and the equal weight rule[117, 145–147] is convenient. Note that one then needs a three-dimensional histogram $P(E, m, m_1)$, E being the exchange energy, m the total magnetization in the thin film, and m_1 the magnetization in the surface, in order to be able to do reweighting in the full parameter space of independent control variables (T, H, H_1). Hence, the storage requirements for P are non-trivial. This problem was solved by Dillmann *et al.*[125] noting that all measurements of E, m, m_1 can be represented by integers, each integer needing 4 Bytes, and hence one can store the time series of 10^6 observations with a storage of 12 MBytes, irrespective of the choices of L and D.

Multihistogram reweighting with respect to the bulk field H is crucial for the determination of the field $H_{\text{coex}}(T)$ in the $(H, T)_{\text{plane}}$ (cf. Fig. 10) along which two-phase coexistence occurs $T < T_c(D)$. The "equal weight rule"[117, 142, 145–147] is then applied: In the space of variables (E, m, m_1), the two phases show up as separate peaks of $P(E, m, m_1)$ [or $P(m, m_1)$, respectively, see Fig. 17(a), when one studies an isotherm one can integrate out E, of course]. These peaks have precisely the same weight at $H = H_{\text{coex}}(T)$ while for $H \neq H_{\text{coex}}(T)$ (but not too far away from it) the two peaks can still be identified but have different weights.

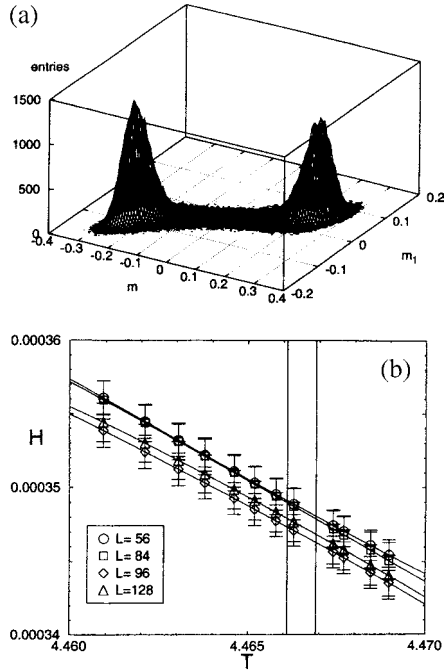

Fig. 17. (a) Unnormalized histogram $P(m, m_1)$ of a thin Ising film with $D = 32$, $L = 96$, $J_s/J = 1$, $H_1/J = 0.015$, $H/J = 0.00028$ at $k_BT/J = 4.471$, which is close to the two-phase coexistence line $H_{\text{coex}}(T)$. (b) Two-phase coexistence line in the plane of variables H/J and k_BT/J for $D = 28$, estimated for four different choices of L from the "equal weight" rule and indicating the statistical errors: The two vertical lines indicate the error interval of the critical temperature $T_c(D)$. Note that for finite L the distribution $P(m, m_1)$ also has a double-peak structure for T slightly above $T_c(D)$, as long as L does not exceed the correlation length ξ,[99] so there are also simulation data points for $T > T_c(D)$. From Dillmann *et al.*[125]

With multihistogram reweighting, a small number of simulation points suffices to generate the curve $H_{\text{coex}}(T)$ with reasonable precision, see Fig. 17(b). Since near $T_c(D)$ the free energy differences between the two phases are very small away from coexistence, the statistical error in the estimation of $H_{\text{coex}}(T)$ is not negligible. The systematic errors visible in Fig. 17(b) [curves for different L do not superimpose within their statistical errors] is due to the fact that the aspect ratio L/D for the smaller choices of L was not quite large enough. The estimation of $T_c(D)$ in Fig. 17(b) is deferred to Section 3.5.

One very simple method to improve the accuracy of the single spin-flip simulations is the technique of "preferential surface site selection":[100, 101] for the study of wetting transitions[126–131] and capillary condensation, spins located in lattice planes directly adjacent to the walls or close to the surface

are considered with a higher *a priori* probability for a spin flip than spins deep in the bulk. In this way one can concentrate most of the statistical effort into these regions of the system where the largest magnetization fluctuations occur. Conversely, for the problem of interface localization-delocalization one samples the lattice points close to $z = D/2$ most often, since very good sampling of the slow and sluggish interface fluctuations is needed.[66, 132–135] In a typical case with "preferential surface site selection" surface sites are visited 10 times more often than sites in the bulk.

At this point, we also mention the quantities that usually are recorded. The sampling of layer magnetizations m_1 and layer energies U_n is rather straightforward, and bulk quantities m_b, U_b and surface excess quantities m_s, U_s also follow from these profiles,

$$m_n = L^{-2} \sum_{i \in \text{layer } n} \langle S_i \rangle, \qquad m_b = \frac{1}{20} \sum_{n=11}^{30} m_n, \qquad U_b = \frac{1}{20} \sum_{n=11}^{30} U_n \tag{135}$$

where the specific example of indices quoted for m_b and U_b refers to a case where for $D = 40$ estimates for bulk quantities were extracted from the inner 20 layers of the thin film.[128] For the case of two equivalent surfaces, the excess quantities are

$$m_s = \frac{1}{2} \sum_{n=1}^{D} (m_b - m_n), \qquad U_s = \frac{1}{2} \sum_{n=1}^{D} (U_b - U_n). \tag{136}$$

Exploiting fluctuation relations we can define layer susceptibilities

$$k_B T \chi_n = L^2 D \left\{ \left\langle \frac{1}{L^2} \sum_{i \in n} S_i \frac{1}{L^2 D} \sum_j S_j \right\rangle - m_n m \right\}, \tag{137}$$

$$k_B T \chi_{nn} = L^2 \left\{ \left\langle \left[\frac{1}{L^2} \sum_{i \in n} S_i \right]^2 \right\rangle - m_n^2 \right\} \tag{138}$$

where in Eq. (137) m denotes the total magnetization of the film, $m = (L^2 D)^{-1} \sum_i \langle S_i \rangle$.

In the cases of interface localization-delocalization and capillary condensation, the total susceptibility of the thin film and the fourth-order cumulant of the magnetization were also studied,

$$k_B T \chi = L^2 D \left\langle \left[\frac{1}{L^2 D} \sum_i S_i \right]^2 \right\rangle - m^2, \tag{139}$$

$$U_L = 1 - \left\{ \left\langle \left[\frac{1}{L^2 D} \sum_i S_i \right]^4 \right\rangle \Big/ 3 \left\langle \left[\frac{1}{L^2 D} \sum_i S_i \right]^2 \right\rangle^2 \right\}; \tag{140}$$

and we shall see that these quantities are useful for the finite size scaling analysis to be discussed in the following section. Similarly, the total specific heat C_v is obtained from an analogous fluctuation formula for the energy,

$$k_B T^2 C_v = [\langle \mathscr{H}^2 \rangle - \langle \mathscr{H} \rangle^2]/L^2 D. \tag{141}$$

While finite size scaling is useful for both second-order and weakly first-order phase transitions, it is more convenient to locate transitions that are strongly first-order, and hence show pronounced hysteresis, by thermodynamic integration methods. This is done by considering two paths (1,2) where the temperature is varied from some starting value T_0 to the temperature T of interest while keeping the magnetic fields $H^{(1)}$, $H^{(2)}$ constant. These fields are chosen so that they correspond to phases with different sign of the magnetization, and we wish to locate the transition field $H_c(T)$ between these two phases.[131] The free energy difference per lattice site between the two states $(T, H^{(1)})$ and $(T, H^{(2)})$ is then ($\beta = 1/k_B T$ here, $\beta_0 = 1/k_B T_0$)

$$\beta \Delta F = \beta_0 \Delta F_0 + \int_{\beta_0}^{\beta} \Delta U(\beta')\, d\beta', \tag{142}$$

where $\Delta U(\beta')$ is the difference in total energy per lattice site between the two states at inverse temperature β! One must choose β_0 so low (e.g., $\beta_0 J = 1.2$) that thermal excitations in the reference states can be neglected and hence $\Delta F_0 \approx \Delta U(\beta_0)$. Free energy differences with respect to these states, $(T, H^{(1)})$ and $(T, H^{(2)})$, can then be constructed,

$$\Delta F^{(1)}(T, H) = -\int_{H^{(1)}}^{H} m^{(1)}\, dH', \quad \Delta F^{(2)}(T, H) = -\int_{H^{(2)}}^{H} m^{(2)}\, dH' \tag{143}$$

Although the total energy per lattice site clearly is always of order unity, $\Delta U(\beta)$ typically is of order 10^{-2} to 10^{-1}. Recording ΔU directly we measure small free energy differences easily and with high accuracy. Correspondingly, $H_c(T)$ could be estimated with a relative accuracy of a few percent or better.[131]

3.2. Finite Size Scaling Analyses of These Phase Transitions and Their Difficulties

Finite size scaling analysis of Monte Carlo results for model systems of statistical mechanics now is a standard tool.[94–99] Hence, we shall assume the reader is familiar with the basic physics behind this approach and focus

only on the difficulties which result from the crossover scaling between different universality classes that we have encountered in Section 2.3. For example, in the case of capillary condensation Eq. (92) or (97) can be extended by including the aspect ratio L/D as an additional scaling variable,

$$f_{\text{sing}}(D, T, H, H_1, L) \approx D^{-3} \tilde{f}(D^{1/\nu} t, L/D, HD^{\Delta/\nu}, H_1 D^{\Delta_1/\nu}). \quad (144)$$

Since for finite L, the free energy and its derivatives are smooth functions of $t = (T - T_{cb})/T_{cb}$, it is more convenient to use $D^{1/\nu} t$ rather than $x = D\,|t|^{\nu}$ as a scaling variable. From Eq. (144), we immediately obtain scaling forms for the specific heat, the magnetization, the susceptibility, and the fourth order cumulant of the thin film,

$$C_v = D^{\alpha/\nu} \tilde{C}(D^{1/\nu} t, L/D, HD^{\Delta/\nu}, H_1 D^{\Delta_1/\nu}), \quad (145)$$

$$m = D^{-\beta/\nu} \tilde{m}(D^{1/\nu} t, L/D, HD^{\Delta/\nu}, H_1 D^{\Delta_1/\nu}), \quad (146)$$

$$\chi = D^{\gamma/\nu} \tilde{\chi}(D^{1/\nu} t, L/D, HD^{\Delta/\nu}, H_1 D^{\Delta_1/\nu}), \quad (147)$$

$$U_L = \tilde{U}(D^{1/\nu} t, L/D, HD^{\Delta/\nu}, H_1 D^{\Delta_1/\nu}). \quad (148)$$

In the limit $L/D \to \infty$ the scaling functions $\tilde{C}$, $\tilde{m}$, $\tilde{\chi}$ and $\tilde{U}$ exhibit true singularities at values $D^{1/\nu} t_c$, $H_c D^{\Delta/\nu}$ corresponding to the capillary condensation critical point $T_c(D)$, $H_c(D)$, but all these singularities are rounded off for finite L/D. This means that both C_v and χ exhibit maxima of finite height at temperatures $T^c_{\max}(D)$, $T^{\chi}_{\max}(D)$ which will be displaced relative to $T_c(D)$. From Eqs. (145) and (147), one readily predicts (we omit here the dependence on the variable $H_1 D^{\Delta_1/\nu}$ which is held fixed, and on $HD^{\Delta/\nu}$; there is a shift of the maximum relative to $H_c(D)$ as well, as already shown in Fig. 17(b))

$$\frac{T^c_{\max}(D) - T_c(D)}{T_{cb}} D^{1/\nu} = \Delta\tilde{T}^c_{\max}(L/D), \quad (149)$$

$$\frac{T^{\chi}_{\max}(D) - T_c(D)}{T_{cb}} D^{1/\nu} = \Delta\tilde{T}^{\chi}_{\max}(L/D). \quad (150)$$

The cumulant U_L at $T = T_c(D)$ is not a universal constant but rather still a function of the aspect ratio L/D,

$$U_L(T = T_c(D)) = \tilde{U}(L/D)\,. \quad (151)$$

One can one expect $U_L = \tilde{U}(\infty) = U^*_{\text{2d Ising}} \approx 0.61$[148] only in the limit $L/D \to \infty$. In Eqs. (149), (150), and (151), the functions $\Delta\tilde{T}^c_{\max}$, $\Delta\tilde{T}^{\chi}_{\max}$ and

$\tilde{U}$ are non-trivial crossover scaling functions. From a related analysis[111] one can also predict the finite size behavior of the height of the maxima. One finds for $L \gg D$

$$C_V^{\max} \propto D^{\alpha/\nu} \ln(L/D) \tag{152}$$

$$\chi^{\max} \propto D^{(\gamma/\nu - \gamma_2/\nu_2)} L^{\gamma_2/\nu_2}, \tag{153}$$

and the vanishing of the absolute value of the order parameter at $T_c(D)$ is also of interest,

$$\langle |m - m(T_c(D), L/D \to \infty)| \rangle_{T=T_c(D)} \propto D^{(\beta_2/\nu_2 - \beta/\nu)} L^{-\beta_2/\nu_2}. \tag{154}$$

Because of Eq. (151), there is no longer a unique intersection point of the cumulants at $T = T_c(D)$. Figure 18 shows that this is indeed a serious problem:[125] the cumulant intersections are scattered considerably, and the associated ordinate value U^* differs considerably from the theoretical value.[148] Many of these crossing-points still differ from the actual critical temperature as in the case[125] $T_c(D)/J = 4.4665(4)$.

An alternative,widely used recipe to find the critical temperature involves the extrapolation of the locations of maxima in the specific heat and susceptibility, or of the cumulant intersection points, versus $L^{-1/\nu}$. Considering the intersection of $U_L(T)$ and $U_{bL}(T)$ with a scale factor $b > 1$,

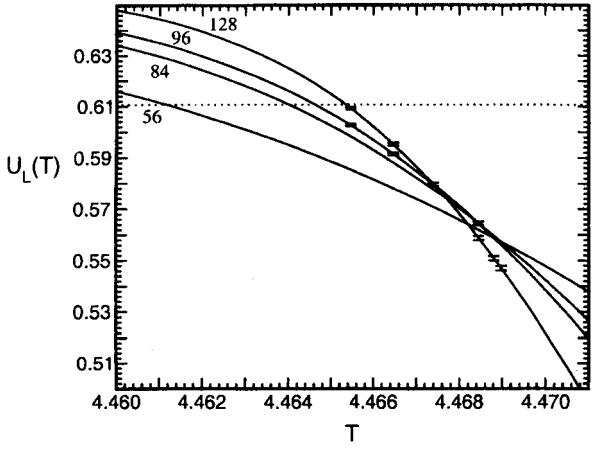

Fig. 18. Cumulants $U_L(T)$ plotted vs. T for $D = 28$ and various choices of L as indicated on the curves, for thin Ising films on the simple cubic lattice and $J_s/J = 1$, $H_1/J = -0.015$. H follows a path determined from the equal weight rule, as explained in Fig. 17 (for $D = 28$, $H_c(D)/J \approx 0.000348(3)$). The dotted line indicates the theoretical value U^* from Blöte *et al.*[148] From Dillmann *et al.*[125]

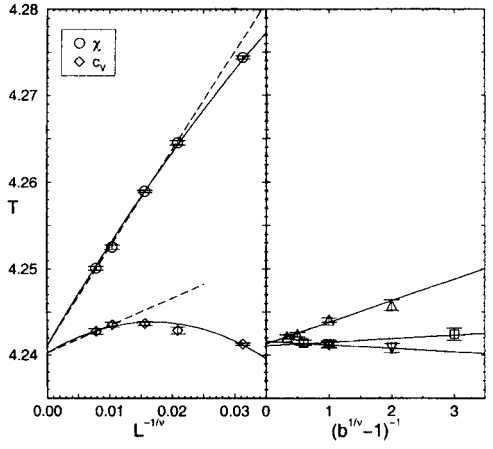

Fig. 19. (left part) Locations of specific heat maxima ($T^c_{\max}$: diamonds) and of susceptibility maxima ($T^\chi_{\max}$: circles) plotted vs $L^{-1/\nu}$ for $D=8$ using the same model as specified in Fig. 18. (right part) Cumulant intersection temperatures for $D=8$ plotted vs $(b^{1/\nu}-1)^{-1}$ for $L=32$ (triangles), $L=48$ (squares) and $L=64$ (inverted triangles). In the left part, the dashed curves show linear fits and the solid curves correspond to the master curves in Fig. 20. From Dillmann *et al.*[125]

we can argue[149] that corrections to finite size scaling lead to a shift of the intersection point that varies proportional to $[b^{1/\nu}-1]^{-1}$ for large b. Figure 19 shows an attempt to carry out such an extrapolation for $D=8$[125] (other choices of D look similar). In this case $T^c_{\max}$ approaches $T_c(D)$ in a non-monotonic fashion, and the curve of $T^\chi_{\max}$ vs. $L^{-1/\nu}$ is distinctly non-linear. Fitting asymptotic straight lines to both data sets one obtains results for $T_c(D)$ that are roughly compatible with each other and with the extrapolation of the cumulant intersection (Fig. 19). Although the accuracy of $T_c(D)$ obtained in this way is several orders of magnitude less than in the case of the bulk three-dimensional Ising model,[94, 116, 150] the data are accurate enough to allow a meaningful test of the scaling predictions, Eqs. (101).

The consistency of this analysis can be checked further by testing for the scaling behavior predicted in Eqs. (149) and (150), as demonstrated in Fig. 20. Here all data points are included for all values of D and L that have been studied[125] and $T_c(D)$ is chosen such that the best data collapse is achieved. The plot reveals the non-monotonic variation of the temperature at which the specific heat has its maximum is an intrinsic property of this scaling function, describing the system shape effects in terms of the aspect ratio D/L of the simulation box. The interpolating curves in Fig. 20 are simple parabolic fits which translate back into the solid lines in the left part of Fig. 19.

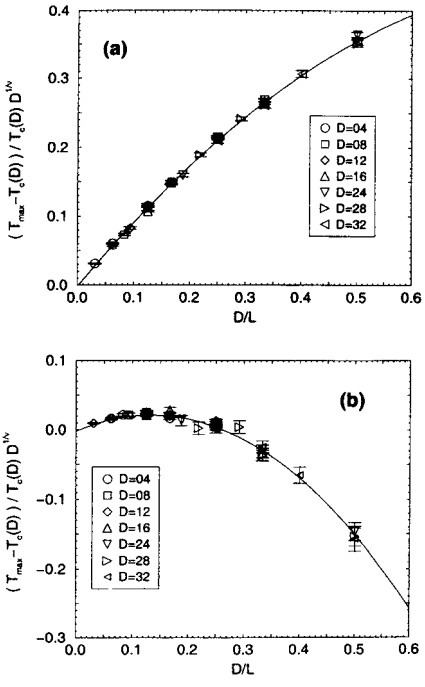

Fig. 20. Master curves for the temperatures of: (a) susceptibility maxima; (b) specific heat maxima, for simple cubic Ising thin films with $J_s/J = 1$ and a surface field $H_1/J = 0.015$ acting on both walls. In each case H is chosen from the equal weight rule (cf. Fig. 17). The curves are simple parabolic fits. From Dillmann *et al.*[125]

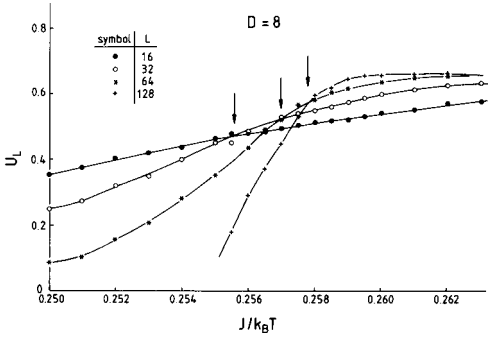

Fig. 21. Cumulants $U_L(T)$ plotted vs inverse temperature for thin Ising films on the simple cubic lattice for $D = 8$, $J_s/J = 1$, $H_1 = -H_D = -0.55J$, and several choices of L. The arrows indicate the locations of cumulant crossings of two neighboring lattice sizes. From Binder *et al.*[134]

While in the case of capillary condensation the proximity of $T_c(D)$ to the bulk critical temperature is intimately linked to the crossover between two- and three-dimensional critical behavior (and complicates the analysis of the respective Monte Carlo results),[125] in the case of the interface localization-delocalization transition one can choose H such that $T_c(D)$ is well below T_{cb}, with a correlation length ξ_b at $T_c(D)$ of the order of one or two lattice spacings, and the crossover towards bulk three-dimensional critical behavior plays no role. Furthermore, for the ideal antisymmetric case ($H_D = -H_1$) symmetry requires that phase coexistence for $T < T_c(D)$ occurs at $H = 0$, and hence no uncertainty due to possible inaccuracies in the estimation of $H_c(D)$ enters. Nevertheless, the data also reveal strong corrections to finite size scaling, and there is a huge scatter in the cumulant intersections (Fig. 21).[134] The accurate extrapolation of such locations of cumulant crossings is difficult, and the same is true for the locations of the maxima in specific heat and susceptibility (Fig. 22).[134] The final estimate for $T_c(D)$ suffered from appreciable error, $J/k_B T_c(D) = 0.2655 \pm 0.0002$, even for very thin films ($D = 6$) where rather large aspect ratios were studied (e.g., $L/D = 256/6$).[134] It was possible to obtain a reasonable data collapse in a finite size scaling plot with 2d Ising exponents[15] only for $D = 6$ and rather large values of $L (L \geqslant 128)$, as shown in Fig. 23. For $D = 8$ and $D = 12$, the analogous plots already exhibit rather systematic deviations from finite size scaling.[15] If corrections to finite size scaling were negligible, one would expect[94–99, 149] that the absolute value of the order parameter $\langle |m| \rangle$ and the cumulant $U_L(T)$ would scale as

$$\langle |m| \rangle L^{\beta_2/\nu_2} = \tilde{m}(L^{1/\nu_2} t), \quad \beta_2 = 1/8, \quad \nu_2 = 1, \quad t = 1 - T/T_c(D) \tag{155}$$

The exponent $\gamma_2 = 7/4$ arise from the asymptotic behavior of the scaling function $\tilde{m}$ for $t < 0$, since[149]

$$\langle |m| \rangle \propto \sqrt{\langle m^2 \rangle} = (k_B T \chi / L^2 D)^{1/2} \propto (-t)^{-\gamma_2/2}/L \tag{156}$$

and hence, using hyperscaling in $d = 2$ ($\beta_2/\nu_2 = 1 - \gamma_2/2\nu_2$) we find that

$$L^{\beta_2/\nu_2} \langle |m| \rangle \propto L^{-(1-\beta_2/\nu_2)} (-t)^{-\gamma_2/2} = (-t L^{\gamma_2/\nu})^{1/2}. \tag{157}$$

Noting that the finite size scaling of the cumulant $U_L(T)$ near $T_c(D)$ in $d = 2$ can be written as

$$U_L(T) = \tilde{U}(L/\xi_{\|}) \overset{t}{\approx}{}^{0} U^* - c^*(L/\hat{\xi}_{\|}^{+})\, t + o(t^2), \tag{158}$$

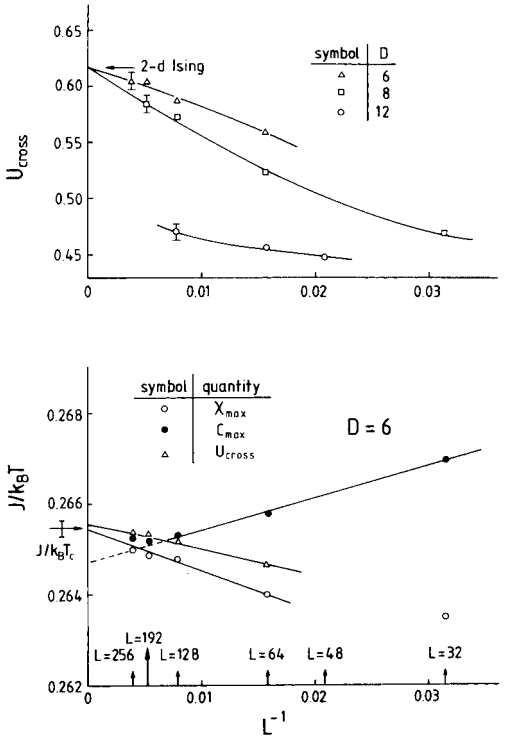

Fig. 22. (Upper part) Cumulant crossings U_{cross} plotted vs L^{-1} for thin Ising films of thicknesses $D = 6$, 8 and 12, $J_x/J = 1$ and $H_1 = -H_D = -0.55J$. Curves are only guides to the eye. The arrow indicates an estimate for the universal value U^* of the two-dimensional Ising universality class. (Lower part) Extrapolations of the temperatures of cumulant intersections, susceptibility maxima, and specific heat maxima for $D = 6$. The arrow (with error bar) marks the final estimate of $J/k_BT_c(D)$, while straight lines indicate possible extrapolations. From Binder *et al.*[134]

where c^* is another universal constant, we should, in principle, be able to estimate the dependence of the critical amplitude $\hat{\xi}_{\parallel}^{+}(D)$ on D from the slope of $U_L(T)$ in the plot versus Lt at $Lt = 0$ (Fig. 23(b)). Unfortunately, the scatter of the data makes such an analysis unwarranted in practice.

It turns out that all these problems with the finite size scaling analysis of second-order interface localization-delocalization phase transitions can be traced back to the Ising to mean field crossover alluded in Sections 2.2 and 2.3. A combination of crossover scaling (cf. Eqs. (125)–(134)) with the above finite size scaling description[15] is then needed. This means that the order parameter, the susceptibility, cumulant etc. become functions of two scaling variables[15] $t \exp(\kappa D/2)$, $L^{1/\nu}t$

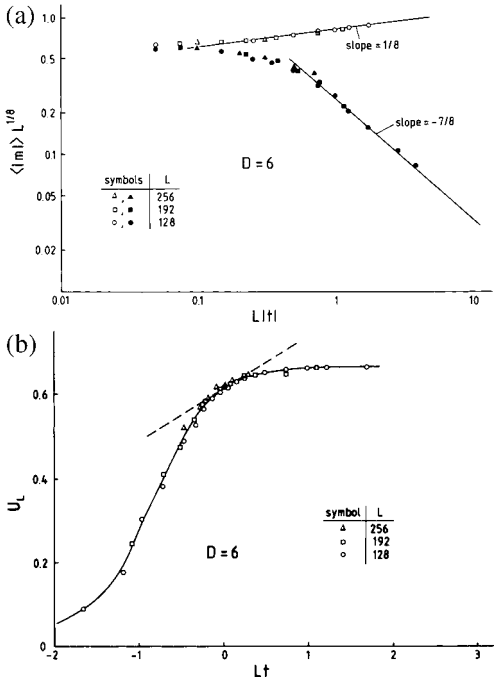

Fig. 23. (a) Log–log plot of $\langle |m| \rangle L^{1/8}$ vs. $L|t|$ for a thin Ising film with $D = 6$ and choosing other parameters as specified in Fig. 22. Data for $T < T_c(D)$ are shown by open symbols, data for $T > T_c(D)$ by full symbols. The straight lines were fitted using the correct values for the order parameter and susceptibility exponents ($\beta_2 = 1/8, \gamma_2 = 7/4$). (b) Cumulant $U_L(T)$ plotted vs. Lt for $D = 6$. The dashed line has the slope of the scaling function at $T = T_c(D)$ (i.e., at $Lt = 0$). The solid curve is a guide to the eye only. From Binder *et al.*[15]

$$\begin{aligned} \langle |m| \rangle \quad &= \quad \frac{1}{D} \exp(\kappa D/4)\, t^{1/2} \tilde{\tilde{m}}(t \exp(\kappa D/2), L^{1/\nu_2} t) \\ &\xrightarrow{\text{small } t,\ \text{large } L} \frac{1}{D} \exp(\kappa D/16)\, t^{1/8} \tilde{\tilde{m}}'(Lt) \\ &\xrightarrow{t=0} \quad \frac{1}{D} \exp(\kappa D/16)\, L^{-1/8} \end{aligned} \tag{159}$$

From reasoning of this type one recognizes that the amplitudes in front of finite size scaling power laws also vary exponentially with D. Of course,

t can be eliminated from one of the two scaling variables in Eq. (159), to yield[15]

$$\langle |m| \rangle = \frac{1}{D} \exp(\kappa D/16)\, t^{1/8} \tilde{\tilde{m}}(\exp(\kappa D/2), L, Lt)$$

$$\xrightarrow{t=0} \frac{1}{D} \exp(\kappa D/16)\, L^{-1/8} \tilde{\tilde{m}}_{\text{crit}}(\exp(\kappa D/2)/L) \tag{160}$$

Similarly, one can argue that the susceptibility at $T_c(D)$, or at the temperature $T_{\max}$ where it has its maximum, and the cumulant $U_L(T_c(D))$

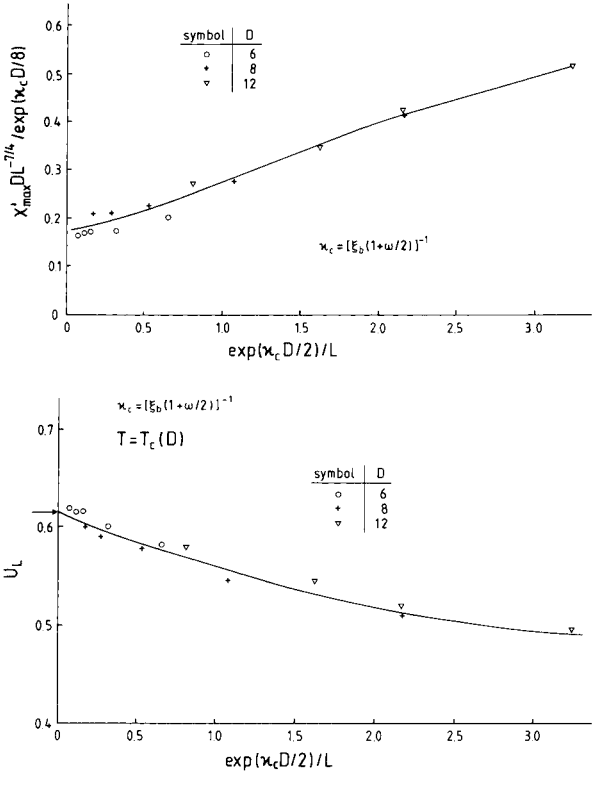

Fig. 24. Plot of the scaled susceptibility maximum $\chi'_{\max}$ (cf. Eq. (161)) and cumulant (Eq. (162)) vs. the crossover scaling variable $\exp(\kappa_c D/2)/L$ for $D = 6$, 8 and 12 and all lateral linear dimensions that were available. Here $\kappa_c = [\xi_b(1+\omega/2)]^{-1}$ was used. Curves are guides to the eye only. From Binder *et al.*[15]

become functions of a finite size crossover variable $\exp(\kappa D/2)/L$, i.e.,

$$\chi'_{\max} = L^2 D(\langle m^2\rangle - \langle |m|\rangle^2)/k_B T_{\max}$$

$$= \frac{1}{D}\exp(\kappa D/8)\, L^{7/4}\tilde{\tilde{\chi}}_{\max}(\exp(\kappa D/2)/L), \tag{161}$$

$$U_L(T) = \tilde{\tilde{U}}(\exp(\kappa D/2)/L, Lt) \xrightarrow{t=0} \tilde{\tilde{U}}_c(\exp(\kappa D/2)/L). \tag{162}$$

Figure 24 shows that the Monte Carlo data are reasonably consistent with these conjectured scaling results.

Yet other finite size effects are encountered for first-order interface localization-delocalization phase transitions.[66] If small enough systems are studied, such that the free energy barrier separating the phases that coexist at the first-order transition is overcome sufficiently often in the course of the simulation to produce meaningful statistics, one can indeed show that both $\chi'_{\max}$ and the specific heat maximum $C_{\max}$ show the expected scaling with the volume of the system,[66] i.e. (note that the volume is L^2D but we vary L at fixed D)

$$\chi'_{\max} \propto L^2, \qquad C_{\max} \propto L^2. \tag{163}$$

An example where this behavior is demonstrated is given in Fig. 25.

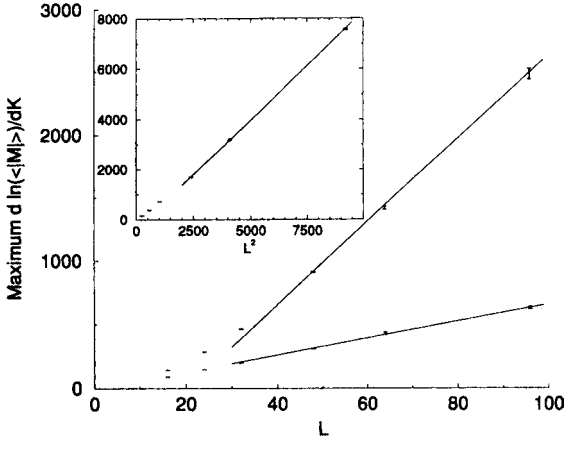

Fig. 25. Plot of the maximum $[\partial \ln(\langle |m|\rangle)/\partial K]_{\max}$, with $K = J/k_B T$, vs. L for thin Ising films with competing wall fields $H_1 = -H_D = -0.55J$ for $D = 6$ and three different choices of $J_s/J : J_s/J = 1.3$ (lower curve), $J_s/J = 1.45$ (upper curve) and $J_s/J = 1.5$ (inset). The theoretical behavior of second-order transitions in the 2d Ising universality class ($\propto L$) and for a first-order transition in the inset ($\propto L^2$) is indicated by the straight lines. From Ferrenberg *et al.*[66]

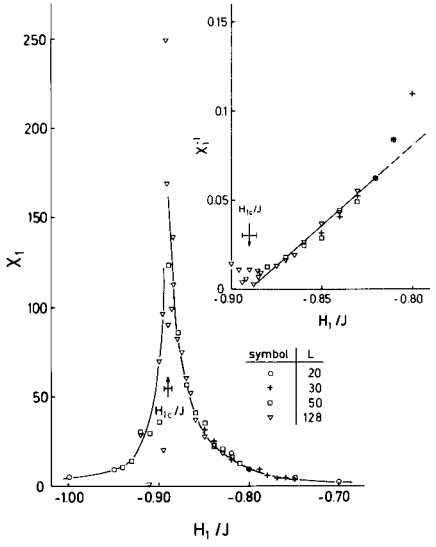

Fig. 26. Surface-layer susceptibility χ_1 plotted vs. surface field H_1 at $J_s = J$, $J/k_BT = 0.35$, and $H = 0$. The inset shows χ_1^{-1} plotted vs. H_1/J on an expanded scale. Several choices of L are indicated for $D = 40$. The arrow shows the resulting estimate for H_{1c}/J. From Binder *et al.*[129]

For the study of wetting transitions, a systematic finite size scaling analysis has not been attempted. Bear in mind that finite size effects in the direction perpendicular to the unbinding interface are quite different from effects in parallel directions (this fact has been demonstrated explicitly for interfaces between coexisting phases of polymer mixtures confined by "competing walls.")[151] Instead, the strategy that was followed was to choose rather large but fixed values of D, e.g., $D = 40$ for $J/k_BT = 0.35$. Of course, we cannot rule out the possibility that residual finite size effects associated with such a value of D are still present and introduce systematic errors in the results; however, in view of the inevitable, large statistical errors it would be very hard to analyze such effects. Then, L is varied and one attempts to identify parameters (large enough L, not too small $H_1 - H_{1c}$ or $|H|$, respectively) for which finite size effects can be neglected. Figure 26 shows a typical Monte Carlo data that have been taken for the study of second-order wetting transitions and indicates the accuracy that has been reached.

3.3. Critical Wetting with Short Range Forces

In this section, we briefly review the results[126–129] of thin film Ising models of Eq. (3) studied for $H_1 = H_D$ and various choices of inverse

temperature $K = J/k_BT$ as well as the ratio J_s/J between the exchange constant in the surface planes of the simple cubic lattice and the exchange constant in the bulk. In the Monte Carlo simulations the system geometry always was $L \times L \times D$ with periodic boundary conditions only in x and y directions. $D = 40$ layers were used for $K \geqslant 0.25$,[126–128] while closer to the bulk critical temperature thicker films were studied ($D = 80$ for $K = 0.23$ and $D = 160$ for $K = 0.226$ and $K = 0.224$, respectively; note $K_c = J/k_BT_{cb} \approx 0.22196$.[94, 150] The parallel linear dimension L was varied typically over some range up to $L = 128$ (details are given elsewhere.[128, 129])

Figure 27 shows "raw data" of Monte Carlo simulations where wetting was studied by varying H_1 for $J_s/J = 1$ at $K = 0.25$.[126] Initial states always had all spins pointing up, and the system then evolved towards a (metastable) equilibrium. Note that for $H_1 < 0$ and $H = 0$ the

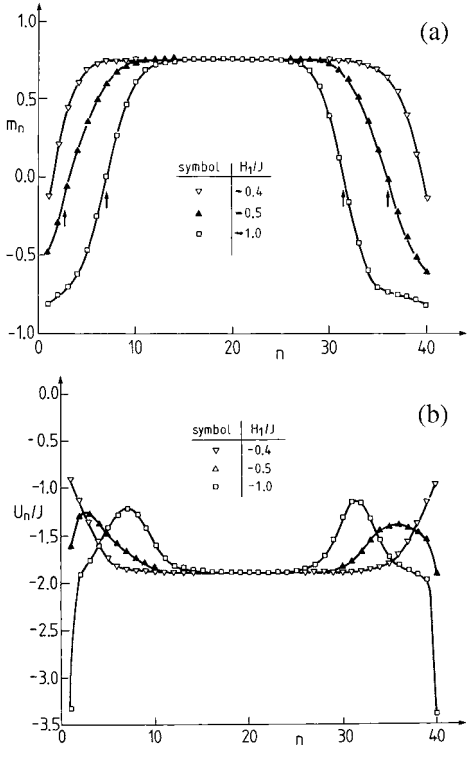

Fig. 27. Profile of (a) the layer magnetization m_n; and (b) the layer energy U_n across a thin Ising film with $H_1 = H_D$, for a $30 \times 30 \times 40$ lattice with $J_s/J = 1$ and $K = 0.25$, and three choices of the surface field. The arrows in (a) show the position where U_n (part (b)) has maxima. From Binder and Landau[126]

stable thermal equilibrium state of the film would have a negative magnetization in the bulk, but for large enough D the states with negatively magnetized surface layers and positive bulk magnetization have long enough lifetimes to produce meaningful averages in the simulations.[126–129] For the three choices of H_1 shown, the data in the central region (layer index n in the range $16 \leqslant n \leqslant 25$) are independent of H_1 and the values of m_n and U_n (Fig. 27) in that region agree very well with results obtained for bulk systems using fully periodic boundaries (so that there are no free surfaces). For $H_1 = -0.4J$ the magnetization m_1 at the surface is already slightly negative, but it is quite obvious that these data still belong to the non-wet regime of the surface. For $H_1 = -0.5J$ the magnetization at the surface is already strongly negative, and the magnetization profile exhibits an inflection point at a location which roughly corresponds to the location of the maximum of the energy profile. Thus, an interface is present near each surface, but it is clear that these interfaces are still bound to the respective walls. Note that $m_1 > -m_b$, while for $H_1/J = -1.0$ we find that $m_1 < -m_b$. In this case the energy profile also exhibits a nearly flat region between the maximum and the wall—the interface is unbound from the wall, characteristic for a state of wet surfaces. Of course, if we could simulate the system for sufficiently long, the interfaces would diffuse away from the walls until they ultimately met in the center of the film and annihilated each other. In this way the system would reach its stable thermal equilibrium state with uniformly negative magnetization. Thus, the Monte Carlo results on the "wet" side of the wetting transition have to be considered with some precautions: although quantities measured locally on the surface, like χ_1 (Fig. 26), look perfectly reasonable both for $H_1 < H_{1c}$ and for $H_1 > H_{1c}$, extrapolation from the non-wet side (Fig. 26) has been used to estimate the location of the wetting transition most precisely.

Figure 28 tests the theoretical predictions for the behavior of m_s (cf. Eqs. (52), (53) and (118)). Logarithmic variations of m_s when approaching the critical wetting transition from the non-wet side for $H = 0$ (case A) and when approaching the coexistence curve from the single phase region ($H \to 0$) on the wet side of the transition (case B) are clearly seen, as expected from the theory (cf. Section 2.3). However, the logarithmic laws tested in Fig. 28 are common to both mean field theories of wetting and the renormalization group treatment (cf. Eq. (118)). This means that a test of Eq. (121) is more interesting since the field dependence of χ_1 at $H_1 = H_{1c}$ should include the anomalous exponent $\nu_{\|}$ (remember $\nu_{\|} \approx 4$ is expected);[113] see Fig. 29. As a further check, $\Delta m_1 = m_1(H) - m_1(H = 0)$ is included, since $\Delta m_1 \propto H^{1-1/2\nu_{\|}}$ would also yield information about $\nu_{\|}$. Surprisingly, these data[129] (as well as earlier, less precise, data for $J/k_BT = 0.25$[127]) gave no clear indication of significant deviations from

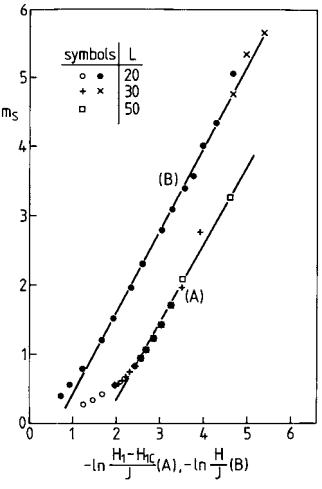

Fig. 28. Surface excess magnetization m_s plotted vs. $-\ln[(H_1-H_{1c})/J]$ for $J_s/J=1$, $J/k_BT=0.35$, $H=0$ (case A) and m_s plotted vs. $-\ln(H/J)$ for $J_s/J=1$, $J/k_BT=0.30$, $H_1/J=-1.0$ (case B). For case A, $H_{1c}/J\approx-0.89$, and for case B, $H_{1c}/J\approx-0.77$. From Binder *et al.*[127]

mean field theory but were compatible with $\nu_{||}=1$. Note that for $H/J\leqslant 0.002$ the slow onset of a crossover to a different power law is not ruled out (one would expect a much flatter curve for χ_1 and a correspondingly steeper variation of Δm_1 if $\nu_{||}=4$, namely $\chi_1\propto H^{-1/8}$, $\Delta m_1\propto H^{7/8}$!), and it has been suggested that the critical region where $\nu_{||}$ can ultimately be seen is extremely narrow.[73–76] Another possibility, which the Monte Carlo

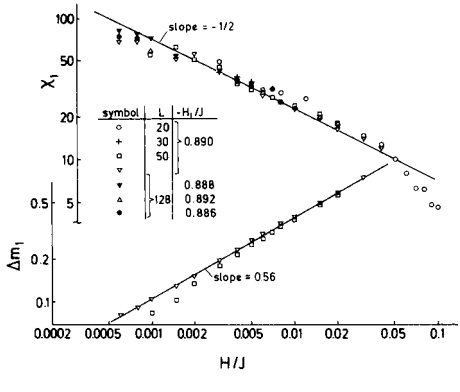

Fig. 29. Surface layer susceptibility χ_1 (upper part) and excess magnetization $\Delta m_1=m_1(H)-m_1(0)$ (lower part) on a log–log plot vs. bulk field at $H_1=H_{1c}$, $J_s=J$, $J/k_BT=0.35$. From Binder *et al.*[129]

data cannot rule out either, is that fluctuations could turn the wetting into a weakly first order transition[63]—however, the Monte Carlo data give no evidence of such behavior. At this point, it seems fair to say that the reason why the Monte Carlo simulations were unable to verify Eqs. (116)–(121) is not definitely known. It is possible that the "single-coordinate"-capillary wave Hamiltonian, Eq. (49) must be replaced by the more complicated "two collective coordinate"-theory, Eq. (89). Although this does not seem to change the final result for $\nu_{\|}$, it does suggest that the asymptotic regime for this fluctuation-dominated behavior is very small. Interestingly, a recent experiment where critical wetting with short range forces could be realized in a system,[152] where in a liquid binary mixture (methanol and alkanes) the wetting transition was tuned to occur very close to T_{cb}, gives only evidence for mean field behavior.

Fortunately, the Monte Carlo studies were rather successful in their attempts to check the various predictions made by Nakanishi and Fisher[13] about the behavior of the wetting phase diagram near the bulk critical point (Fig. 4). First of all, these verified that for the sufficiently strong surface exchange enhancement first-order wetting indeed occurs. Figure 30 presents an example.[128] The wetting transition is clearly of first order for $J_s/J \geqslant 1.25$, while the wetting tricritical point is close to $J_s/J = 1.2$. This conclusion is corroborated by an analysis of m_s, U_s and χ_{11} as well.[128] From such studies the locus of tricritical wetting transitions (Fig. 31) as well as the associated critical field (Fig. 32) could be estimated.[129] As predicted (cf. Eq. (115)), the line of tricritical wetting transitions for $T \to T_{cb}$ indeed extrapolates towards the surface-bulk multicritical point.[100] The singular variation near that point seen in Fig. 31 is compatible with

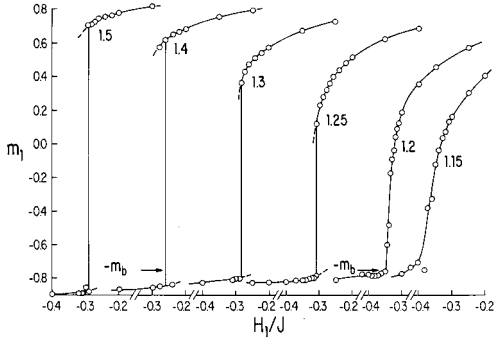

Fig. 30. Surface layer magnetization m_1 plotted vs. H_1/J at $J/k_BT = 0.25$ and several values of J_s/J as indicated. Arrows indicate the negative value of the bulk magnetization, $-m_b$. From Binder and Landau.[128]

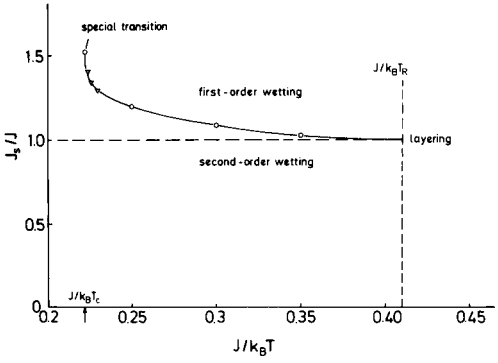

Fig. 31. Projection of the surface phase diagram onto the plane of variables J_s/J and J/k_BT, exhibiting the line of tricritical wetting transitions, separating the region of first-order wetting (above this line) from second-order wetting (below this line). The tricritical wetting line ends at J/k_BT_{cb} in the so-called "special transition" (or "surface-bulk multicritical point,") and at lower temperature it ends at the roughening temperature T_R, where layering transitions replace wetting.[14] From Binder *et al.*[129]

Eq. (115), with a crossover exponent ϕ close to $1/2$ ($\phi \approx 0.45$ gives the "best fit,"[129]) but an accurate estimation is precluded by the inaccuracy with which the surface exchange enhancement J_{sc}/J at the "special transition" is known.[100–103] Figure 32 shows that the critical fields H_{1c} at the critical and tricritical wetting transitions are also compatible with the expected power laws, $H_{1c} \propto (1-T/T_{cb})^{\Delta_1}$ and $H_{1t} \propto (1-T/T_{cb})^{\Delta_1^{SB}}$ as

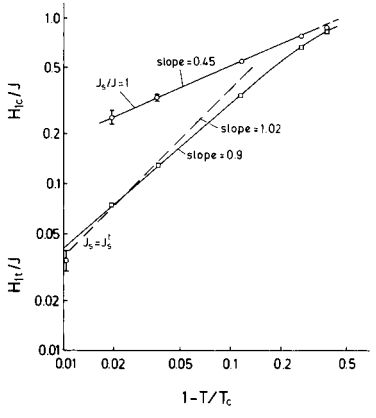

Fig. 32. Log–log plot of the temperature dependence of the critical field H_{1c} at the critical wetting transition for $J_s/J = 1$ (upper part) and at the tricritical wetting transition (lower part). Dashed and solid lines show possible power law fits and the corresponding (effective) exponents that can be extracted from these Monte Carlo data. From Binder *et al.*[129]

predicted in Eq. (114). The exponent estimates for Δ_1, Δ_1^{SB} that one can read off from Fig. 32 agree with expectations[7, 8, 100–104] to within a few percent.

3.4. Interface Localization-Delocalization in Ising Models

We first focus on Monte Carlo results for the case $J_s/J = 1$, where the corresponding wetting transition in the semi-infinite nearest-neighbor Ising model is of second order and occurs for $H_1/J = 0.55$ at $J/k_B T_w(H_1) \approx 0.25$ (cf. Section 3.3). As a typical example of the "raw data" from Monte Carlo simulations of the perfectly antisymmetric model ($H_D = -H_1$), Fig. 33 presents data for the layer energy U_n and layer susceptibility χ_{nn} for $D = 20$, for both $T > T_c(D)$ and $T < T_c(D)$[134] (order parameter profiles m_n and layer susceptibility χ_n for this choice of D can be found in the same reference,[134] along with data for other choices of D). Note that within the accuracy of this study, $T_c(D = 20)$ and T_w were hardly distinguishable, $J/k_B T_c(D = 20) = 0.2475 \pm 0.0015$. For $T > T_{cb}$, these profiles are essentially flat in the center of the film, while near the walls there is an inhomogeneity which decays proportional to $\exp(-z/\xi_b)$ when z is the distance from the wall, and ξ_b the correlation length in the bulk. For $T_c(D) < T < T_{cb}$, however, the profiles develop a clear peak in the center of the film, resulting from the presence of a fluctuating interface there, which separates the domain with negative magnetization (for $z < 0$) from the domain with positive magnetization (for $z > 0$). It is also obvious that for $T > T_c(D)$ the profiles are symmetric around $z = D/2$, which is the average position of the (delocalized) interface.

We recall that the system for $T_c(D) < T \lesssim T_{cb}$ is in a "disordered phase" only with respect to the symmetry-breaking interface localization/delocalization transition occurring at $T_c(D)$, where a spontaneous magnetization appears in the film as a whole (Fig. 6). Already at T_{cb} a rounded transition to the layered structure of two oppositely oriented domains, separated by an interface parallel to the walls, has occurred.

The picture is very different for $T < T_c(D)$. Now the symmetry around $z = D/2$ is clearly broken, and in Fig. 33 the interface is bound to the right wall of the film. Of course, for the strictly antisymmetric case ($H_1 = -H_D$) the situations with the interface bound to the left wall and the right wall are precisely equivalent and degenerate. In Fig. 33, the initial condition was chosen such that all spins pointed down in all layers except the layer $n = 20$ where the spins pointed up. The peak position $\langle z_{\max} \rangle$ of quantities such as χ_{nn} increases smoothly from $z = D/2$ (at $T = T_c(D)$) to larger values (slightly below $z = D$) as the temperature decreases.

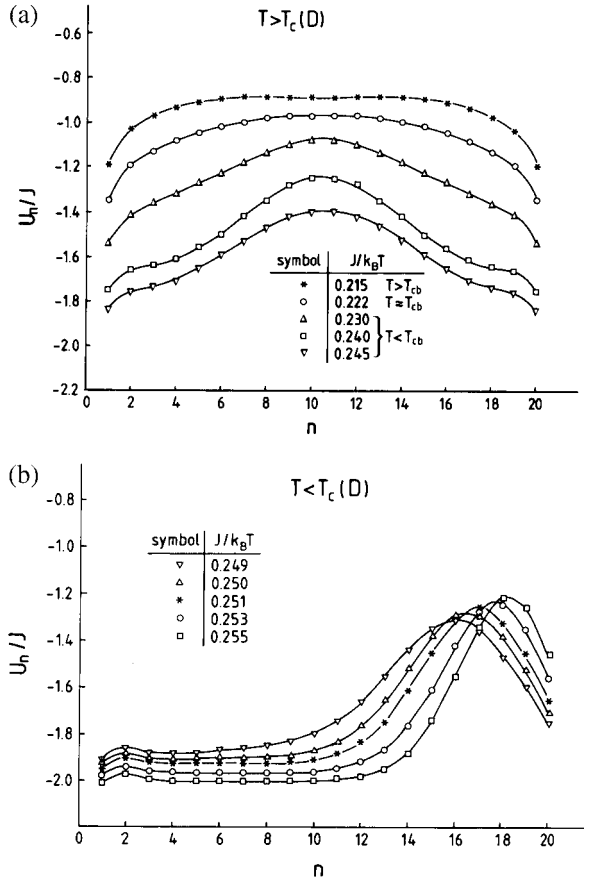

Fig. 33. Profiles of the layer energy U_n/J (a, b) and the layer susceptibility $\chi_{nn}J$ (c, d) plotted vs. layer number n, for thin Ising films of thickness $D = 20$ layers, $J_s/J = 1$, $H_1/J = -H_D/J = -0.55$, and several inverse temperatures J/k_BT, as indicated. Parts (a, c) refer to $T > T_c(D) \approx 4J/k_B$, parts (b, d) to $T < T_c(D)$. Curves through the simulation data are guides to the eye only. From Binder *et al.*[134]

While the position of the peaks of χ_{nn} (or χ_n) in Fig. 33 is a good estimate of the position of the interface, the width of these peaks should not be associated with the intrinsic width of the interface profile: the mean field estimate for the intrinsic width $2\xi_b$ of the interface would only be about 2 lattice spacings, while the width of the peaks in Fig. 33(c) and (d) is much larger. In fact, this width depends crucially on the film thickness D, as will be treated in detail below, and can (at least crudely) be accounted for in terms of capillary wave theory.

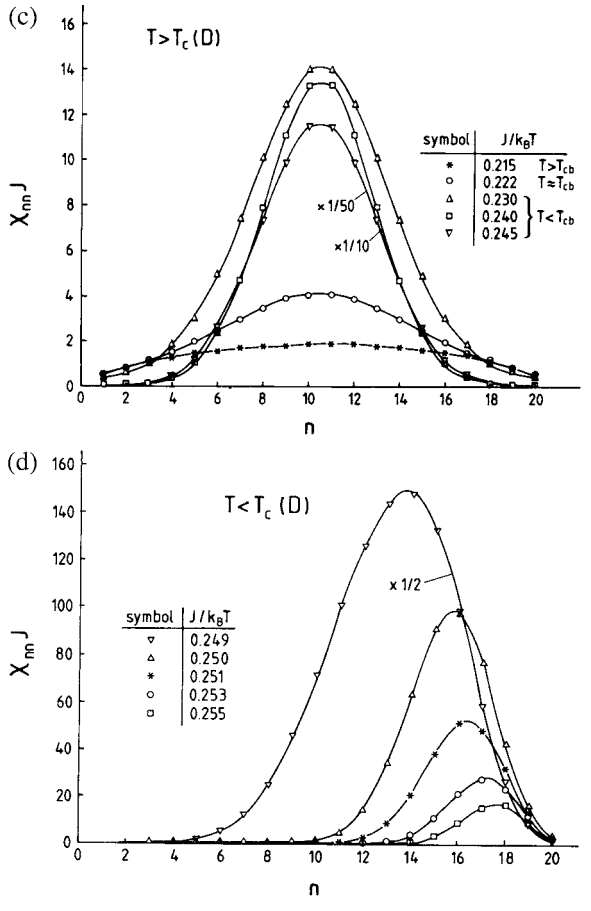

Fig. 33. *(Continued)*

As was discussed in Sections 2.2 and 2.3, the interface localization-delocalization phase transition can be viewed as a transition belonging ultimately to the universality class of the two-dimensional Ising model. Thus, plotting the energy of the thin film vs. J/k_BT (Fig. 34a), one would expect singular behavior in the slope of the E vs. T^{-1} curves at $T = T_c(D)$, reflecting the logarithmic divergence of the specific heat. However, Fig. 34 (a) reveals that within the accuracy of the study[134] reviewed here, hardly any anomaly could be detected. This finding does not mean that the expected logarithmic divergence of the specific heat is truly absent—the singularity is weak in the sense that the critical amplitude is very small, moreover there is very strong finite size rounding. This is demonstrated in

more detail for $D = 6$, which is the most favorable case for observation of the Ising-like critical behavior, as was argued in Section 2.3. on the basis of a crossover scaling analysis. But as Fig. 34(b) shows, even for a film as thin as $D = 6$, both the peaks of χ' and C are completely wiped out when linear dimensions $L = 32$ or $L = 64$ are chosen. For larger values of L, the peaks of χ' and C sharpen, as expected, but the statistical errors simultaneously become very large, making a qualitatively reliable analysis rather difficult, even in this case. The restriction to $L \geqslant 128$ is needed to allow verification of Ising behavior in a finite size scaling analysis,[15] cf. Fig. 23.

In the following, we focus on the behavior of the disordered phase, in the temperature region $T > T_c(D)$ but below the bulk critical temperature.

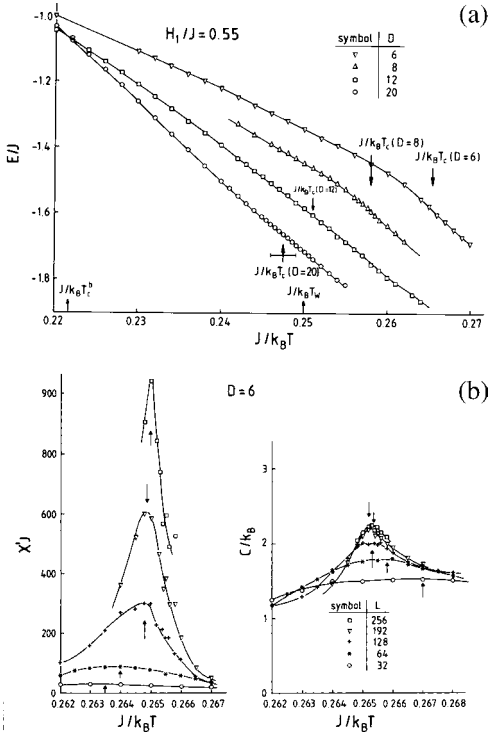

Fig. 34. (a) Internal energy per spin E/J of thin Ising films of thickness D with $J_s/J = 1$, $H_1 = -H_D = -0.55J$ plotted vs. inverse temperature for four film thicknesses. Arrows show the estimates for the critical temperatures $T_c(D)$ obtained from the finite size scaling analysis. All data shown are for linear dimension $L = 128$ in the directions parallel to the surfaces of the film. (b) Susceptibility $\chi' J = L^2 D(\langle m^2 \rangle - \langle |m| \rangle^2)\, J/k_B T$ (left part) and specific heat C/k_B (right part) of thin Ising films of thickness $D = 6$ plotted vs. $J/k_B T$, including L from $L = 32$ to $L = 256$. From Binder *et al.*[134]

The system is then locally ordered, with two domains of opposite magnetization coexisting in the system separated by an interface which can fluctuate more or less freely around its average position in the center of the thin film.[15, 16, 59] For large D the effective potential which favors the interface being located at $z = D/2$ is very weak, and displacing the interface homogeneously to the left or the right of this position is almost like a "soft mode." This property causes anomalously large response functions. In fact, both the total susceptibility of the thin film and the maximum value $\chi^{\max}$ reached by the layer susceptibility (in the center of the film for $T > T_c(D)$, cf. Fig. 33(c)) increase exponentially with film thickness D. such behavior is qualitatively consistent with the phenomenological analysis of Sections 2.2 and 2.3, (cf. Fig. 35).

Since theory has predicted (cf. Eq. (82)) that the critical amplitude of the susceptibility scales as $\exp(\kappa D/2)$, it is of interest to analyze the quantity $\ln(\chi_{nn}^{\max})/D$ to obtain an estimate for $\kappa/2$. Figure 36 shows that for $D \geqslant 12$ this quantity, when plotted against D, indeed levels off,[134] but the values of these plateaus disagree with the expected values $(2\xi_b)_{nn}^{-1}$ obtained

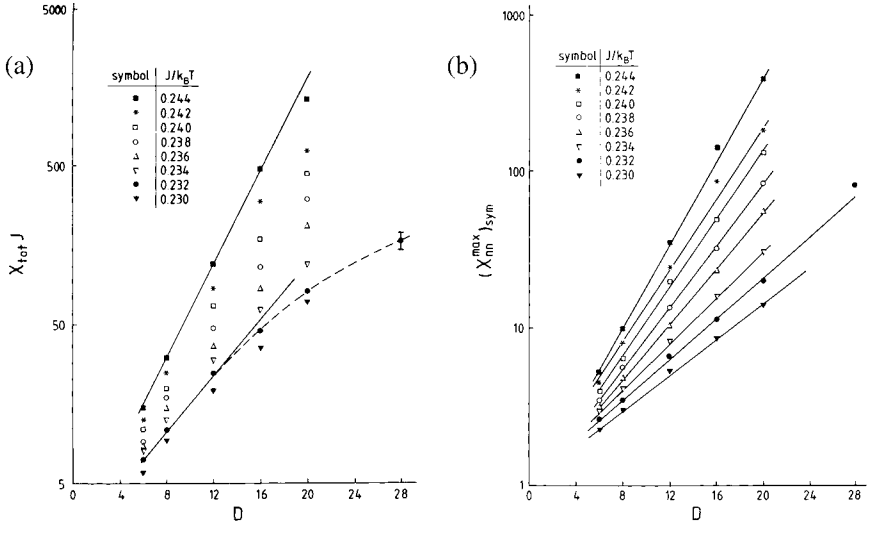

Fig. 35. Semi-log plot of the total susceptibility $\chi_{\text{tot}}J = L^2D\langle m^2\rangle/k_BT$ (a) and the layer susceptibility $(\chi_{nn}^{\max})_{\text{sym}}$, symmetrized with respect to the center of the film, plotted vs. the film thickness D at various temperatures T above the wetting temperature $T_w(H_1)$, for $H_1 = -H_D = -0.55J$ and $J_s = J$. Solid lines indicate an exponential variation. The broken curve in (a) is only a guide to the eye (note that the data point at $D = 28$ may suffer both from systematic errors due to the smallness of L and insufficient sampling time). From Binder *et al.*[134]

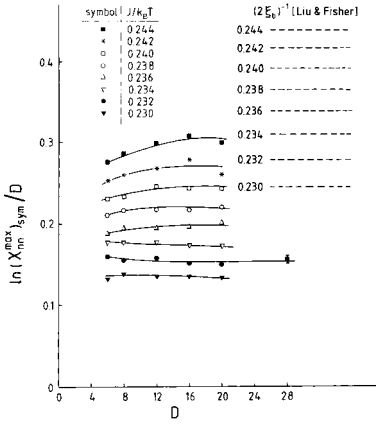

Fig. 36. Plot of $\ln(J\chi_{nn}^{\max})_{\text{sym}}/D$ vs. D, for thin confined Ising films with $J_s/J=1$, $H_1=-H_D=-0.55J$, and various temperatures in the range $T_w<T<T_{cb}$. Broken straight lines show the predictions of the corresponding asymptotic straight lines from the mean field theory of Parry and Evans,[59] namely $(2\xi_b)^{-1}$, using estimates from the series of Liu and Fisher[153] for ξ_b. From Binder *et al.*[134]

using estimates for the bulk correlation length ξ_b from series expansions.[153] This discrepancy is analyzed in Fig. 37 in more detail, where Monte Carlo data[154] for $(2\xi_b)^{-1}$ are also included to emphasize that this discrepancy is not due to problems with the accuracy of the series expansions. However, if one adopts the result of Parry *et al.*[86–91] (cf. Eqs. (89)–(91)) that the characteristic perpendicular length scale is effectively renormalized by a factor $(1+\frac{\omega+\Delta\omega}{2})$, where $\Delta\omega$ near T_w can be neglected, one concludes that $\kappa/2$ should not be $(2\xi_b)^{-1}$ but rather

$$\kappa/2=[\xi_b(2+\omega)]^{-1}. \tag{164}$$

Figure 37 shows that Eq. (164) is in reasonable agreement with the Monte Carlo data.[15] This choice for κ was then also used in the crossover scaling analysis (Fig. 24); use of $\kappa=\xi_b^{-1}$ in this crossover plot produces significantly worse data collapse.[15] Figures 36 and 37 hence constitute the first evidence that the extension of capillary wave theory (cf. Eq. (49)) from its simple one-collective-coordinate version to the two-collective coordinate description (89) is practically significant. Further evidence for Eq. (164) came from simulations of models for polymer mixtures[155] to be reviewed in Section 3.6.

Lastly, we discuss the problem of interpreting the width of the interface profile between coexisting phases in this regime, $T_w<T<T_{cb}$, where interface displacements show "soft mode" behavior. For short range

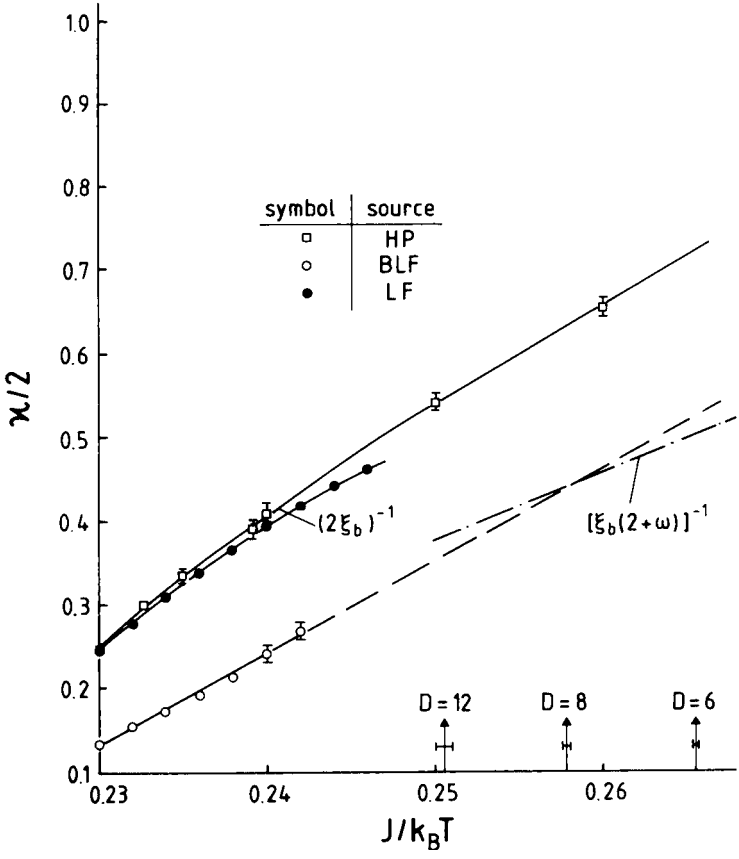

Fig. 37. Plot of the inverse length scale $\kappa/2$ vs. J/k_BT. Full dots represent estimates of $(2\xi_b)^{-1}$, ξ_b being the true correlation range in a lattice direction, obtained from the leading term of the Pade approximant to the low temperature series analysis of Liu and Fisher (LF).[153] Open squares are corresponding Monte Carlo estimates of Hasenbusch and Pinn[154] (HP), while open circles are the direct estimates of Binder, Landau, and Ferrenberg (BLF)[134] extracted from $\ln(\chi_{mn}^{\max})/D$, as shown in Fig. 36. The dash-dotted curve shows the suggested formula of Parry *et al.*[86-91] that $\kappa/2 \approx [\xi_b(2+\omega)]^{-1}$, where $\omega \approx 0.86$[113] was used. Arrows (with error bars) at the abscissa show location of $T_c(D)$ for $D = 12$, 8, and 6, respectively. From Binder *et al.*[15]

potentials between the walls and the interface, as considered throughout this article, there is a scaling law for the interfacial width[134, 151, 156, 157]

$$w^2 = w_0^2 + \frac{k_B T}{16\sigma}\kappa D + \text{const}, \tag{165}$$

where w_0 is the "intrinsic width" of the interface, and the additive constant is related to the short wave-length cutoff in the capillary wave spectrum and parameters of the effective Hamiltonian, Eq. (61). Since this constant is hard to estimate quantitatively, it often is neglected.[156] This is legitimate for large enough D. Figure 38 shows, however, that in the thin Ising films significant interface broadening does occur in the range from $D = 6$ to

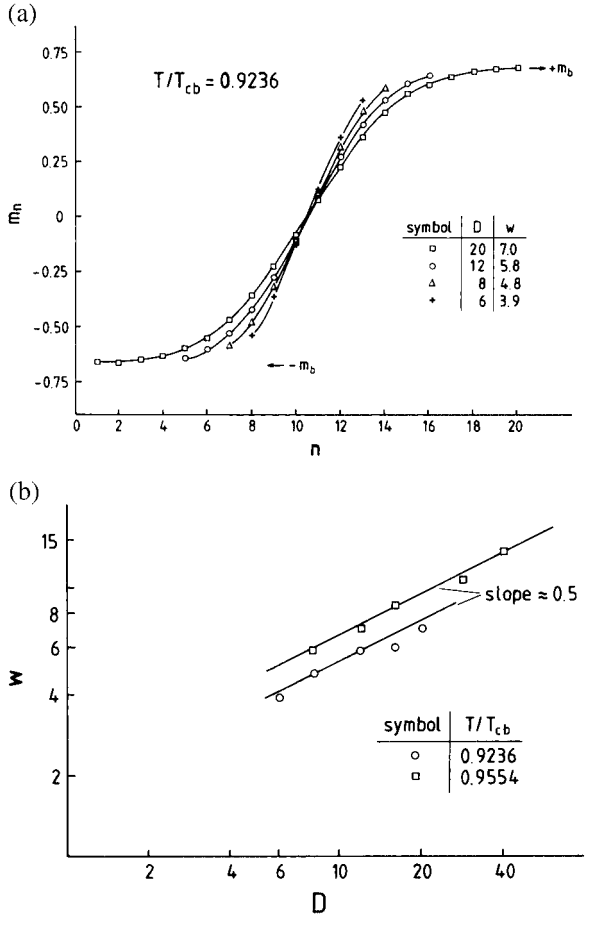

Fig. 38. Magnetization m_n in the nth layer of an Ising $L \times L \times D$ lattice, n labeling the lattice planes in z-direction, at $J/k_BT = 0.240$ ($T/T_{cb} \approx 0.9236$). The abscissa scales refers to the case $D = 20$; other values of D are plotted such that the profile mid-points coincide. Arrows show the values $\pm m_b$. Observed widths w are quoted in the figure. (b) Log–log plot of w versus D, including data from part (a) and analogous data for $J/k_BT = 0.232$ (i.e., $T/T_{cb} = 0.9554$). From Kerle *et al.*[156]

$D = 40$, and the asymptotic power law $w \propto \sqrt{D}$ holds down to such thin films as $D = 8$. Thus the "squeezing" of the intrinsic profile of the interface, Fig. 14, which should also be present in Fig. 38 since for $D \leqslant 8$ the magnetization profile m_n no longer reaches the bulk values $\pm m_b$ for $n = 1$ and $n = D$, affects only very thin films.

We briefly sketch the arguments that yield Eq. (165).[134, 151, 156, 157] We start from a convolution approximation to relate the apparent profile $m^{(\mathrm{app})}(z)$ to the intrinsic profile $m^{\mathrm{int}}(z-h)$, h being the interface position,

$$m^{(\mathrm{app})}(z) \approx \int_{-D/2}^{+D/2} \mathrm{d}h\, P(h)\, m^{(\mathrm{int})}(z-h). \tag{166}$$

For simplicity, the intrinsic profile is taken as the standard tanh-profile between coexisting bulk phases (i.e., the "squeezing effect" mentioned above is neglected) with the coordinate origin chosen to be in the center of the thin film,

$$m^{(\mathrm{int})}(z) = m_b \tanh(z/w_0) \approx m_b \operatorname{erf}[z\sqrt{\pi}/(2w_0)]. \tag{167}$$

Assuming then, consistent with Eq. (70), that $P(h)$ is a Gaussian,

$$P(h) = [2\pi\langle h^2\rangle]^{-1/2} \exp[-h^2/2\langle h^2\rangle], \tag{168}$$

we obtain

$$w^2 \approx w_0^2 + \frac{\pi}{2}\langle h^2\rangle = w_0^2 + \frac{k_B T}{4\sigma} \ln(\xi_{\|} q_{\max}), \tag{169}$$

where in the last step we equate $\langle h^2\rangle$ with the fluctuation $\langle(\delta l)^2\rangle$ obtained in Eq. (74). Using $\xi_{\|} \propto \exp(\kappa D/4)$, see Eq. (84), we obtain Eq. (165). This equation is in almost quantitative agreement with the Monte Carlo results for a range of temperatures,[156] showing once more the self-consistency of this analysis.

3.5. Capillary Condensation

In an early simulational study of capillary condensation in the Ising (lattice gas) model,[131] emphasis was not on the vicinity of the critical point $T_c(D)$ and $H_c(D)$ but instead on the behavior of the model at temperatures distinctly below criticality. Rather strong surface fields ($H_1/J = H_D/J = -0.75$ or -0.25, respectively) were chosen in order to have a situation where (in the corresponding semi-infinite system) a wetting transition occurs at temperatures distinctly below the bulk critical region.

In the following we review the most pertinent findings of this study, also using a "language" appropriate to the lattice gas interpretation of the Ising model, i.e., transforming the spin variable $S_i = \pm 1$ to a density variable $c_i = 0, 1$ according to $c_i = (1 - S_i)/2$. Then the local average density in the n^{th} layer parallel to the wall is denoted as $\rho_n = \langle c_i \rangle_{i \in n}$. Depending on the initial condition for the Monte Carlo runs, the confined fluid film is either a high density liquid or a low density gas with some rather strong density enhancement near the walls (Fig. 39). Although in the case shown for $D \to \infty$ and chemical potential $\mu \to \mu_{coex}$ the surface would be wet, i.e., the interfaces separating the wetting layers from the bulk should be unbound from the walls, the interface is still centered at the layer $n = 2$ which is immediately adjacent to the wall. Thus for small D (and for non-zero values of $\mu - \mu_{coex}$ of interest, where the gas phase in the thin film geometry is still stable) the wetting phenomena are completely rounded off. However, the tendency to form wetting layers causes pronounced asymmetry between the profiles of the two coexisting phases (Fig. 40), and this asymmetry is also seem in the corresponding isotherms (Fig. 41) where the total density is plotted as a function of the chemical potential difference. From the pronounced hysteresis seen in these curves it is clear that accurate location of the transition can only be achieved from a knowledge of the free energies of the two phases obtained from thermodynamic integration methods, as described in Section 3.1. A particular consequence of the

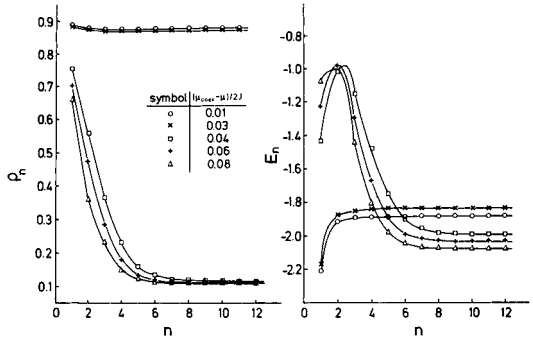

Fig. 39. Density profile ρ_n (left part) and energy profile E_n (right part) for a capillary of thickness $D = 24$ at $k_B T/J = 4.0$, for the case $H_1/J = -0.75$, and several choices of the bulk field $H/J = (\mu_{coex} - \mu)/(2J)$ [Note that in the lattice gas model, the chemical potential μ at the coexistence curve is known exactly, $\mu_{coex} = 2qJ$, q being the coordination number of the lattice]. For the corresponding semi-infinite system, $k_B T_w/J = 3.30 \pm 0.01$, i.e., at $k_B T/J = 0.40$ the surface would be wet for $\mu = \mu_{coex}$. Profiles are symmetric around the middle of the film, so only layers from $n = 1$ to $n = D/2$ are shown. Note that solid curves are guides to the eye only. From Binder and Landau.[131]

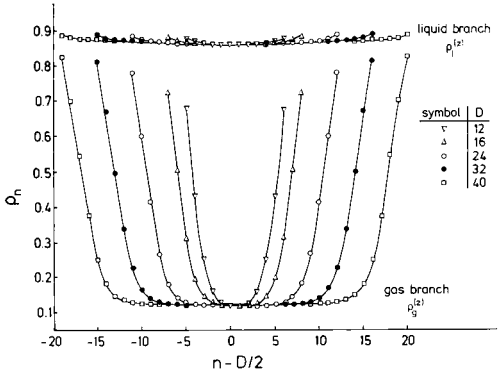

Fig. 40. Layer density profiles ρ_n plotted vs. n for five choices of D and the chemical potential μ chosen for each D to be at exact phase coexistence between a liquid branch (upper part) and a gas branch (lower part). Parameters $J_s/J = 1$, $H_1/J = H_D/J = -0.75$ and $k_BT/J = 4.0$ were chosen throughout. From Binder and Landau.[131]

asymmetry of the isotherms (note that for a symmetric mixture in the bulk, considered here, the isotherms are antisymmetric around the point $\rho = 1/2$, $\mu = \mu_{\text{coex}}$ in the bulk) is that the magnitude of the density jumps in Fig. 41 is much smaller than in the bulk.

From isotherms as shown in Fig. 41 we obtain the phase diagram of the thin film both in the (T, μ) plane and in the (T, ρ) plane,[131] see Fig. 42. In the temperature T-field H plane the phase diagram has precisely

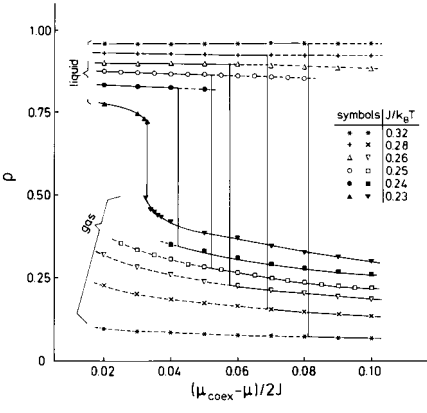

Fig. 41. Average density ρ of a capillary of thickness $D = 16$ plotted vs.the chemical potential difference, for $J_s/J = 1$, $H_1/J = -0.75$, and several temperatures, as indicated in the figure. The first-order transitions are indicated by the vertical straight lines; metastable states are shown by broken curves. From Binder and Landau.[131]

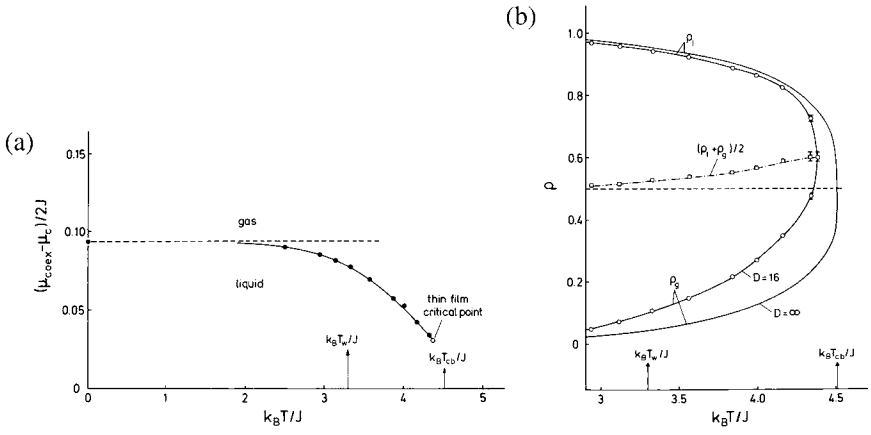

Fig. 42. (a) Phase diagram of a capillary of thickness $D = 16$ for $J_s/J = 1$ and $H_1/J = -0.75$. The broken straight line gives the asymptotic low temperature value of the chemical potential at which liquid-gas coexistence occurs. Arrows indicate the location of the bulk wetting transition k_BT_w/J and the bulk critical temperature k_BT_{cb}/J, respectively. Full dots indicate transitions located from thermodynamic integration. The full curve is a guide to the eye only. (b) Liquid-gas coexistence curve for a capillary of thickness $D = 16$ and a wall potential $H_1/J = -0.75$ compared to the bulk coexistence curve ($D = \infty$). Arrows indicate the location of the bulk wetting transition k_BT_w/J and the bulk critical temperature T_{cb}. The "rectilinear diameter," constructed from the liquid density (ρ_l), and the gas density (ρ_g), ($\rho_d = (\rho_l + \rho_g)/2$), is shown by the dot-dashed line. Error bars are only shown when they exceed the size of the symbols. From Binder and Landau.[131]

the shape expected on general grounds (cf. Fig. 10, where the opposite sign of H_1 was assumed, however). For a thin film, e.g., $D = 16$, the second-order wetting transition at T_w does not cause any anomaly in the phase diagram; however, the situation should be different for first-order wetting transitions where a triple point is predicted to occur for large enough D, when the remnant of the prewetting transition line meets the capillary condensation transition of the bulk film.[29, 131] Figures 43 and 44 describe this situation in a schematic way, but no systematic Monte Carlo studies of the Hamiltonian Eq. (3) are yet available to probe this behavior.

We now turn to a test of the Kelvin equation, Eq. (104), which we rewrite here in the notation appropriate for a liquid-gas system

$$\mu_{\text{coex}} - \mu = \frac{2}{D} \frac{\Omega_{gs}(T, \mu_{\text{coex}}, H_1) - \Omega_{ls}(T, \mu_{\text{coex}}, H_1)}{[\rho_l - \rho_g + (2/D)(\rho_{ls} - \rho_{gs})]}, \tag{170}$$

where Ω_{gs}, Ω_{ls} are the surface excess contributions of the grand potential in the gas (g) or liquid (l) phases, ρ_l, ρ_g are the bulk densities and ρ_{ls}, ρ_{gs} the

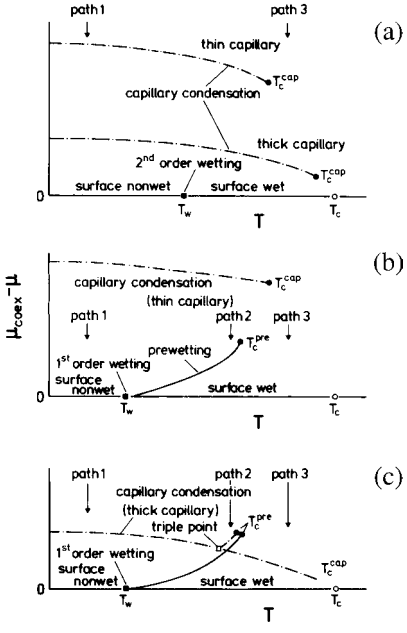

Fig. 43. Schematic phase diagrams for wetting and capillary condensation in a thin film lattice gas model i.e., a slitlike capillary. (a) refers to a case where an equivalent semi-infinite system has a second-order wetting transition at T_w and $\mu = \mu_{coex}$. The dash-dotted curves show the capillary condensation phase transition at $\mu = \mu_c(D, T)$, ending at a capillary critical point $T_c^{cap} = T_c(D)$. The model Eq. (3) studied in this section always yields this type of phase diagram if $J_s = J$. The paths indicated by arrows refer to the corresponding isotherms shown in Fig. 44. (b) and (c) refer to a case where a semi-infinite system undergoes a first-order wetting transition at T_w and $\mu = \mu_{coex}$, as in the model of Eq. (3) for $J_s > J$, cf. Fig. 31. Then for $\mu < \mu_{coex}$ a transition may occur when the thickness of an adsorbed layer at the wall jumps from a small finite value to a larger finite value (prewetting), cf. Fig. 44. For thin capillaries (b) this transition no longer exists since $\mu_{coex} - \mu_c(D, T)$ is too large, while for very thick capillaries a remnant of this prewetting transition persists (c). Full dots denote two-dimensional critical points, open circles show bulk three-dimensional criticality, full squares denote wetting transitions, and the open square denotes a capillary triple point. From Binder and Landau.[131]

surface excess densities in the respective phases. From Monte Carlo data[131] one recognizes (Fig. 45) that the relation $\mu_{coex} - \mu_c(T, D) \propto D^{-1}$ is indeed very well fulfilled if the surfaces of the capillary are in the non-wet part of the surface phase diagram (i.e., $T < T_w(H_1)$), while for $T > T_w(H_1)$ pronounced curvature in the plot is present. Expecting that $\rho_{gs}(\mu) \propto |\ln(\mu_{coex} - \mu)|$ for a wet surface of a semi-infinite system, Binder and Landau[131] argued that the term $-\rho_{gs}$ in the denominator of the above

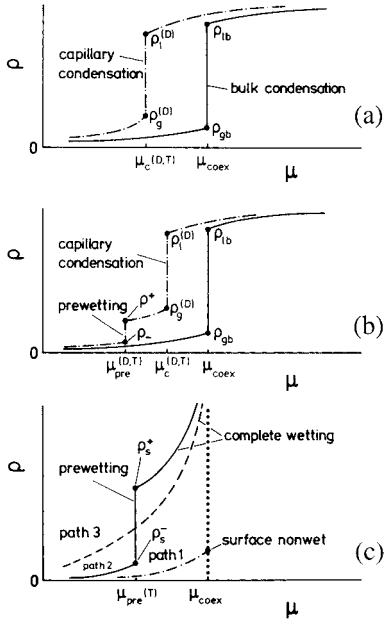

Fig. 44. Schematic isotherms corresponding to the transitions along the paths shown in Fig. 43. Cases (a) and (b) plot the density ρ vs. chemical potential μ for a bulk system (full curves) and a capillary (dash-dotted curves), while (c) shows the variation of the surface excess density ρ_s of a semi-infinite system for comparison (compare also Fig. 2, lower part). (a) refers to cases where a prewetting line is not crossed [cf. Fig. 43(a) and 43(b)], while (b) refers to case (c) of Fig. 43 where an isotherm crosses a prewetting line at $\mu_{coex}(D, T)$. Then a transition from a thin adsorbed film to a thicker adsorbed film occurs at the walls of the capillary, corresponding to a jump in the overall density in the capillary from ρ_- to ρ_+. This prewetting transition does not show up in the average density of a bulk semi-infinite system but only in its surface excess density ρ_s (c). This quantity also distinguishes non-wet surfaces, $\rho_s(\mu_{coex})$ being finite, from wet surfaces, $\rho_s(\mu \to \mu_{coex}) \to \infty$, cf. Fig. 2. From Binder and Landau.[131]

equation actually should be singular, i.e., $-\rho_{gs} \propto \ln D$. Hence the leading correction to the Kelvin equation in the wet regime should be of order $(\ln D)/D$. This idea is tested in Fig. 46, but a plot of $D(\mu_{coex} - \mu)$ vs. $(\ln D)/D$ gives only a slightly better fit to a straight line than does a plot vs. $1/D$. More precise simulation data over a large range of D would be desirable to clarify this point. We also note that an alternative but equivalent, and very elegant, formulation of this problem was given by Parry and Evans[158] who describe the shift of the transition as follows,

$$\mu_{coex}(D, T) - \mu \propto \frac{1}{D - 2l[\mu_c(D, T)]}, \tag{171}$$

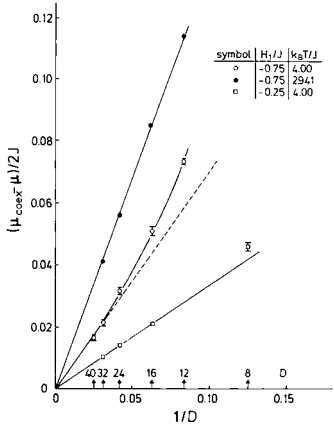

Fig. 45. Plot of the shift of the chemical potential $\mu = \mu_c(T, D)$ relative to μ_{coex} at the liquid-gas condensation transition in the thin film versus inverse thickness $1/D$ of the capillary. Two temperatures and two choices of the wall potential H_1/J are included. In the case $H_1/J = -0.75$, $k_BT/J = 4.00$ the surface of a semi-infinite lattice gas system would be wet, while otherwise it is non-wet. Error bars are only shown when they exceed the size of the points. The curve through the open circles is only a guide to the eye to demonstrate the deviation from the straight line (dashed). From Binder and Landau.[131]

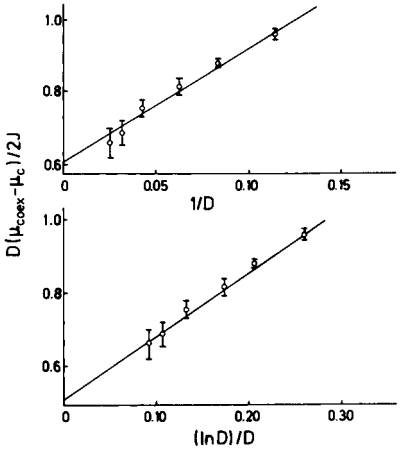

Fig. 46. Plot of $D(\mu_{\text{coex}} - \mu_c(T, D))/2J$ vs. $1/D$ (upper part) or $(\ln D/D)$ (lower part), for the nearest-neighbor Ising lattice gas model with $k_BT/J = 4.0$, $J_s = J$, and $H_1/J = -0.75$. From Binder and Landau.[131]

where l is the distance of the liquid-gas interface from the wall. The physical interpretation of this equation is that it is only the thickness $D-2l$ available to the gas for condensation that matters. Since $\ln D$, l and ρ_{gs} are proportional to each other for large D, this formula also suggests that the leading correction is of order $(\ln D)/D$.

However, for practically realizable D subleading corrections (of order $1/D$) also may be rather important. Such terms occur, e.g., in the mean-field theory of capillary condensation in type I-superconductors.[159]

To complete this section, we turn to the test of the Fisher–Nakanishi[24, 25] scaling relations Eqs. (98) and (99) for the shift of the capillary condensation critical point. Due to the enormous statistical effort required, a very precise estimation of the critical point for $H_1/J = -0.75$ was very difficult even for films as thin as $D = 16$ (cf. Fig. 42), and because of this no attempt could be made in the early study[131] to locate the critical point for larger D. Dillmann *et al.*[125] reconsidered this problem, but chose a much smaller surface field ($H_1/J = 0.015$) so that they could use a cluster algorithm (Section 3.1). From the finite size and crossover scaling analysis already described in Section 3.2, $H_c(D)$ and $T_c(D)$ could be extracted for $4 \leqslant D \leqslant 32$;[125] but log–log plots of $H_c(D)$ and $T_c(\infty)-T_c(D)$ vs. D show small but significant deviations from linear behavior. Such deviations are

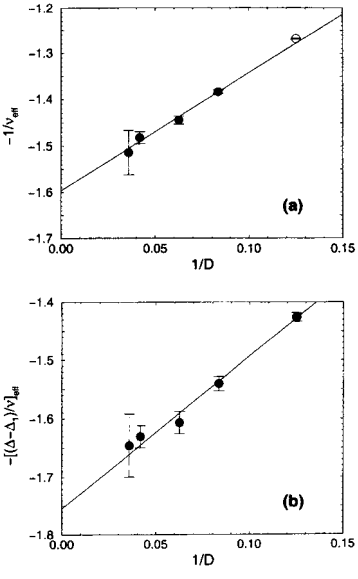

Fig. 47. Plot of $-1/\nu_{\text{eff}}$ (a) and of $-[(\Delta-\Delta_1)/\nu]_{\text{eff}}$ (b) vs. $1/D$. For further explanations cf. text. From Dillmann *et al.*[125]

to be expected, of course, since the asymptotic regime where corrections to finite size scaling are negligible has not yet been reached for the range of linear dimensions used. Thus, better results are obtained by fitting effective exponents using only three successive thicknesses ($D = 4$, 8, 12; $D = 8$, 12, 16,...; $D = 24$, 28, 32), which can be extrapolated versus $1/D$ reasonably well. The results converge nicely towards the theoretical predictions (Fig. 47), namely $-1/\nu \approx -1.587$ and $-(\Delta - \Delta_1)/\nu \approx -1.75$. Very roughly, the two-dimensional Ising critical behavior could also be verified in the vicinity of these transition points, but only for the very thin films such as $D = 6$ and $D = 8$.[125] Studies using larger D, which then would require substantially larger lateral linear dimensions L for the finite size scaling analysis, would be very desirable but are clearly very difficult.

3.6. Simulation of a Lattice Polymer Model

The general features of wetting, interface localization-delocalization and capillary condensation are universal, i.e., they do not depend on the details of the underlying model but rather on the dimensionality and the range of interactions. Consequentially, most of the simulation work has focused on the Ising model due to its computational efficiency. In this subsection, however, we shall discuss wetting in binary polymer blends within the framework of the bond fluctuation model.[160] Being interested in the universal behavior, we represent the long extended macromolecules by chains of N coarse grained monomers on a simple cubic lattice. Each monomer blocks the eight corners of a cube from further occupancy, and monomers along a chain are connected by one of 108 bond vectors. There are two species of monomers, denoted A and B. Monomers of the same type attract each other via a square well potential of depth ϵ/k_BT which extends over the nearest 54 lattice sites, while monomers of different types repel each other with the same interaction energy. Much is known about the phase behavior[161, 162] In the following we restrict ourselves to symmetrical mixtures, i.e., both chains have identical chain length and architecture. The mixture is confined in a thin film by two hard impenetrable walls. These attract A monomers which are less than 2 lattice spacings away with an energy $\epsilon_w (> 0)$, and repel B monomers in this region with the same strength. This bond fluctuation model[160, 161] captures the relevant features of dense polymer mixtures, while retaining the computational advantages of a lattice model. Many methodological advances in Ising model simulations can be readily applied to the complex fluid mixture. The model can be simulated in the semi-grandcanonical ensemble[163] by "flipping" the identity of an entire chain from A to B, or vice versa. The chemical exchange potential $\Delta\mu$ corresponds to a bulk magnetic field in the Ising model.

Analogous to the Ising model, histogram extrapolation techniques[144] have been employed to estimate the properties at parameters in the vicinity of the simulation point, and much of the finite size scaling techniques (e.g., cumulant intersection method) carry over from simple lattice models.[164]

The simulation of these complex fluids is computationally much more demanding than simulating the Ising model. For instance, calculating the energy change for "flipping" the identity of a whole chain which is comprised of N monomers, each of which interacts via a square well potential which extends over 54 lattice sites, is computationally much more costly than flipping a spin with 6 neighbors on a cubic lattice. Additionally, the conformations of the chains on the lattice have to be equilibrated. Nevertheless, these complex fluids offer, at least in principle, particular advantages:

- In the strong segregation limit interface and surface tensions are independent of the chain length N, and so the wetting transition also occurs at a temperature which is independent of N. This is in marked contrast to the critical point of the polymer mixture. Due to the low entropy of mixing, the critical temperature T_c of the bulk increases linearly with N; hence, the wetting transition temperature is typically lower than the critical temperature by a factor N and the wetting transition is typically of first order. Only interface fluctuations then play a role, the bulk phases are completely segregated into pure A and pure B phases. In the Ising model this separation is more difficult to achieve because of the roughening transition at $T_R/T_c \approx 0.54$.

- Owing to its size, a polymer interacts with many neighbors. This is quantified by the degree of interdigitation $\bar{N} = (\rho R_e^3/N)^2$, where $\rho = 1/16$ is the monomer density and $R_e \approx 3.05\sqrt{N}$ is the chain's end-to-end distance for the simulations presented below. Except for the immediate vicinity of the critical point, the phase behavior of the bulk is accurately described by mean field theory. Moreover, the degree of interdigitation $\bar{N}$ offers a convenient way to reduce the capillary parameter ω, which scales like $1/\sqrt{\bar{N}}$.

In the following we shall focus on the consequences of a strongly first-order wetting transition on the phase behavior in a thin film.

First Order Wetting. Measuring a strongly first-order wetting transition via the metastability of a microscopically thin layer of the preferred phase at the surface might be inaccurate. Rather than determining the wetting transition temperature, one obtains an estimate for the wetting spinodal (cf. Eq. (56)). Therefore we determine the location of the wetting

transition via the Young equation.[1] Let A be attracted by the surface by a potential $\epsilon_w > 0$. The A-component wets the surface if $\Delta\sigma \equiv \sigma_{BW} - \sigma_{AW} = \sigma_{AB}$, where σ_{AW} and σ_{BW} are the surface tension of the wall in contact with the A-rich and B-rich phase, respectively, and σ_{AB} is the interface tension between the coexisting bulk phases. The latter can be measured accurately in the Ising[149, 165] or polymer models[81, 155] via reweighting techniques. If the two coexisting phases are symmetric—like in our polymer model or the Ising model—the difference in the surface tensions $\sigma_{BW} - \sigma_{AW}$ can be determined very accurately by realizing that $\Delta\sigma$ equals the difference of the tension between a surface, which attracts the A component σ_{AW} in contact with an A-rich bulk and the tension of a surface, which attracts the B component $\sigma_{AW\_}$ in contact with an A-rich bulk. This difference can be accurately measured via thermodynamic integration

$$\Delta\sigma = \frac{1}{L^2} \int_{-\epsilon_w}^{\epsilon_w} \mathrm{d}\epsilon'_w \, \frac{E_w(\epsilon'_w)}{\epsilon'_w} \tag{172}$$

where E_w denotes the interaction between the components and the wall, and L the lateral system extension.[4] If the wetting transition is strongly first-order, the thickness of the B-rich surface layer remains always very thin (even for $\epsilon'_w = -\epsilon_w$), and hence the typical configurations do not differ strongly along the path of the integration—a fact which makes the method particularly convenient. If the wetting transition was only weakly first-order (or second-order) a thick layer of B would gradually build up as we decreased ϵ'_w to $-\epsilon_w$ and the equilibration times would be considerably longer. In Fig. 48 we exemplify how to locate the wetting transition via the Young equation.[1] From the intersection of the curves we can read off the wetting transition temperatures for different strengths of the surface interactions. The fact that the curves intersect at a finite angle indicates first-order wetting transitions. With decreasing strength of the surface interactions, the wetting transition temperature increases towards the critical temperature of the bulk and becomes weaker; but for all values ϵ_w investigated, we find first-order transitions.

Phase Diagram in Thin Films. The phase diagram of a thin film with symmetric and antisymmetric surface fields is presented in Fig. 49 and compared to the bulk phase behavior. The pronounced influence of the first-order wetting and the concomitant prewetting can be readily observed. In the vicinity of the critical points, the binodals have been extracted from the Monte Carlo data[65, 155] via a finite size scaling analysis (cf. Section 3.2).

[4] Alternatively, we can determine the free energy difference via simulation in an expanded ensemble, where ϵ_w is a Monte Carlo variable.

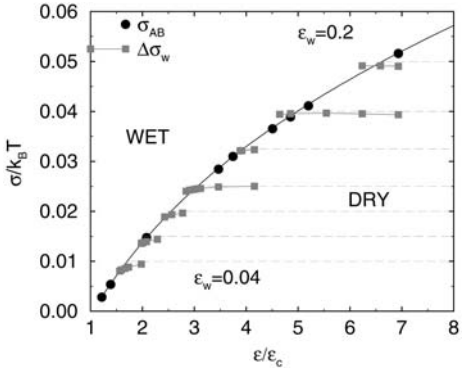

Fig. 48. Locating the wetting transition via the Young equation. The solid line with circles represents the interface tension between the coexisting phases as a function of the scaled inverse temperature $\epsilon/\epsilon_c = T_{cb}/T$. The squares indicate the difference in the surface free energy $\Delta\sigma$. Different curves correspond to different surface interactions ϵ_w (decreasing from top to bottom). The dashed horizontal lines correspond to the simple estimate $\Delta\sigma = 4\rho\epsilon_w$, which ignores the possibility of an enrichment layer and packing effects of the polymer fluid. From the intersection points we accurately estimate the wetting transition temperature. From Müller and Binder.[155]

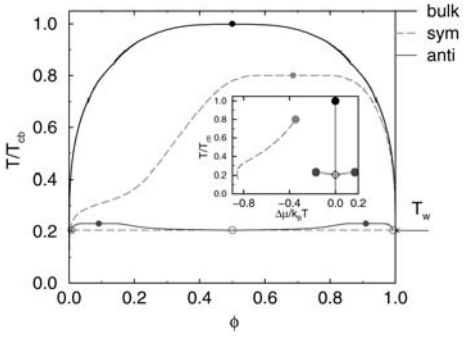

Fig. 49. Phase diagram of a binary polymer blend in the bond fluctuation model with chain length $N = 32$. The upper curve shows the binodals in the infinite system, the middle one corresponds to a thin film of thickness $D = 48 \approx 2.8R_e$ and symmetric boundary fields $\epsilon_w = 0.16$, which both attract species A. The lower curve corresponds to a thin film with antisymmetric surfaces. The arrow marks the location of the wetting transition as located via the Young equation. Full circles indicate critical points, open circles and dashed horizontal line denote the triple point. The inset presents the phase diagram as a function of temperature and exchange potential. Circles mark critical points, and the diamond indicates the wetting transition temperature. On the scale of the figure it is indistinguishable from the triple temperature of the film. Note that the wetting transition occurs at low temperatures $T_w/T_{cb} = 0.2$. From Müller and Binder.[65]

The coexistence value of the chemical potential has been determined via the equal weight rule.[146]

In the case of symmetric surface fields, the critical point is shifted to lower temperatures and larger composition of the A-component. This is qualitatively similar to the behavior of the Ising model. Since a single phase diagram costs about 50,000 h of single processor CPU-time on a CRAY T3E, we have not attempted to study the dependence of the critical point of the film thickness or the strength of the surface fields but instead have focused on the signature of the first-order wetting transition in a thin film. For symmetric surface interactions the A-poor binodal exhibits a "bulge" in the vicinity of the wetting transition temperature. In the A-poor phase there is a thin enrichment layer of A at the wall, while the B component prevails in the middle of the film. The composition profile across the film is similar to Fig. 40, which shows the corresponding data for the Ising model. As we increase the temperature and pass through the wetting transition temperature, the AB interface is repelled from the surface and this gives rise to the change in curvature of the A-poor binodal. The coexistence chemical potential as a function of temperature is shown in the inset of Fig. 49. The repulsion of the AB interface and the growth of the A-enrichment layer manifest themselves in a change of the temperature dependence of the coexistence chemical potential. For the film thickness considered in the Monte Carlo simulations, the coexistence curve does not intersect the prewetting line. If the film were thicker, the phase diagram would exhibit a second two-phase region, which would correspond to the coexistence of a thin and a thick layer of A on the prewetting line (cf. Fig. 43).[29, 166] While it is computationally too expensive to explore this by Monte Carlo simulations, this has been corroborated by self-consistent field calculations[155] for our polymer model. As Nakanishi and Fisher[24, 25] have pointed out, the wetting transition of the semi-infinite system is completely rounded by the finite thickness of the film, but the prewetting transition can give rise to a phase transition in thin films. Indeed, if the wetting transition is second-order (cf. the results for the Ising model in Fig. 41(b)), there is no prewetting line and the binodals in a thin film do not exhibit a signature of the wetting transition.

The phase diagram for antisymmetric surface fields is also shown in Fig. 49. At high temperatures enrichment layers of the components are gradually built up at the corresponding surfaces and an AB interface, which runs parallel to the surfaces, is stabilized in the middle of the film. Lateral phase separation occurs only below the prewetting critical temperature. If the wetting transition is of first order and the film thickness sufficiently thick (cf. Section 1) the interface localization-delocalization transition is of first order and there are two two-phase coexistence regions, which

merge below a triple point. Below the triple temperature, there is a single two phase region. The simulations corroborate the qualitative features of the phenomenological considerations of Section 1.

In experiments, the idealization of strictly symmetric or strictly antisymmetric surface interactions is difficult to realize. Hence, one might ask the question which degree of asymmetry is permissible without losing the features of capillary condensation or interface localization-delocalization. The crossover between the two qualitatively different types of phase diagrams is also interesting in itself. Unfortunately, there are no Monte Carlo data from the Ising model or the polymer model available and we resort to mean field calculations for the polymer model.

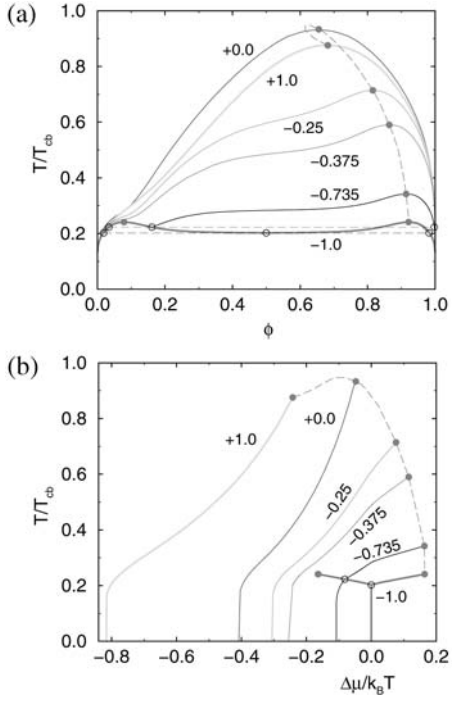

Fig. 50. Phase diagram of a binary polymer blend for $D = 2.6R_e$ within mean field approximation. (a) The binodals as a function of the relative strength of the surface interactions (as indicated in the key): $+1$ corresponds to capillary condensation, 0 corresponds to one surface not having any preference, and -1 corresponds to interface localization-delocalization. Circles mark critical points, open symbols and dashed horizontal lines correspond to triple points. (b) Phase coexistence as a function of the chemical potential and temperature. The "quasi-prewetting" lines for ratios -0.735 and -1 and $\Delta\mu < 0$ are indistinguishable, because they are associated with the surface with fixed interaction. From Müller *et al.*[21]

In Fig. 50 we show how the phase diagram depends on the asymmetry of the surface interactions. The bottom surface always attracts the A-component of the mixture and the semi-infinite system exhibits a first-order wetting transition. We tune the interaction of the top surface from attracting A with the same strength than the bottom to attracting B. As we reduce the preference of the top surface for species A, the critical point and the critical composition tend towards their bulk values, i.e., the critical temperature increases and the critical composition becomes more symmetric. The coexistence curve in the T-$\Delta\mu$ plane approaches the symmetry axis. Upon making the top surface attractive for the other component B, we gradually change the character of the phase transition towards an interface localization-delocalization transition. In this case there are enrichment layers of the A-component at the bottom and the B-component at the top, and the two coexisting phases differ in the location of the AB interface which runs parallel to the surfaces. As the preferential interaction of the top surface increases, the critical temperature decreases and the critical composition becomes richer in A. When the coexistence curve intersects the prewetting line of the bottom surface at $\Delta\mu < 0$, a triple point forms at which an A-rich phase and two B-rich phases with a thin and a thick A-enrichment layer coexist. When the bottom surface attracts A with exactly the same strength as the top surface attracts B (antisymmetric surfaces), the phase diagram becomes symmetric.

It is interesting to ask how for asymmetric surface interactions, such as shown in Fig. 50 for a confined polymer mixture, or for an Ising model with $J_S > J_{SC}$, $H_1/H_D = \lambda$, the limit $D \to \infty$ is approached. No numerical calculations were performed for this case, but we can mention a plausible speculation: For $D = \infty$ one has wetting transition temperatures $T_w^{(1)}$ and $T_w^{(D)}$ for $-1 \leqslant \lambda < 0$, which coincide only for $\lambda = -1$, while for $\lambda \to 0$ $T_w^{(1)} \to T_{cb}$. When $T < T_w^{(D)}$, the interface is bound either to the left wall ($z \to 0$) or the right wall ($z \to D$). At $T = T_w^{(D)}$, a first order interface unbinding at the right wall ($z \to D$) occurs, and in the phase diagram the prewetting line appears. For $0 \leqslant T \leqslant T_w^{(1)}$ there is a two-phase coexistence between states of opposite order parameter ($\pm m_b$) in the "thick" film ($D \to \infty$). The part of the same two-phase coexistence line from $T_w^{(1)} < T < T_{cb}$ appears discontinuously as the limit $D \to \infty$ is taken, but is not yet present in the phase diagram for arbitrarily large but finite D, because of the rounding of the transition at T_{cb} (note also that for very large but finite D there is also a shift of this two-phase coexistence away from $\Delta\mu = 0$ by an amount of the order $1/D$ in the whole region $0 \leqslant T \lesssim T_w^{(1)}$. At $T_w^{(1)}$ a second prewetting line occurs in the limit $D \to \infty$, which ends in another prewetting critical point. While this prewetting line joins at $T_w^{(1)}$ the coexistence line (at $\Delta\mu = 0$) for $D \to \infty$ with a kink, for

very large but finite D this kink is rounded off, and the bulk two-phase coexistence (which was at $\Delta\mu = 0$ for $D \to \infty$) and the two-phase coexistence along the prewetting line join smoothly into a common two-phase coexistence line, along which the character of the two-phase coexistence gradually changes from bulk-type to prewetting-type. The end point of this line (which becomes the prewetting critical point $T_c^{\mathrm{pre}(1)}$ for $D \to \infty$) for finite D is the thin film critical point $T_c^{(1)}(D)$ which differs from the critical point $T_c^{(D)}(D)$ related to prewetting-type phase separation at the other wall of the film. For $\lambda \to 0$ also $T_w^{(1)} \to T_{cb}$, of course, and for $\lambda > 0$ and $D \to \infty$ we would have again a wetting transition temperature $T_w^{(1)} < T_{cb}$ and a prewetting line $T_c^{\mathrm{pre}(1)}$, but now on the same side of the line $\Delta\mu = 0$ as the other prewetting line ending at $T_c^{\mathrm{pre}(D)}$. Irrespective of the sign of λ for large but finite D the bulk transition at T_{cb} and the wetting transition $T_w^{(1)}$ disappear because of finite size rounding. While $T_w^{(D)}$ changes its character from a wetting transition into a thin film triple point, $T_c^{\mathrm{pre}(D)}$ for finite D changes its character from critical prewetting into a thin film critical point $T_c^{(D)}$. Note that the asymmetry in the behavior near T_{cb} for $\lambda > 0$ and $\lambda < 0$ has a simple physical meaning: for $\lambda > 0$ a phase transition is possible from a state with no interface to a state with two interfaces parallel to the walls; for $\lambda < 0$ there is a single interface parallel to the walls, and, hence, no phase coexistence is possible.

Finite Size Scaling at Finite Thickness D in the Vicinity of the Tricritical Interface Localization-Delocalization Transition. Upon reducing the film thickness, we reduce the critical temperatures for the antisymmetric film and the two two-phase regions extend over a smaller temperature range. At a film thickness D_t (cf. Section 2.3), the two critical points merge and there is a tricritical interface localization-delocalization transition. For even smaller film thickness the transition is of second order. This behavior has been studied by Monte Carlo simulations of the bond fluctuation model,[65] as will be briefly reviewed next.

An example of the behavior of the cumulant $\langle m^2 \rangle / \langle |m| \rangle^2$ of the order parameter $m = \phi_A - \phi_B$ as a function of the inverse temperature for a thin film ($D \approx 0.84 D_t$, cf. Eq. (65)) is presented in Fig. 51. For the limited range of lateral system sizes L, which are accessible in our simulations, the cumulants yield a reasonably well defined intersection point around $\epsilon / k_B T = 0.059(1)$. The value of the cumulant at the intersection point differs, however, from the universal value of the 2d Ising universality class. This fact indicates pronounced corrections to scaling. Comparing the probability distribution of the order parameter (normalized to unit variance and norm) at our estimate of the critical temperature to the universal distribution of the 2d Ising universality class, we identify the reason. For

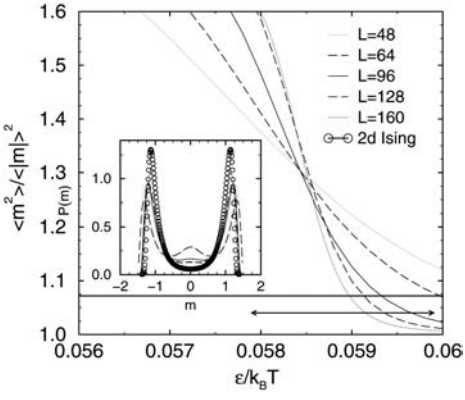

Fig. 51. Cumulant intersection for a binary polymer $N = 32$ confined into a film with antisymmetric surfaces ($D = 12, \epsilon_w = 0.16$). Our estimate of the critical temperature $\epsilon_c/k_BT = 0.0589(10)$ is indicated by the double arrow. The horizontal line marks the universal cumulant value for the 2d Ising universality class. The inset presents the distribution function of the order parameter at our estimate of the critical temperature, and compares the Monte Carlo data to the universal distribution of the 2d Ising universality class (circles). From Müller and Binder.[65]

small lateral system sizes, the probability distribution is not bimodal—like the 2d Ising curve—but exhibits a third peak at symmetrical composition $m = 0$. The three-peak structure of the probability distribution is characteristic of the distribution at a 2d tricritical point. If we monitored the distribution for a small lateral system size (e.g. $L = 48$) only, the distribution would never resemble the 2d Ising curve but would always show a three peak structure in the temperature range of interest, i.e., the lateral system size is so small that it does not exceed the correlation length at the crossover from the 2d tricritical to the 2d Ising critical behavior. As we increase the lateral system size, the concomitant finite size rounding sets in at a smaller distance from the critical point, the central peak gradually disappears and the distribution function approaches the shape of the 2d Ising curve. This change gives evidence for the crossover from 2d tricritical to 2d Ising behavior (cf. Section 2.2 and Fig. 16) and signals the vicinity of the tricritical film thickness D_t.

The probability distribution of the order parameter is also useful for locating the tricritical transition. To this end we have extrapolated the results of different film thickness to a temperature such that the central peak is a factor 1.2 higher than the outer peaks. This value corresponds to the behavior of the universal distribution of the 2d tricritical universality class.[167] The results of this procedure for various film thicknesses are presented in Fig. 52. For $D < D_t$ the valleys between the three peaks are too

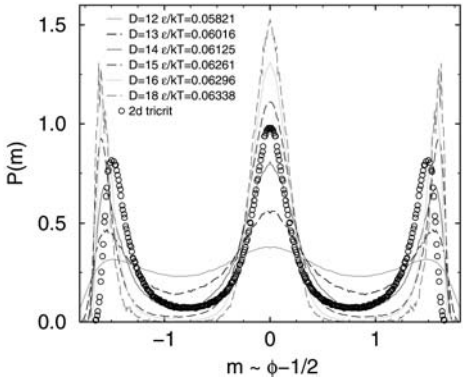

Fig. 52. Locating the tricritical wetting transition in a binary polymer blend. The probability distribution of the order parameter is compared to the universal function of the tricritical universality class in two dimensions.[167] The film thickness is indicated in the key and the lateral system size is $L = 96$. The inverse temperature is adjusted such that the central peak is a factor 1.2 higher than the outer ones. The universal distribution of the 2d tricritical universality class[167] is shown by the circles. From Müller and Binder.[65]

shallow. The temperature is above the second-order transition. For $D > D_t$ the valleys are too deep. In this case the transition is first-order and the temperature is close to the triple point. The configurations between the peaks are dominated by configurations which simultaneously contain a thin and a thick enrichment layer at a surface, and their probability is suppressed by the (albeit low) interface tension between a thin and a thick enrichment layer. From the data in Fig. 52 we estimate the tricritical film thickness to be $D_t \approx 0.89 R_e$, R_e being the end-to-end distance of the polymer. Simulations of larger systems confirm that the distribution approaches the 2d tricritical shape.[65]

Renormalization of the Effective Interface Potential. Fluctuations are important not only in the vicinity of critical points, but also above the roughening temperature where capillary waves are also present. They broaden the width of interface profile (cf. Section 2.2), but they also renormalize the effective interface potential (cf. Section 2.3). By monitoring the probability $P(l)$ of finding the AB interface a distance l away from a surface, we can directly extract the effective interface potential $V_{\text{eff}}(l) = -k_B T \ln P(l)/L^2 + \text{const}$ from the simulations. Results for a binary polymer blend confined into a thick film with antisymmetric surfaces slightly above the triple point are presented in Fig. 53. $V_{\text{eff}}(l)$ exhibits the characteristic shape in the vicinity of a first-order wetting transition (cf. Section 1 and Fig. 5): a free energy barrier separates the minimum close

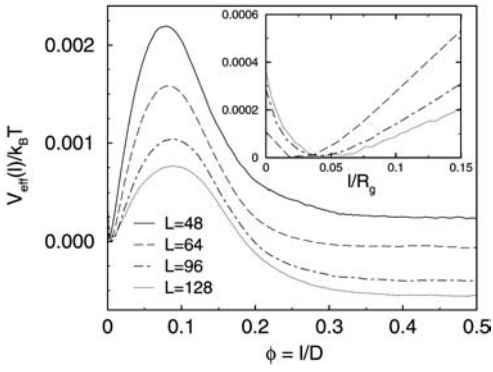

Fig. 53. Direct evidence for the renormalization of the effective interface potential via its dependence on the lateral system size. The effective interface potential is extracted from the Monte Carlo simulations of a binary polymer blend in a film $D = 48$ at a temperature $k_BT/\epsilon = 14.5$ slightly above the first-order wetting transition temperature $k_BT_w/\epsilon = 14.1$. The inset enlarges the behavior at the minimum close to the surface. From Müller and Binder.[65]

to the surface from the values at large separations between the interface and the surface. The simulation data have been shifted vertically such that g vanishes at the minimum close to the surface. Within mean field approximation the interface potential $V_{\text{eff}}(l)$ does not depend on the lateral system size. This is not at all what we observe in the simulations: the free energy difference between the minima at the surface and at the center of the film (i.e., at large distances) changes its sign and the minimum close to the surface becomes broader and shifts to larger distances as we increase the lateral system size and thereby allow for additional modes of capillary waves in the simulation box.

The curvature of the minima at the surface and in the middle of the film are quite different. It imparts a lateral correlation length $\xi_{||}$ on capillary waves (cf. Section 2.2 and Eq. (71)). $\xi_{||}$ is much smaller for the minimum close to the surface than for the minimum at the center of the film, where it diverges exponentially with the film thickness D. This lateral correlation length $\xi_{||}$ or the lateral system size L act as long wavelength cutoff for capillary waves. Increasing L we gradually "switch on" capillary waves, which lower the free energy compared to a strictly flat interface configuration. When the interface is in the middle of the film, there are more capillary modes and consequentially the minimum at the center decreases more than the minimum at the surface. A quantitative comparison of the Monte Carlo data with the behavior of an interface in a harmonic potential corroborates this qualitative explanation.[65]

4. CONCLUSIONS

In this review, we have focused on the three-dimensional nearest-neighbor ferromagnetic Ising model confined between two parallel surfaces a distance D apart, upon which surface fields H_1 and H_D act. We have emphasized that this model is a very useful testing ground for theories that attempt to describe phenomena in confined fluids, e.g., wetting transitions, interface localization-delocalization and anomalous broadening of interface profiles, and capillary condensation. We have first presented a tutorial introduction to the main theoretical concepts, emphasizing in particular how these phenomena are compatible with the scaling description that should hold near the bulk critical point of the Ising model and working out consequences resulting from the theory of finite size scaling.

Wetting and capillary condensation near bulk criticality is a topic that was pioneered in a series of papers by Fisher and Nakanishi[13, 24, 25] that provided particular motivation for the Monte Carlo studies[15, 66, 125–135] that were reviewed here. When the Monte Carlo studies could yield conclusive results, the scaling scenarios of Fisher and Nakanishi (who predicted the scaling of the location of a capillary condensation critical point with D[24, 25] as well as the scaling of wetting transition fields with the distance from a bulk critical point in a semi-infinite Ising system,[13] etc.) were confirmed. Of course, the accuracy of the Monte Carlo results is still rather limited, and extensions of the work reviewed here are still desirable—e.g., studies of capillary condensation for much thicker films than $D = 32$ lattice spacings[125] are needed, the surface-bulk multicritical point needs to be located more accurately, and the associated exponents need to be estimated more precisely.[100–104] It would also be desirable to locate critical and tricritical wetting transitions still closer to the bulk critical temperature than it was done by Wansleben *et al.*;[129] etc.

While such studies—when they become available—will presumably not reveal fundamental surprises, the situation is quite different, as far as the theory of critical wetting is concerned.[63, 64, 67–76, 86–91, 112, 113] Since the theory of critical wetting with short range forces relies heavily on the use of a capillary wave-type Hamiltonian, cf. Eqs. (49) and (50), and predicts a non-universal critical exponent $\nu_{||}$ (cf. Eq. 117) that depends on a parameter ω, Eq. (91), the first question to be asked is whether or not the starting point of the description is correct. One obvious uncertainty, the value for the parameter ω for the Ising model, was clarified by Fisher and Wen[113] who showed that $\omega \approx 0.86$ both at the bulk critical temperature and over a range of temperatures below it, so $\nu_{||} \approx 4$ at the temperatures for which Monte Carlo results are available. Nonetheless, both the simulations[128, 129] and recent experiments[152] showed no significant deviations from the mean

field result, $\nu_{||} = 1$ (cf. Eq. (76)). Another question is, can one really justify the simple effective potential with a few exponentially decaying terms that compete with each other (cf. Eq. (76)) for the Ising model? This issue was considered by Fisher and Jin[63, 64] who suggested that actually one should have a (weakly) first-order wetting transition in the Ising model. If this result is true, the phase diagrams shown in Figs. 4 and 31 would need revision, and the apparent vanishing of the jump in Fig. 30 would need a different interpretation, namely a crossover from a strong first-order wetting transition to a very weak first-order wetting transition as J_s/J decreases. Of course, it is always possible that a very weak first-order transition in a simulation (as well as in experiments!) is mistakenly identified as a second-order transition. On the other hand, there are no specific predictions of any quantities resulting from the work of Fisher and Jin[63, 64] that could provide a more critical test of what actually happens. In our view, this problem deserves more attention both from the theoretical side and with very accurate simulations.

Parry *et al.*[86–91] made the particularly interesting suggestion that the one-collective coordinate description, Eq. (49), needs to be abandoned and replaced by a two-collective coordinate description, Eq. (89), for the effective Hamiltonian. It would be very desirable to explore the consequences that this description implies for the Monte Carlo study by more detailed, accurate simulations. Encouragingly, the result that one can take the effect of the coupling between the two collective coordinates l_1, l_2 in Eq. (89) into account approximately by using Eq. (49) with a renormalized potential, where the decay constant $\kappa = \xi_b^{-1}$ in Eq. (50) is replaced by $\kappa = [\xi_b(1+\omega/2]^{-1}$ (cf. Eq. (164)) has been confirmed by simulations for both Ising models[15] and models of polymer mixtures.[155] However, it seems that Eq. (89) does not produce any change in the exponent $\nu_{||}$ or its dependence on ω,[76, 91] so at this point it seems as though the only possible reconciliation between simulations (and experiments) on critical wetting with short range forces with the corresponding renormalization group theory[67–76] would be if the asymptotic critical region were so narrow that it has been reached neither in simulation[127–129] nor experiment.[152]

Thin Ising films with competing walls, $H_1 = -H_D$ are also very interesting. Theory predicts[16, 59, 60] that there is a phase transition that converges to the wetting transition temperature T_w as $D \to \infty$, unlike the capillary condensation critical point (observable e.g., for $H_1 = H_D$) $T_c(D)$ where $T_c(D) \to T_{cb}$ as $D \to \infty$. This transition was predicted to be either second-order[16, 59] or, depending on the parameters, first-order.[60] Indeed all these cases have been found in Monte Carlo simulations of both Ising models[66, 132–134] and models for symmetrical polymer mixtures.[65] A particularly interesting consequence of these studies is the prediction that a

system that undergoes first-order wetting as well as first-order localization-delocalization phase transition in thick films may have second-order interface localization-delocalization transitions if the thickness falls below some tricritical value D_t. This change in the order of the transition is also reflected in different topologies of the phase diagram of the thin film, in particular when (in the case of the mixture) the concentration (rather than the chemical potential difference $\Delta\mu$, i.e., the magnetic field of the Ising model) is the independent variable.[17, 18, 65] A generalization to the case where no particular symmetry between the surface fields holds (cases intermediate between $H_1 = H_D$ and $H_1 = -H_D$) has also been presented for the polymer case, within the framework of the self-consistent field theory.[21] Although for $D \to \infty$ the transition temperature (for $H_1 = -H_D$) coincides with the wetting transition temperatures T_w, the critical behavior of the total system has nothing to do with critical wetting. A Ginzburg criterion (Eq. (88)) shows that this transition indeed satisfies mean field behavior, while for finite D it belongs to the class of the two-dimensional Ising model.[15]

While we are not yet aware of any clear experimental evidence for an interface localization-delocalization phase transition, the anomalous behavior of fluctuating interfaces confined between competing walls has been observed for polymer mixtures experimentally.[156, 157] Corresponding simulations[151] show that the width of the interface depends strongly on the thickness of the film D, and it is impossible to extract the "intrinsic width" of the interface from the data. This problem of separating the intrinsic width from capillary wave-type broadening is, in our opinion, a very general and unsolved problem that occurs for all types of interface profiles.[30, 61, 80–82] It is related to the fact that it is unclear in which way short wavelength capillary waves crossover to the bulk-like excitations on the scale of the bulk correlation length ξ_b (in a crude and doubtful way this crossover is simply taken into account via a cutoff at large wavenumbers in the capillary wave spectrum.)[82]

Finally, we emphasize that the present review has not treated any work that uses long range forces due to the walls, although this case would clearly be very important for the understanding of experiments.[4–6] For the Ising model with short range forces on the walls, we have restricted attention to the case of $d = 3$ dimensions and have disregarded the rich literature on wetting in $d = 2$ (e.g., refs. 168–172) and on thin (quasi-one-dimensional) Ising strips (e.g., refs. 173 and 174). In the 2d case, fluctuation effects are much more important, and mean field theories that were mentioned earlier are no longer a reliable guide to the understanding of wetting and related phenomena. Nevertheless, due to the availability of exact solutions[168, 170] and powerful transfer matrix methods (e.g., ref. 173) a rather

satisfactory phenomenological understanding of the two-dimensional case is in fact available. In particular, the interpretation of the interface in the 2d Ising model at low temperatures as a contour that behaves like a self-avoiding walk[171] has provided very useful insight into all these phenomena. Also, in this case there is no roughening transition at nonzero temperatures, and one can calculate the coupling constant σ of the capillary wave Hamiltonian exactly and show that in $d = 2$ it differs in general from the interfacial free energy f_{int}/k_BT: while for $T \to 0$ $f_{\text{int}} \to 2J$ one finds that[62, 171] this "interface stiffness" $k_BT\sigma \to \infty$.

ACKNOWLEDGMENTS

We thank E. V. Albano, O. Dillmann, R. Evans, A. M. Ferrenberg, W. Janke, D. M. Kroll. and S. Wansleben for their fruitful collaboration on partial aspects of the work reviewed here. We are particularly grateful to M. E. Fisher for helpful comments and inspiring discussions and for sending preprints of his pertinent papers prior to publication. We acknowledge stimulating discussions with many colleagues, in particular S. Dietrich, J. O. Indekeu, J. Klein, R. Lipowsky, A. O. Parry, F. Schmid, and A. Werner. The research reviewed here was also supported by NSF under grants No. DMR-9100692, DMR 86-03605, DMR 9405018, DMR-9727714, and DMR0094422, by the Deutsche Forschungsgemeinschaft under grants No. SFB262/D1 and Bi 314/16 and Bi 314/17, by NATO grants No. CRG 921202 and PST-CLG 977430, and by the Alexander von Humboldt foundation.

REFERENCES

1. T. Young, *Philos. Trans. Roy. Soc. London* **95**:65 (1805)
2. J. W. Cahn, *J. Chem. Phys.* **66**:3667 (1977).
3. On an atomic scale, the density profile of a fluid against a hard wall shows well-known density oscillations (i.e., a "layered structure"). We assume here that we are so close to the bulk critical point, that the correlation length of density fluctuations is much larger than interatomic distances and can be used as a linear dimension of coarse-graining cells. Using the average of the density over such coarse graining cells as an order parameter in Fig. 2 rather than the density itself, we average the layered structure out.
4. D. E. Sullivan and M. M. Telo da Gama, in *Fluid Interfacial Phenomena*, C. A. Croxton, ed. (Wiley, New York 1986), p. 45.
5. S. Dietrich, in *Phase Transitions and Critical Phenomena*, Vol. XII, C. Domb and J. L. Lebowitz, eds. (Academic, New York, 1988), p. 1.
6. M. Schick, in *Liquids at Interfaces*, J. Charvolin, J. F. Joanny, and J. Zinn-Justin, eds. (North-Holland, Amsterdam, 1990), p. 415.
7. K. Binder and P. C. Hohenberg, *Phys. Rev. B* **6**:3461 (1972); ibid B**9**:2194 (1974).

8. K. Binder, in *Phase Transitions and Critical Phenomena*, Vol. VIII, C. Domb and J. L. Lebowitz, eds. (Academic, New York, 1983), p. 1.
9. A. J. Liu and M. E. Fisher, *Phys. Rev. A* **40**:7202 (1989), and references therein.
10. H. W. Diehl and M. Smock, *Phys. Rev. B* **47**:5841 (1993); **48**, 6740(E) (1993).
11. A. J. Bray and M. A. Moore, *J. Phys. A* **10**:1927 (1977).
12. K. Ohno and Y. Okabe, *Phys. Rev. B* **39**:9764 (1989).
13. H. Nakanishi and M. E. Fisher, *Phys. Rev. Lett.* **49**:1565 (1982)
14. We disregard here temperatures far below the bulk critical temperature T_{cb} and thus shall not discuss the fact that near the roughening transition temperature T_R complete wetting is replaced by a sequence of layering transitions, as discussed by R. Pandit, M. Schick, and M. Wortis, *Phys. Rev. B* **25**:5112 (1982) and by K. Binder and D. P. Landau, *Phys. Rev. B* **46**:4844 (1992).
15. K. Binder, R. Evans, D. P. Landau, and A. M. Ferrenberg, *Phys. Rev. E* **53**:5023 (1996).
16. A. O. Parry and R. Evans, *Phys. Rev. Lett.* **64**:439 (1990).
17. M. Müller, K. Binder, and E. V. Albano, *Physica A* **279**:188 (2000), M. Müller, E. V. Albano, and K. Binder, *Phys. Rev. E* **62**:5281 (2000).
18. K. Binder, M. Müller, and E. V. Albano, *Phys. Chem. Chem. Phys.* **3**:1160 (2001).
19. J. Rogiers and J. O. Indekeu, *Europhys. Lett.* **24**:21(1993).
20. E. Carlon and A. Drzewinski, *Phys. Rev. Lett.* **79**:1591 (1997).
21. M. Müller, K. Binder, and E. V. Albano, *Europhys. Lett.* **50**:724 (2000).
22. S. J. Gregg and K. S. W. Sing, *Adsorption, Surface Area and Porosity* (Academic, New York, 1982).
23. W. T. Thomson (Lord Kelvin), *Philos. Mag.* **42**:448 (1871).
24. M. E. Fisher and H. Nakanishi, *J. Chem. Phys.* **75**:5857 (1981).
25. H. Nakanishi and M. E. Fisher, *J. Chem. Phys.* **78**:3279 (1983).
26. R. Evans and P. Taranzona, *Phys. Rev. Lett.* **52**:557 (1984).
27. R. Evans, *J. Phys. Condens. Matter* **2**:8989 (1990).
28. L. D. Gelb, K. E. Gubbins, R. Radhakrishnan, and M. Sliwinska-Bartkoviak, *Rep. Progr. Phys.* **62**:1573 (1999).
29. D. Nicolaides and R. Evans, *Phys. Rev. B* **39**:9336 (1989).
30. A. Milchev and K. Binder, *J. Chem. Phys.* **114**:8610 (2001).
31. A. Milchev and A. Milchev, *Europhys. Lett.* **56**:695 (2001).
32. L. G. MacDowell, M. Müller, and K. Binder, *Colloids Surf. A* **206**:277 (2002).
33. J. W. Gibbs. *The Collected Works of J. Willard Gibbs* (Yale University Press, London, 1957), p. 288.
34. P. G. deGennes, *Rev. Mod. Phys.* **57**:827 (1985).
35. J. O. Indekeu, *Internat. J. Modern Phys.* **138**:309 (1994), and references therein.
36. T. Getta and S. Dietrich, *Phys. Rev. E* **57**:655 (1998), and references therein.
37. J. Drelich, *Colloids Surf. A* **116**:43 (1996).
38. C. Bauer and S. Dietrich, *Euro. Phys. J. B* **10**:767 (1999).
39. M. P. Gelfand and R. Lipowsky, *Phys. Rev. B* **36**:8725 (1987).
40. T. Bieker and S. Dietrich, *Phys. A* **252**:85 (1998) and *Phys. A* **259**:466 (1998), and refereces therein.
41. A. Milchev and K. Binder, *J. Chem. Phys.* **117**:6852 (2002).
42. A. J. Liu and G. S. Grest, *Phys. Rev. A* **44**:R7894 (1991).
43. D. B. Abraham, in *Phase Transitions and Critical Phenomena*, Vol. 10, C. Domb and J. L. Lebowitz, eds. (Academic Press, New York, 1986).
44. F. Igloi and J. O. Indekeu, *Phys. Rev. B* **41**:6836 (1990), and references therein.
45. J. O. Indekeu, *Phys. A* **177**:428 (1991).
46. I. Schmidt and K. Binder, *Z. Phys. B* **67**:369 (1987).
47. S. Puri and K. Binder, *Z. Phys. B* **86**:263 (1992).

48. K. Binder and H. L. Frisch, *Z. Phys. B* **84**:403 (1991).
49. R. Pandit and M. Wortis, *Phys. Rev. B* **25**:3226 (1982).
50. J. D. Weeks, in *Ordering in Strongly Fluctuating Condensed Matter Systems*, T. Riste, ed. (Plenum Press, New York, 1980), p. 293.
51. H. Van Beijeren and I. Nolden, in *Structure and Dynamics of Surfaces II*, W. Schommers and P. Blankenhagen, eds. (Springer, Berlin, 1987), p. 259.
52. B. Widom, in *Phase Transitions and Critical Phenomena*, Vol. 2, C. Domb and M. S. Green, ed. (Academic Press, London 1972), p. 79.
53. J. S. Rowlinson and B. Widom, *Molecular Theory of Capillary* (Clarendon, Oxford, 1982).
54. F. P. Buff, R. A. Lovett, and F. H. Stillinger, *Phys. Rev. Lett* **15**:621 (1965).
55. J. D. Weeks, *J. Chem. Phys.* **67**:3106 (1977).
56. J. D. Weeks, *Phys. Rev. Lett.* **52**:2160 (1984).
57. H. W. Diehl, in *Phase Transitions and Critical Phenomena*, Vol. 10, C. Domb and J. L. Lebowitz, eds. (Academic Press, London, 1986), p. 75.
58. M. E. Fisher, *Rev. Mod. Phys.* **46**:597 (1974).
59. A. O. Parry and R. Evans, *Phys. A* **181**:250 (1992).
60. M. R. Swift, A. L. Owczarek, and J. D. Indekeu, *Europhys. Lett.* **14**:475 (1991).
61. K. Binder, M. Müller, F. Schmid, and A. Werner, *J. Statist. Phys.* **95**:1045 (1999).
62. V. Privman, *Internat. J. Modern Phys. C* **3**:857 (1992).
63. M. E. Fisher and J. A. Jin, *Phys. Rev. Lett.* **69**:792 (1992); A. J. Jin and M. E. Fisher, *Phys. Rev. B* **47**:7365 (1993).
64. M. E. Fisher, A. J. Jin, and A. O. Parry, *Ber. Bunsenges. Phys. Chem.* **98**:357 (1994).
65. M. Müller and K. Binder, *Phys. Rev. E* **63**:021602 (2001).
66. A. M. Ferrenberg, D. P. Landau, and K. Binder, *Phys. Rev. E* **58**:3353 (1998).
67. E. Brezin, B. I. Halperin, and S. Leibler, *Phys. Rev. Lett.* **50**:1387 (1983).
68. E. Brezin, B. I. Halperin, and S. Leibler, *J. Phys. (Paris)* **44**:775 (1983).
69. R. Lipowsky, D. M. Kroll, and R. K. P. Zia, *Phys. Rev. B* **27**:4499 (1983).
70. D. S. Fisher and D. A. Huse, *Phys. Rev. B* **32**:247 (1985).
71. E. H. Hauge and K. Olaussen, *Phys. Rev. B* **32**:4766 (1985).
72. R. Lipowsky and M. E. Fisher, *Phys. Rev. B* **36**:2126 (1987).
73. E. Brézin and T. Halpin-Healey, *J. Phys. (Paris)* **48**:747. (1987).
74. E. Brézin and T. Halpin-Healey, *Phys. Rev. Lett.* **58**:1220. (1987).
75. T. Halpin-Healey, *Phys. Rev. B* **40**:772 (1989).
76. A. O. Parry and J. C. Boulter, *Phys. Rev. E* **53**:6577 (1996).
77. M. Napiorkowski and S. Dietrich, *Z. Phys. B* **89**:263 (1992); *Phys. Rev. E* **47**:1836 (1993).
78. A. O. Parry and C. J. Boulter, *J. Phys. Condens. Matter* **6**:7199 (1994).
79. K. Mecke and S. Dietrich, *Phys. Rev. E* **59**:6766 (1999).
80. A. Werner, F. Schmid, M. Müller, and K. Binder, *Phys. Rev. E* **59**:728 (1999).
81. M. Müller and L. G. MacDowell, *Macromolecules* **33**:3902 (2000).
82. K. Binder and M. Müller, *Internat. J. Modern Phys. C* **11**:1093 (2000).
83. V. L. Ginzburg, *Fiz. Tverd. Tela (Leningrad)* **2**:2031 (1960) [*Sov. Phys. Solid State* **2**:1824 (1960)].
84. J. Als-Nielsen and R. J. Birgeneau, *Amer. J. Phys.* **45**:554 (1970).
85. M. A. Anisimov, S. B. Kiselev, J. V. Sengers, and S. Tang, *Phys. A* **188**:487 (1992).
86. C. J. Boulter and A. O. Parry, *Phys. Rev. Lett.* **74**:3403 (1995).
87. A. O. Parry and C. J. Boulter, *Phys. A* **218**:77 (1995).
88. C. J. Boulter and A. O. Parry, *Phys. A* **218**:109 (1995).
89. A. O. Parry, C. J. Boulter, and P. S. Swain, *Phys. Rev. E* **52**:R5768 (1995).

90. P. S. Swain and A. O. Parry, *Europhys. Lett.* **37**:207 (1997).
91. A. O. Parry, *J. Phys.: Condens. Matter* **8**:10761 (1996).
92. C. J. Boulter, *Mod. Phys. Lett.* **15**:993 (2001).
93. J. C. Le Guillou and J. Zinn-Justin, *Phys. Rev. B* **21**:3976 (1980).
94. K. Binder and E. Luijten, *Phys. Rep.* **344**:179. (2001).
95. M. E. Fisher, in Critical Phenomena, *Proc. 1970 E. Fermi Int. School of Physics*, M. S. Green, ed. (Academic, London, 1971), p.1.
96. M. E. Fisher and M. N. Barber, *Phys. Rev. Lett.* **28**:1516 (1972).
97. M. N. Barber, in *Phase Transitions and Critical Phenomena*, Vol. 8, C. Domb and J. L. Lebowitz, eds. (Academic, New York, 1983), p. 145.
98. V. Privman, ed., *Finite Size Scaling and the Numerical Simulation of Statistical Systems* (Singapore, World Scientific, 1990).
99. K. Binder, in *Computational Methods in Field Theory*, H. Gausterer and C. B. Lang, eds. (Springer, Berlin, 1992), p. 59.
100. K. Binder and D. P. Landau, *Phys. Rev. Lett.* **52**:318 (1984).
101. D. P. Landau and K. Binder, *Phys. Rev. B* **41**:4633 (1990).
102. C. Ruge, S. Dunkelmann, F. Wagner, and J. Wulf, *J. Statist. Phys.* **73**:293 (1993).
103. C. Ruge and F. Wagner, *Phys. Rev. B* **52**:4209 (1995).
104. H. W. Diehl and M. Shpot, *Nucl. Phys. B* **528**:595 (1998).
105. H. W. Diehl, *Internat. J. Modern Phys. B* **11**:3503 (1997).
106. A. D. Bruce and N. B. Wilding, *Phys. Rev. Lett.* **86**:193 (1992).
107. K. Binder, *Thin Solid Films* **20**:367 (1974).
108. T. W. Capehart and M. E. Fisher, *Phys. Rev. B* **13**:6021 (1976).
109. M. E. Fisher and H. Au-Yang, *Phys. A* **101**:255 (1980); H. Au-Yang and M. E. Fisher, *Phys. Rev. B* **21**:3956 (1980).
110. F. Freire, D. O'Connor, and C. R. Stephens, *J. Statist. Phys.* **74**:219 (1994); D. O'Connor and R. C. Stephens, *Phys. Rev. Lett.* **72**:506 (1994).
111. Y. Rouault, J. Baschnagel, and K. Binder, *J. Statist. Phys.* **80**:1009 (1995).
112. D. M. Kroll, R. Lipowsky, and R. K. P. Zia, *Phys. Rev. B* **32**:1862 (1985).
113. M. E. Fisher and H. Wen, *Phys. Rev. Lett.* **68**:3654 (1992).
114. C. J. Boulter and F. Clarysse, *Eur. Phys. J. E* **5**:465 (2001).
115. E. Riedel and F. J. Wegner, *Z. Phys.* **225**:195 (1969).
116. M. Hasenbusch, *Internat. J. Modern Phys. C* **12**:91 (2001).
117. D. P. Landau and K. Binder, *A Guide to Monte Carlo Simulations in Statistical Physics* (Cambridge University Press, Cambridge, 2000).
118. R. H. Swendson and J. S. Wang, *Phys. Rev. Lett.* **58**:86 (1987).
119. U. Wolff, *Phys. Rev. Lett.* **62**:361 (1989).
120. R. H. Swendsen, J. S. Wang, and A. M. Ferrenberg, *The Monte Carlo Method in Condensed Matter Physics* (Springer, Berlin, 1992), p. 75.
121. J. S. Wang, *Phys. A* **161**:249 (1989).
122. P. G. Lauwers and V. Rittenberg, *Phys. Lett. B* **233**:197 (1989).
123. V. S. Dotsenko, W. Selke, and A. L. Talapov, *Phys. A* **170**, 278 (1990).
124. O. Redner, J. Machta, and L. F. Chayes, *Phys. Rev. E* **58**:2749 (1998); L. Chayes, J. Machta, and O. Redner, *J. Statist. Phys.* **93**:17 (1998); J. Machta, *Internat. J. Modern Phys. C* **10**:1427 (1999).
125. O. Dillmann, W. Janke, M. Müller, and K. Binder, *J. Chem. Phys.* **114**:5853 (2001).
126. K. Binder and D. P. Landau, *J. Appl. Phys.* **57**:3306 (1985).
127. K. Binder, D. P. Landau, and D. M. Kroll, *Phys. Rev. Lett.* **56**, 2276 (1986).
128. K. Binder and D. P. Landau, *Phys. Rev. B* **37**:1745 (1988).
129. K. Binder, D. P. Landau, and S. Wansleben, *Phys. Rev. B* **40**:6971 (1989).

130. K. Binder and D. P. Landau, *Phys. Rev. B* **46**:4844 (1992).
131. K. Binder and D. P. Landau, *J. Chem. Phys.* **96**:1444 (1992).
132. K. Binder, A. M. Ferrenberg, and D. P. Landau, *Ber. Bunsenges. Phys. Chem.* **98**:340 (1994).
133. K. Binder, D. P. Landau, and A. M. Ferrenberg, *Phys. Rev. Lett.* **74**:298 (1985).
134. K. Binder, D. P. Landau, and A. M. Ferrenberg, *Phys. Rev. E* **51**:2823 (1995).
135. D. P. Landau and K. Binder, in *STATPHYS 19*, B. Hao, ed. (World Scientific, Singapore, 1996), p. 446.
136. N. Metropolis, A. W. Rosenbluth, M. N. Rosenbluth, A. H. Teller, and E. Teller, *J. Chem. Phys.* **21**:1087 (1953)
137. M. Hasenbusch and S. Meyer, *Phys. Rev. Lett.* **66**:530 (1991).
138. B. J. Schulz, K. Binder, and M. Müller, *Int. J. Mod. Phys. C* **13**:477 (2002).
139. F. Wang and D. P. Landau, *Phys. Rev. Lett.* **86**:2050 (2001).
140. A. B. Bortz, M. M. Kalos, and J. L. Lebowitz, *J. Comput. Phys.* **17**:10 (1975).
141. A. M. Ferrenberg, D. P. Landau, and Y. J. Wong, *Phys. Rev. Lett.* **69**:3382 (1992)
142. W. Janke, in *Computational Physics: Selected Methods, Simple Exercises, Serious Applications*, K. H. Hoffmann and M. Schreiber, eds. (Springer, Berlin, 1996), p. 10.
143. S. Kirkpatrick and E. Stoll, *J. Comput. Phys.* **40**:517 (1981).
144. A. M. Ferrenberg and R. H. Swendsen, *Phys. Rev. Lett.* **63**:1195 (1989)
145. K. Binder and D. P. Landau, *Phys. Rev. B* **30**:147 (1984).
146. C. Borgs and R. Kotecky, *J. Statist. Phys.* **61**:79 (1990); C. Borgs, R. Kotecky, and S. Miracle-Sole, *J. Statist. Phys.* **62**:529 (1991).
147. C. Borgs and W. Janke, *Phys. Rev. Lett.* **68**:1738 (1992); W. Janke, *Phys. Rev. B* **47**:1453 (1993).
148. H. W. Blöte, E. Luijten, and J. R. Heringa, *J. Phys. A* **28**:6289 (1995).
149. K. Binder, *Phys. Rev. Lett.* **47**:693 (1981); *Z. Phys. B* **43**:119 (1981).
150. D. P. Landau, *Phys. A* **205**:41 (1994).
151. A. Werner, F. Schmid, M. Müller, and K. Binder, *J. Chem. Phys.* **107**:8175 (1997).
152. D. Ross, D. Bonn, and J. Meunier, *Nature* **400**:737 (1999); *J. Chem. Phys.* **114**:2784 (2001).
153. A. J. Liu and M. E. Fisher, *Phys. A* **156**:35 (1989).
154. M. Hasenbusch and K. Pinn, *Phys. A* **192**:342 (1993).
155. M. Müller and K. Binder, *Macromolecules* **31**:8323 (1998).
156. T. Kerle, J. Klein, and K. Binder, *Phys. Rev. Lett.* **77**:1318 (1996).
157. T. Kerle, J. Klein, and K. Binder, *Eur. Phys. J. B* **7**:401 (1999).
158. A. O. Parry, R. Evans, *J. Phys. A* **25**:275 (1992).
159. E. Montevecchi and J. O. Indekeu, *Phys. Rev. B* **62**:14359 (2000).
160. I. Carmesin and K. Kremer, *Macromolecules* **21**:2819 (1988). H.-P. Deutsch and K. Binder, *J. Chem. Phys.* **95**:2294 (1991).
161. M. Müller, *Macromol. Theory Simul.* **8**:343 (1999).
162. M. Müller and F. Schmid, in *Annual Reviews of Computational Physics VI*, D. Stauffer, ed. (World Scientific, Singapore, 1999), p. 59.
163. A. Sariban and K. Binder, *Macromolecules* **21**:711 (1988).
164. H.-P. Deutsch and K. Binder, *Macromolecules* **25**:6214 (1992).
165. B. A. Berg, U. Hansmann, and T. Neuhaus, *Z. Phys. B* **90**:229 (1993).
166. R. Evans and U. Marini Bettolo Marconi, *Phys. Rev. A* **32**:3817 (1985).
167. N. B. Wilding and P. Nielaba, *Phys. Rev. E* **53**:926 (1996).
168. D. B. Abraham, *Phys. Rev. Lett.* **44**:1165 (1980)
169. T. M. Burkhardt, *J. Phys. A: Math. Gen.* **14**, L63 (1981); J. T. Chalker, ibid **14**:2431 (1981); S. T. Chui and J. D. Weeks, *Phys. Rev. B* **23**:2438 (1981); H. Hilhorst and J. M. J. van Leeuwen, *Phys. A* **107**:319 (1981); D. M. Kroll, *Z. Phys. B* **41**:345 (1981); M. Vallade and J. Lajczerowicz, *J. Phys. (Paris)* **42**:1505 (1981).

170. D. B. Abraham and E. R. Smith, *Phys. Rev. B* **26**:1480 (1982); *J. Statist. Phys.* **43**:621 (1986).
171. M. E. Fisher, *J. Statist. Phys.* **34**:667 (1984).
172. E. V. Albano, K. Binder, D. W. Heermann, and W. Paul, *J. Statist. Phys.* **61**:161 (1990).
173. A. Maciolek, *J. Phys. A: Math. Gen.* **29**:3837 (1996).
174. E. V. Albano, K. Binder, and W. Paul, *J. Phys.: Condens. Matter* **12**:2701 (2000), and references therein.